Towards method miniaturization for determination of sterols in liver organoids: an investigation of nano liquid chromatography-mass spectrometry (nLC-MS)

Thesis for the Master's degree in Chemistry

60 study points

Henriette Nordli

Department of Chemistry

UNIVERSITY OF OSLO

July 6th, 2021

Towards method miniaturization for determination of sterols in liver organoids: an investigation of nano liquid chromatography-mass spectrometry (nLC-MS)

2021

Towards method miniaturization for determination of sterols in liver organoids: an investigation of nano liquid chromatography-mass spectrometry (nLC-MS)

Henriette Nordli

http://www.duo.uio.no/

Trykk: Reprosentralen, Universitetet i Oslo

Abstract

Obesity and inactivity can lead to a cluster of conditions called metabolic syndrome, which again can lead to non-alcoholic fatty liver disease (NAFLD). NAFLD consists of several stages, where the liver accumulates fats, potentially leading to liver fibrosis and cirrhosis. Cirrhosis is considered a terminal state and requires liver transplantation to save the life of the patient. The only diagnostic tool for NAFLD today is liver biopsy. Hence, less invasive diagnostic tools are currently lacking, like biomarkers, which can be advantageous for early diagnosis. Liver organoids are a promising research model used for disease modeling and recapitulate the human NAFLD *in vivo* environment. Oxysterols are endogenous cholesterol metabolites seen in some of the NAFLD pathways and are proposed as potential biomarker candidates. However, oxysterols are low abundant in biological samples and need a highly sensitive LC-MS method for quantification. Miniaturizing the inner diameter (ID) of the LC column (nLC) is one way to enhance the method sensitivity. Additionally, a trap column can further enhance method sensitivity by allowing large volume injections, and an automatic filtration and filter backflushing system (AFFL) enhances the robustness of the platform. Few studies have investigated the use of miniaturized LC columns in oxysterol determination. The aim of this study was to develop a highly sensitive nLC-MS method, combined with an on-line sample clean-up in the form of a trap column and an AFFL-system, towards quantification of the oxysterols 22R-, 24S-, 25-, and 27-OHC in healthy and NAFLD-induced liver organoids. An automated nLC-MS method combined with an on-line sample clean-up was successfully assembled. 2.5 μm core-shell Super Phenyl-Hexyl (SPH) and 5 μm phenyl-hexyl (PH) particles were chosen and successfully packed in fused silica capillaries (75 μm ID) as the analytical- and trap column, respectively. Significant band broadening was a problem, and a Butterfly Portfolio column heater was included in the platform to enhance column efficiency. It was discovered that the 5 μm PH particles in the trap column were partly responsible for the band broadening observed due to incompatibility with the 2.5 μm SPH particles. Hence, the 2.5 μm SPH particles were found to be suitable in the trap column instead. Relatively efficient nLC columns were packed; however, they proved to be challenging to reproduce and lacked robustness due to short lifetimes, making the oxysterol isomer separation challenging. Core-shell particles continue to prove to be challenging to pack in narrow bore capillaries. Therefore, customizing the packing procedure for these particles should be performed further by, e.g., adding a frit on both ends of the column and optimizing the slurry concentration.

Preface

The work presented in this thesis was performed at the research group for Bioanalytical Chemistry at the Department of Chemistry, University of Oslo, from January 2020 to July 2021. Although the COVID-19 pandemic offered personal and work-related challenges, I am grateful that all the people close to me are safe.

First, I would like to thank my supervisors Professor Elsa Lundanes, Professor Steven Ray Wilson, and Associate Professor Hanne Røberg-Larsen, for their great guidance and inspiring support. A special thanks to Hanne for always being available, answering my questions, and the hands-on guidance.

A thank you to Inge Mikalsen for always providing his help during instrument malfunctions and leakages. His assistance was important for me to cope with the technical problems. I would also like to thank Ph.D.-candidates Christine Olsen and Frøydis Sved Skottvoll for being available for questions and for providing their valuable hands-on experience and guidance on different instruments. Thanks to Lars Bakketeig for sharing and discussing challenges and frustrations regarding the packing of the nLC columns.

A big thanks to my dear friends and study mates Ida Caroline, Karoline, and Maria for great support and talks, both personally and academically. I am grateful for their constant encouragement and motivation through this thesis and throughout my entire education.

At last, a great thank you to my supporting family and friends; I would not have made it through without the great support and motivation from you. A special thanks to my boyfriend Erik for the continuing support, patience, and always being there for me during stressful times.

I want to mention that I am aware that abbreviations should not be used in titles, but this has been done at some places to ease the reading.

Henriette Nordli,
Oslo, Norway, July 2021

Abbreviations

Abbreviation	Term
22R-OHC	22R-Hydroxycholesterol
22R-OHC-d_7	22R-Hydroxycholesterol-d_7
24S-OHC	24S-Hydroxycholesterol
25-OHC	25-Hydroxycholesterol
25-OHC-d_6	25-Hydroxycholesterol-d_6
27-OHC	27-Hydroxycholesterol
27-OHC-d_6	27-Hydroxycholesterol-d_6
2D	Two-dimensional
3D	Three-dimensional
ACN	Acetonitrile
AFFL	Automatic filtration and filter backflushing
C	Concentration
C18	Octadecyl
CE	Capillary electrophoresis
CYP450	Cytochrome P450
DC	Direct current
EADSA	Enzyme-assisted derivatization for sterol analysis
EIC	Extracted ion chromatogram
ER	Endoplasmic reticulum
ESI	Electrospray ionization
FA	Formic acid

FFA	Free fatty acid
FPP	Fully porous particles
FS	Fused silica
FWHM	Full width half maximum
GC	Gas chromatography
HPLC	High performance liquid chromatography
HSC	Hepatic stellate cell
ID	Inner diameter
iPSC	Induced pluripotent stem cell
IS	Internal standard
LC	Liquid chromatography
LOD	Limit of detection
LOQ	Limit of quantification
LXR	Liver X receptor
m/z	Mass to charge ratio
MeOH	Methanol
MP	Mobile phase
MRM	Multiple reaction monitoring
MS	Mass spectrometry
NAFL	Non-alcoholic fatty liver
NAFLD	Non-alcoholic fatty liver disease
NASH	Non-alcoholic steatohepatitis
nESI	Nano electrospray ionization
nLC	Nano liquid chromatography

OD	Outer diameter
PEEK	Polyether ether ketone
PH	Phenyl-hexyl
RF	Radio frequency
ROS	Reactive oxygen species
RP	Reversed phase
RPLC	Reversed phase liquid chromatography
RSD	Relative standard deviation
SEM	Scanning electron microscope
S/N	Signal to noise ratio
SP	Stationary phase
SPH	Super phenyl-hexyl
SST	Stainless steel
TG	Triglycerides
TIC	Total ion current
TQMS	Triple quadrupole mass spectrometry
UHPLC	Ultra-high performance liquid chromatography
UV	Ultraviolet
V	Volume
WS	Working solution

Definitions

Term	Definition
Agglomeration	Particles suspended in a liquid clustering together (reversible) [1].
Aggregation	Particles suspended in a liquid clustering together (irreversible) [1].
Excretion	Metabolic waste products that are eliminated from the body [2].
Extra-column volume	The volume between the effective injection point and the effective detection point, excluding the part of the column containing the stationary phase [3].
Ex vivo	Biological process occurring in or on a biological tissue but in an artificial environment, outside the organism, with the minimum alteration of natural conditions [4].
In vitro	Processes taking place outside a living body [5].
In vivo	Processes taking place in a living body [6].
Ion suppression	Leads to reduced detector response due to the presence of other compounds in the sample competing for ionization or inhibiting efficient ionization of the analytes [7].
Limit of detection	The concentration that gives S/N = 3.
Limit of quantification	The concentration that gives S/N = 10.

Linear velocity	Standardized flow rate adjusted for columns in all dimensions expressed in cm/s (flow rate (cm^3/s) per unit cross-sectional area (cm^2)) [8].
logP	Partition coefficient of a molecule between an aqueous and an organic phase.
Parenchymal cells	The functional tissue of an organ as distinguished from connecting or supporting tissue [9].
Phenotype	The observable characteristics of an organism or a disease [10].
Precision	The closeness of agreement between independent test results. A measure of precision is the standard deviation [11].
Repeatability	The closeness of agreement between independent results obtained with the same method on identical test material under the same conditions (same operator, same apparatus, same laboratory, and after short intervals of time) [11].
Resolution	A characteristic of separation between two adjacent peaks in chromatography [12]. $R_s \geq 1.5$ corresponds to baseline separation.
Rotor	A dynamic part in an HPLC-valve that turns when switched, controlling the direction of the flow.
Sedimentation	A process in which small pieces of a solid material fall to the bottom of a liquid and form a layer [13].
Surface tension	The property of the surface of a liquid that allows it to resist an external force, due to the cohesive nature of its molecules [14].

Stator	A fixed outer part in an HPLC-valve where the tubings and connections are attached.
Suspension	A liquid in which small pieces of solid are contained, but not dissolved [15].

Table of Contents

1 Introduction

Obesity and inactivity can lead to metabolic syndrome, which is a cluster of conditions like imbalanced cholesterol levels, high blood pressure, high blood sugar, and insulin resistance [16, 17]. Metabolic syndrome again raises the risk of developing diabetes type 2, heart disease, and non-alcoholic fatty liver disease (NAFLD) [18, 19]. An overview of the different conditions is illustrated in **Figure 1**.

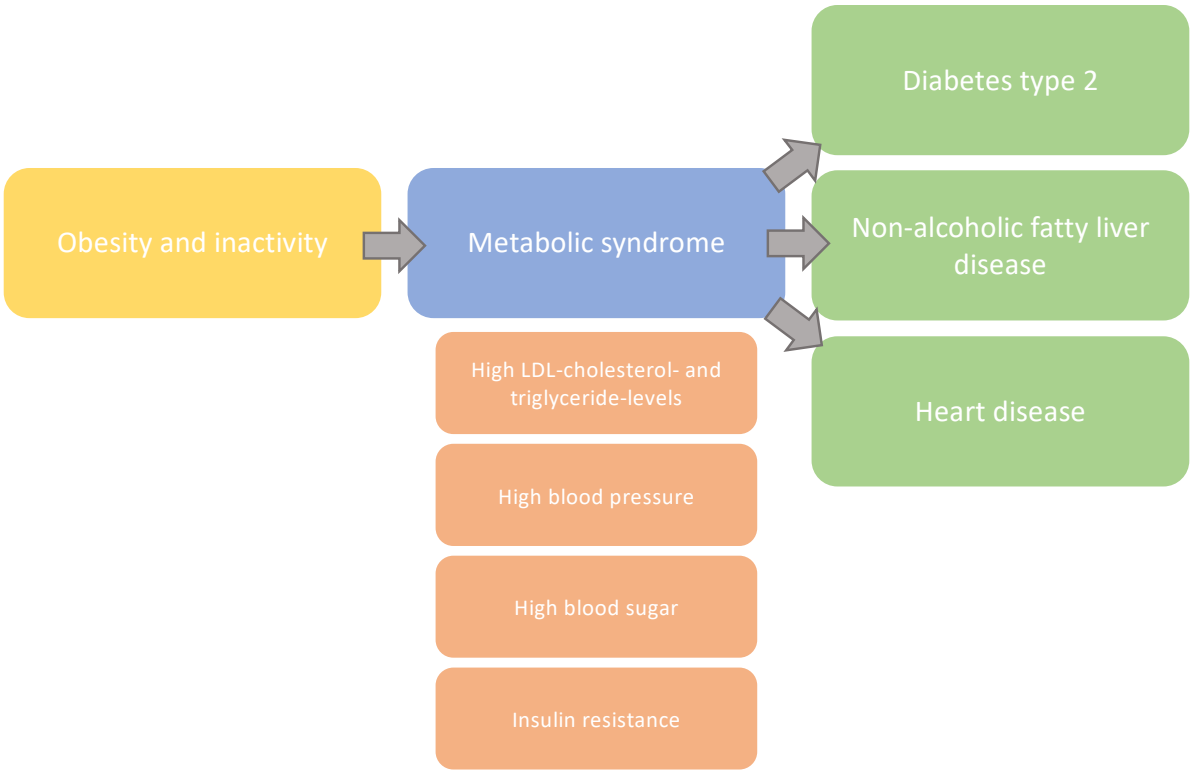

Figure 1. The various conditions linked to obesity and inactivity. The orange boxes illustrate the different conditions of metabolic syndrome, which singly or collectively can contribute to one or several of the conditions in the green boxes.

1.1 Non-alcoholic fatty liver disease

Non-alcoholic fatty liver disease (NAFLD) has become the most common cause of chronic liver disease worldwide, estimated to affect around 25% of the global adult population of the western world [20, 21]. NAFLD develops when the liver accumulates fats due to obesity and inactivity (and not due to alcohol consumption) and is closely related to insulin resistance, metabolic syndrome, and diabetes type 2 [22, 23].

The pathophysiology of NAFLD is complex and not fully understood, but in general, NAFLD consists of several stages, differentiating by the severity of the condition (**Figure 2)** [24]. In the first stage, the hepatocytes, which are the functional metabolizing cells of the liver, accumulate lipids such as triglycerides (TGs) and free fatty acids (FFAs). Accumulation of lipids leads to an enlargement of the liver, often referred to as hepatocyte ballooning, and a stage called steatosis or non-alcoholic fatty liver (NAFL) [24]. NAFL is considered a relatively benign state but can develop into more fatal conditions [25]. Over time, NAFL can progress into a second stage where hepatocyte necrosis leads to inflammation and potential fibrosis of the liver. This second stage is often referred to as non-alcoholic steatohepatitis (NASH) [23]. Fibrosis is when the repair of damaged tissue (inflammation) causes tissue scarring.

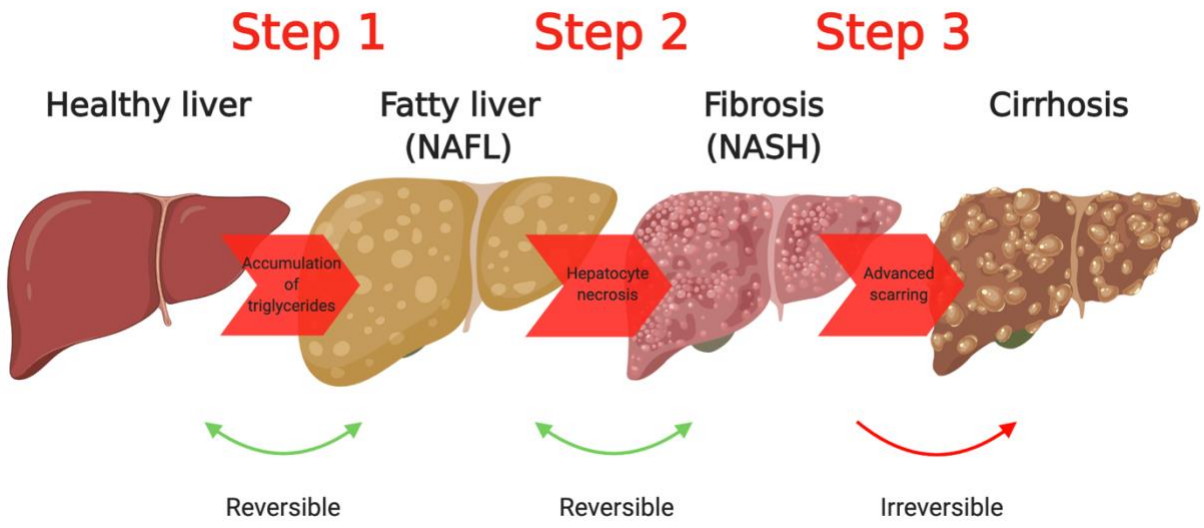

Figure 2. The stages of NAFLD progression from a healthy liver to an enlarged fatty liver, followed by an inflammation-induced fibrotic liver, and an irreversible tissue scarring stage called cirrhosis. The illustration is adapted from [26] and was made in BioRender [27].

Continued damage and repair of liver tissue cause the spread of fibrosis and progression into the third stage; irreversible scarring (cirrhosis) [28]. When the liver has reached cirrhosis, the functional mass of the liver is reduced, the normal structure of the liver is altered, and the liver cannot function properly anymore [22]. There is no treatment for cirrhosis; hence progression to this stage requires a liver transplant to save the life of the patient. NAFLD is predicted among the leading causes for liver transplantation, highlighting the importance of early diagnosis to reverse the disease [29, 30]. For further discussion on the evolution of NAFLD, see **chapter 7.1.1** in **Appendix**.

1.1.1 Current diagnosis of non-alcoholic fatty liver disease

Liver biopsy remains the only standard method for diagnosis of any stage in NAFLD. Hepatic tissue from biopsies is subjected to microscopic examination following standardized scoring of the progression of the disease. Biopsies are highly invasive and put the patient at risk for additional fibrosis resulting from the intervention [31]. Hence, a less invasive diagnostic tool (e.g., using biomarkers in biological samples) with the ability for early-stage diagnosis is strongly desired for NAFLD to reverse the disease and prevent reaching cirrhosis and liver transplantation [32].

1.1.2 Disease modeling in non-alcoholic fatty liver disease

Studies of NAFLD have primarily been performed with animal models and *in vitro* two-dimensional (2D) cell cultures [33-35]. Disease modeling has commonly been approached by feeding high-fat diets to murine models, but this approach has major drawbacks. Inducing inflammation and fibrosis requires feeding for a long time (> one year); hence, studying advanced progression to NASH is highly time-consuming [36]. Additionally, animal models do not fully capture the hepatic and extrahepatic environment in human NASH, and extrapolation to humans may be insufficient [37]. Larger animal models are also expensive and logistically difficult to use [38]. Furthermore, the microscopic assessment of the liver tissue is obtained in only one single analysis at the end of the study, without any baseline biopsy for comparison [39]. Additionally, current *in vitro* 2D cell cultures fail to model the complex multicellular NAFLD-environment (lack non-parenchymal cells responsible for inflammatory and fibrotic responses in the liver [40, 41]). Although advances have been made in recent years, the current state of animal research and 2D cell cultures are not able to mimic the complexity of human biology [36].

1.1.3 Organoids – A new approach for modeling non-alcoholic fatty liver disease

The drawbacks mentioned above with current well-established animal- and *in vitro* models for NAFLD assessment demonstrate the urgent need for model advancement [42]. Organoids may deliver the advancement of better recapitulating human *in vivo* biology [43]. Organoids are derived from either primary cells, induced pluripotent stem cells (iPSCs), or embryonic stem cells (EMCs) [44]. Primary cells are cells taken directly from the living tissue of a donor and further grown *in vitro*. iPSCs are derived from already functionalized cell types from a donor, like easily collected skin cells, and reprogrammed back to stem cells [45]. iPSCs can be differentiated into almost all cell types and self-assemble into three-dimensional (3D) organ-like structures with organ-specific functions similar to their *in vivo* counterparts [46]. Organoids have been employed in disease modeling, personalized medicine, and drug development [46-48], where tissue-specific organoids mimicking the liver, brain, kidney, and intestine have been employed [45]. Organoids were chosen by Nature as the "Method of the Year" in 2017, reflecting its potential [49]. However, being an emerging research model, drawbacks like inter-batch-variability (due to lacking differentiation protocol-standardization) and lacking adult tissue properties (immature) must still be overcome [50].

Non-alcoholic fatty liver disease induced organoids

To induce NAFLD in liver organoids (particularly steatosis- and fibrosis-phenotypes), the organoids must be exposed to FFAs for a prolonged period to cause FFA accumulation (e.g., palmitic or oleic acid, chemical structures are shown in **Figure 3**) [40, 51, 52]. A previous challenge of the NAFLD induction has been the absence of liver resident Kupffer cells (liver immune cells) and hepatic stellate cells (HSCs) in liver organoids. HSCs are the cells responsible for inflammation and fibrosis in the liver. Takebe and colleagues managed to combat the previous challenge and differentiated liver organoids with HSCs- and Kupffer-like cells and recapitulated steatosis, inflammation, and fibrosis through FFA treatment with oleic acid. As a result, enlarged lipid droplets, hepatocyte ballooning, secretion of NAFLD-associated cytokines, and the stiffening of the organoids associated with fibrosis were observed [53].

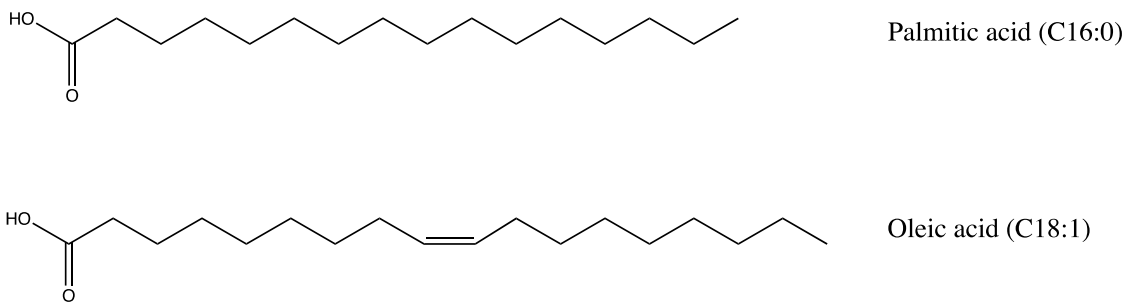

Figure 3. The chemical structure of the fatty acids, palmitic acid, and oleic acid, which are commonly used to induce NAFLD in liver organoids.

1.2 Sterols

1.2.1 Cholesterol

As mentioned, imbalanced cholesterol levels (high low-density lipoprotein (LDL)-cholesterol combined with low high-density-lipoprotein (HDL)-cholesterol) are closely related to obesity and inactivity [54] and are one of several conditions for metabolic syndrome.

Cholesterol is a lipid highly abundant in the cells, located in the lipid bilayer of the cell membrane [55]. Cholesterol consists of four hydrocarbon rings, a non-polar carbon side-chain, and a polar hydroxyl group at position three (**Figure 4**). Cholesterol plays several essential roles in various synthetic pathways, e.g., in bile acids, steroid hormones, and vitamin D synthesis [56]. Three-quarters of the cholesterol in the body is synthesized in the liver, and the rest comes from food [57]. Cholesterol is transported in the body by lipoproteins in the blood, either by high-density lipoproteins (HDL) or low-density lipoproteins (LDL). HDL is responsible for the transport of cholesterol back to the liver for excretion, and LDL transports the cholesterol to the blood arteries. Too much LDL-cholesterol can accumulate cholesterol in the arteries, creating plaque, potentially resulting in blood clots, strokes, or heart attacks [58, 59].

1.2.2 Oxysterols

Oxysterols are intermediate metabolites of cholesterol on their pathway to becoming bile acids before excretion through the gallbladder and the digestive tract [60, 61]. Cholesterol can be oxidized to oxysterols either enzymatically by enzymes of the cytochrome P450-superfamily (CYP450) or hydroxylases, or nonenzymatically by autoxidation by, e.g., H_2O_2 or reactive oxygen species (ROS) such as singlet oxygen, HOCl, and ozone [62]. Depending on the location of the oxidation, the resulting oxysterols have different functions. The hydroxyl group can be bound to the side-chain on the cholesterol (typically enzymatically) or supplement the cholesterols ring structure (typically by autoxidation) [63]. Oxysterols can also form by the addition of a carbonyl or an epoxide group and can exist as both free sterols or esterified- or sulfonated species [64]. Further discussions will mainly concern the side-chain oxysterols 22R-hydroxycholesterol (22R-OHC), 24S-hydroxycholesterol (24S-OHC), 25-hydroxycholesterol (25-OHC), and 27-hydroxycholesterol (27-OHC) oxidized by enzymes; their molecular structures are shown in **Figure 4**. The 27-OHC is more correctly called (25R)-26-OHC [65], but 27-OHC will be used in this thesis as it is commonly used.

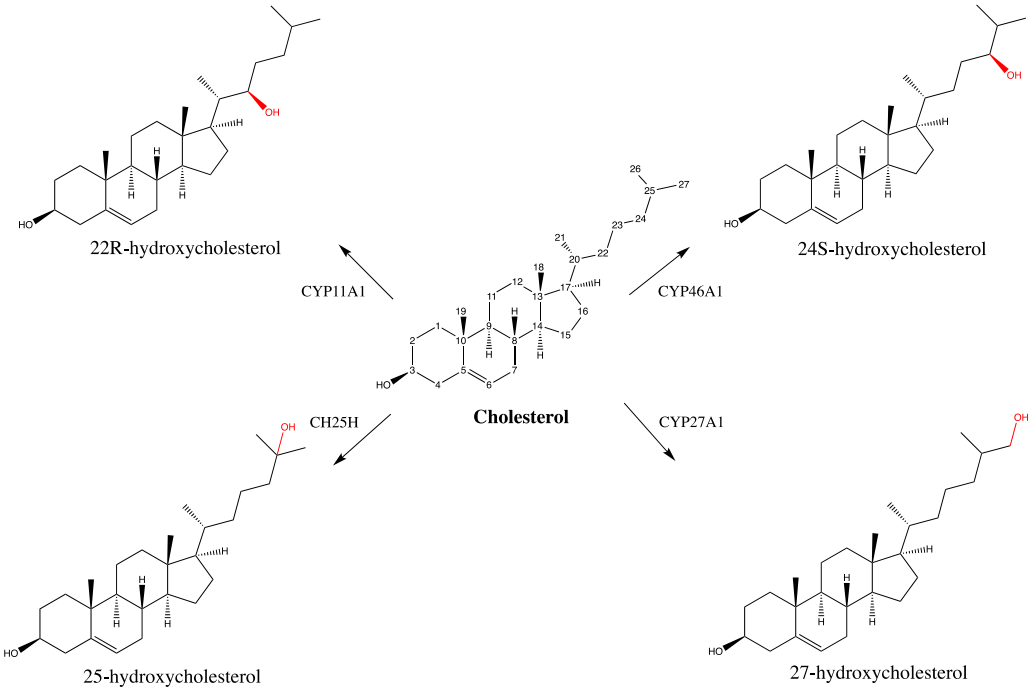

Figure 4. The chemical structure of cholesterol and its metabolites; 22R-OHC, 24S-OHC, 25-OHC, and 27-OHC. The location of the hydroxyl group differentiates the oxysterols and is marked in red. Their respective enzymes for formation are included (CYP11A1, CYP46A1, CH25H, and CYP27A1, respectively).

1.2.3 The biological role of oxysterols

Oxysterols are biologically active molecules, acting as signaling ligands for multiple receptors. 22R-OHC, 24S-OHC, 25-OHC, and 27-OHC act as ligands on the nuclear receptor liver X receptor (LXR), which, when stimulated, induces gene transcription leading to the suppression of cholesterol synthesis [66, 67]. 7β-OHC is a precursor of biologically active molecules including 25-hydroxy-7-oxocholesterol and 26-hydroxy-7-oxocholesterol [68] that activate the G protein-coupled receptor (GPCR) Smoothened in the Hedgehog pathway [66, 69]. 27-OHC is a signaling ligand for the estrogen receptor that studies have shown to be relevant in breast cancer progression [70]. In addition, 24S-OHC, 25-OHC, and 27-OHC, and other side-chain oxysterols can bind to the sterol regulatory-element binding protein-2 (SREBP-2), which favors cholesterol synthesis and uptake when unbound [56, 71].

The potential role of oxysterols in non-alcoholic fatty liver disease

Oxysterols are lipid intermediates often associated with lipotoxicity related to metabolic syndrome, insulin resistance, and type 2 diabetes and have a suspected relationship to NAFLD disease progression [31].

Research suggests that oxysterol binding to LXR activates the gene sterol regulatory element binding protein-1c (SREBP-1c), which further initiates the synthesis of fatty acids inside the liver, as shown in **Figure 5** [72, 73]. The same mechanism has been discovered in NAFLD patients, suggesting that oxysterols play a role in the disease and may be potential biomarkers. Raselli *et al.* showed that patients and mice with NAFLD had increased levels of 24S-OHC and 22R-OHC, respectively, supporting the hypothesis of oxysterols as biomarkers for NAFLD [32]. Additionally, Ikegami *et al.* discovered upregulated levels of the LXR activators 25- and 27-OHC in NAFLD patients compared to controls [72]. Contrary to Raselli *et al.*, who determined the levels of free oxysterols (non-conjugated), Ikegami *et al.* determined the total levels of oxysterols (the sum of conjugated and non-conjugated oxysterols) as they performed a hydrolysis step before derivatization.

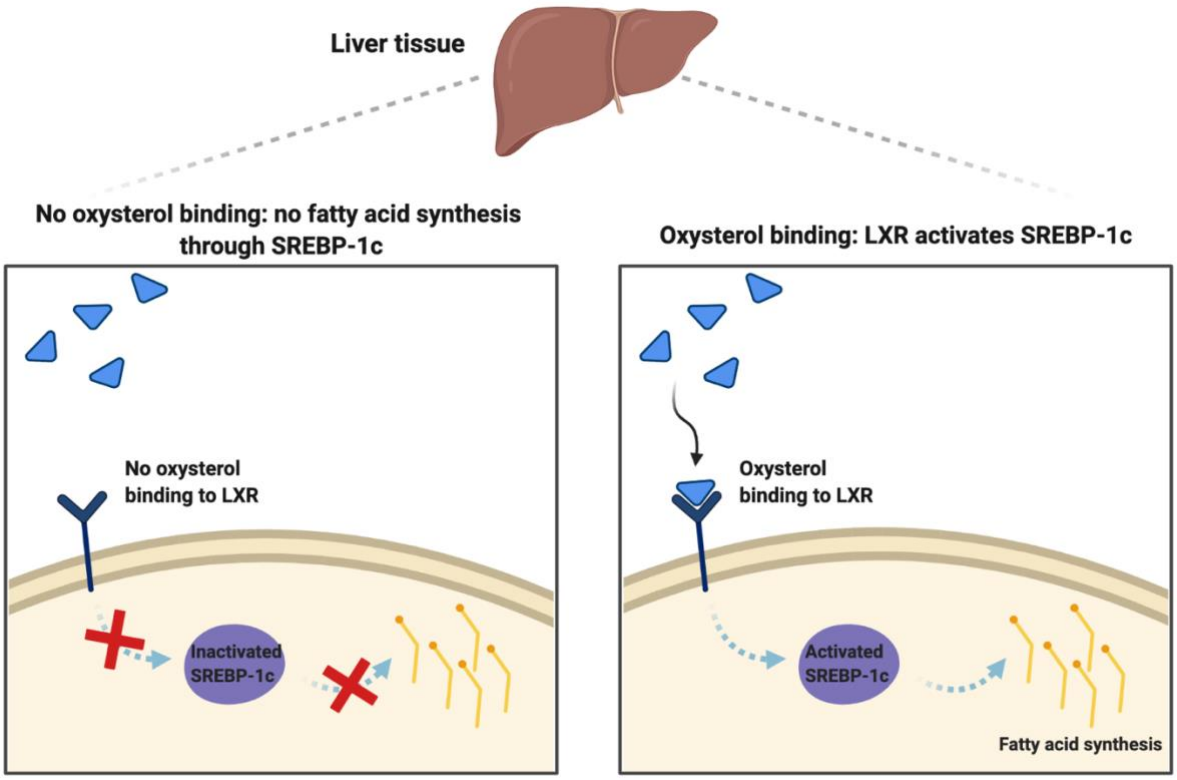

Figure 5. The role of oxysterols binding to the LXR. LXR-binding of oxysterols activates the target gene SREBP-1c synthesizing fatty acids in the liver. The blue triangles illustrate the oxysterols. Adapted from "Insulin Mechanism" by BioRender (2021) [27].

1.3 Determination of oxysterols

Quantification of oxysterols can be performed with both traditional and less explored techniques. Gas chromatography (GC) and liquid chromatography (LC) coupled with mass spectrometry (MS) (GC-MS and LC-MS, respectively) are the most established methods, with GC-MS superior for sterol separation and detection in the last 50 years [74]. GC-MS methods offer satisfactory analysis times (3.5 – 20 min), combined with excellent separation and resolution. However, sample preparation is laborious, including several derivatization steps, commonly by cleavage of conjugates and the addition of trimethylsilyl (TMS) to enhance oxysterol volatility, followed by solid phase extraction (SPE) [75-77]. The cleavage of oxysterol conjugates is a disadvantage for the GC-MS approach. Cleavage by, for example, hydrolysis (for esterified oxysterols) or solvolysis (for the sulfonated oxysterols) limits the method to detection of total levels of oxysterols (both non-conjugated and conjugated oxysterols), as the conjugated oxysterols are made indistinguishable from the free oxysterols in the derivatization step [67]. For this reason, quantification of oxysterols using LC-MS is an emerging field.

Quantification of oxysterols with LC-MS can be performed both with [78] and without [79] derivatization. Derivatization is, however, often favored due to the increased MS-detection sensitivity. Different derivatization reagents used will be discussed in **chapter 1.3.1**. With LC-MS, the levels of free oxysterols can be quantified if the hydrolysis step is omitted [80, 81], allowing determination of both total and free levels of oxysterols and the level of conjugated oxysterols can be calculated. More details on LC and MS are discussed in **chapters 1.5** and **1.4**, respectively.

1.3.1 Derivatization reagents for increased method sensitivity

LC-MS depends on an ionization interface, like electrospray ionization (ESI), to bring analytes from an aqueous state in the LC to a charged gaseous state for MS detection. Due to the neutral origin of oxysterols, they are non-ionizable; hence using ESI results in poor analytical sensitivity [82]. Derivatization of the oxysterols solves this problem by introducing an ionized or ionizable group to enhance method sensitivity. Derivatization reagents commonly used are N,N-dimethylglycine (DMG) [83, 84], picolinyl acid [85] and Girard P and Girard T [78, 86-88]. While DMG is mostly used in the context of Niemann Picks syndrome, Girard P and T are used in neurologic studies, metabolic diseases, and cancer [74]. However, it is possible to

quantify oxysterols by LC-MS without the derivatization step, as proven by McDonald *et al.* They exploited the formation of ammonium adducts of the oxysterols in the MS (ammonium acetate added in the MP) [79]. Omitting the derivatization step has nevertheless shown to be challenging as adducts are not always formed. Additionally, in nLC, the system may suffer from extreme carry-over of the underivatized oxysterols [89].

Derivatization with Girard P or T-reagent is an enzyme-assisted derivatization for steroid analysis (EADSA) developed by Griffiths *et al.* [90]. Derivatization with the Girard T-reagent charge-tags the oxysterols by adding a positive quaternary nitrogen group to the carbonyl group on the ring structure of the oxysterols after the enzyme-assisted oxidation by, e.g., cholesterol oxidase (**Figure 6**) [68]. The enzymatic oxidation takes about one hour (37 °C), while the Girard T reaction needs to take place overnight (in the dark at room temperature) [91, 92]. The time-consuming aspect of this derivatization technique is a major drawback regarding method efficiency [78].

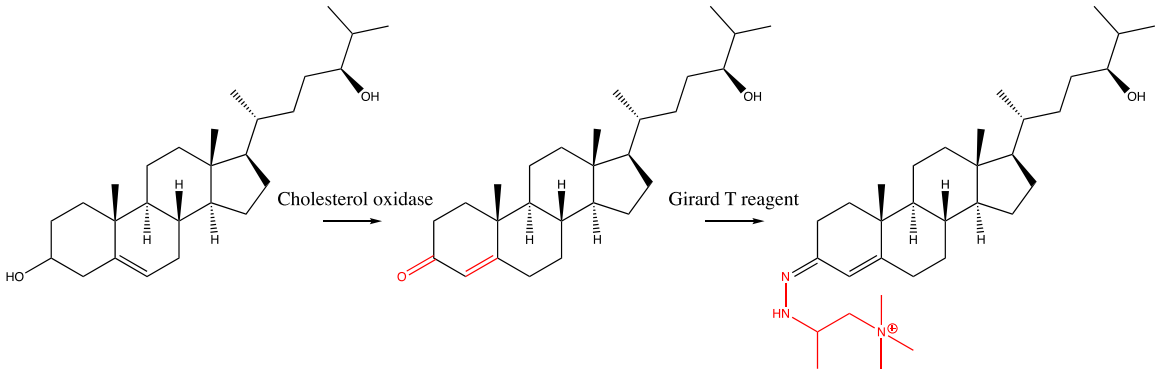

Figure 6. The oxysterol derivatization process of 24-OHC. First, the enzyme cholesterol oxidase oxidizes the 3β-hydroxy-5-ene structure (hydroxyl group on the ring structure) into derivatives of 3-oxo-4-ene (the carbonyl group on the ring structure) before the Girard T reaction, where the Girard T reagent reacts with the 3-oxo group to form the Girard T derivatives of the oxysterols. The changes in the structures are shown in red. The chemical structures were adapted from [78].

1.3.2 Oxysterol isomer separation and selectivity

The oxysterols of interest for this thesis (22R-OHC, 24S-OHC, 25-OHC, and 27-OHC) are isomers, meaning they have identical mass but different molecular structures. The isomers have identical fragmentation patterns in MS/MS and are impossible to distinguish with MS/MS only.

Therefore, the separation of the isomers is solely based on chromatographic separation, highlighting the importance of a well-performing column with a suitable stationary phase (SP) for good selectivity and separation. Chromatographic separation of the oxysterol isomers is also known to be challenging [81]. The selectivity of oxysterol separation is further discussed in **chapter 1.5.1**.

1.3.3 Oxysterol abundance in biological systems

As the abundance of oxysterols in biological systems is very low (e.g., ng/mL range in plasma [68, 80]), they can be challenging to detect with the presence of a high cholesterol background (e.g., mg/mL range in plasma [80, 93]). Therefore, there is a high demand for sufficient sensitivity in oxysterol quantification in biological samples [67]. Additionally, oxysterol-containing samples are often valuable biological samples, such as plasma, tumor, or tissue samples, and sample amount may be limited, arising the need for the LC system to provide high sensitivity due to small sample volume consumption [94].

In addition to derivatization sensitivity enhancement, sensitivity can be enhanced by sample enrichment by large volume injection or employment of miniaturized LC systems (10-100 μm ID columns). Large volume injection allows higher amounts of analytes to be transferred onto the analytical column (further discussed in **chapter 1.5.4**) [94, 95]. Miniaturized LC systems like nLC systems ensure less radial dilution of the samples in the column, introducing more concentrated eluting bands to the detector (further discussed in **chapter 1.5.5**) [96].

1.3.4 Autoxidation

When preparing biological samples containing oxysterols, cholesterol (precursor) autoxidizing is possible when the sample is subjected to air, light, or elevated temperatures, leading to *ex vivo* oxidized cholesterol to mix with endogenous oxysterol [67]. *Ex vivo* autoxidation is hence, a serious issue leading to misinterpretation of endogenous oxysterol-levels [81]. Monitoring autoxidation by adding heavy cholesterol (^{13}C-isotope or deuterated) to the sample can account for this problem to keep track of the possible cholesterol autoxidation. To avoid autoxidation during sample preparation, it is essential to perform all drying steps in an inert atmosphere, such as in a vacuum or by purging with inert gases like nitrogen or argon [67].

1.4 Mass spectrometry

MS is a powerful technique able to provide both quantitative (mass or concentration) and qualitative (structure) information about compounds of interest based on their mass to charge ratios (*m/z*) [97]. MS has a wide application range and is widely employed in chemistry, bioscience, toxicology, environmental sciences, and pharmacy. Both excellent selectivity and sensitivity are important features delivered by MS instruments. As mass is a highly specific property of a molecule, MS provides minor interferences in high-resolution MS. When operated in multiple reaction monitoring (MRM) mode, where ion masses of interest are isolated, additional selectivity is expected. The most sensitive MS instruments have detection limits in the attomole range [78, 98, 99].

1.4.1 Electrospray ionization

As previously mentioned, MS analysis is limited to the detection of ions in the gaseous phase. The LC-MS interface, therefore, includes an ionization source, where the analytes become positive or negative gaseous ions [97]. ESI is amongst the most employed ionization sources. It is an old technique first described by Geoffrey Taylor in 1964 [100] and was first successfully developed experimentally for MS by John Fenn and colleagues in the mid-1980s [101, 102], who was also awarded the Nobel Prize in Chemistry in 2002 for the work with ESI. As ESI ionizes molecules directly from the liquid phase, it is highly compatible with LC [103].

ESI can be run in both positive and negative ion mode, depending on whether the analytes are positively or negatively charged, respectively. In positive ion mode, the sample is preferably sprayed at lower pH so that proton donors are available in the mobile phase (MP) to enhance analyte protonation. A higher pH in the MP with proton acceptors available to enhance deprotonation is recommended in negative mode. Volatile MPs and buffers must be used in ESI-MS as they must be capable of evaporating. ESI holds no molecular mass limitations, which is a great advantage when analyzing larger molecules like protein complexes [103]. Additionally, ESI delivers excellent ionization efficiency, making it suitable for trace analysis [103].

Electrospray ionization theory

The mechanism for ESI is illustrated in **Figure 7.** The electrospray process itself arises from a physical phenomenon called the Taylor cone. A Taylor cone occurs in a liquid when the liquid is in a nozzle, and an electric field is applied at atmospheric pressure. The liquid will initially form an elliptic shape due to an equilibrium between two forces – surface tension and electrostatic forces [103]. The surface tension pulls the liquid back into the nozzle to minimize the energetically unfavorable surface area, while the electrostatic forces pull the liquid out of the nozzle towards the counter electrode. When the voltage exceeds a threshold value where the two forces are in balance, the elliptic shape will change into a conic shape (the Taylor cone) due to dominating electrostatic forces, and a spray is dispersed [103, 104]. For ESI, the electric field is applied across the emitter and the MS inlet, usually at a potential of 1-6 kV, pulling the positive ions towards the MS inlet, and the negative ions are held back (in positive ion mode). The emitted droplets have a diameter of more than 1 μm [104].

The Rayleigh stability criterion limits the electrostatic forces to an equilibrium with the surface tension. The droplets emitted have a surface charge density, and solvent evaporation starts instantly. Evaporation is ensured by adding a heated inert gas (often N_2) co-axially with the emitter as nebulizing gas due to large flow volume. Aided evaporation will leave smaller droplets with a higher surface-charge density as the volume is decreased and the charge is kept constant. As the surface charge density increases, repulsion of the same charges will create a new Taylor cone inside the small droplet. The Rayleigh limit is exceeded (the electrostatic forces prevail the surface tension), which leads to the ejection of even smaller, highly charged droplets (about 200 nm diameter or less). This process repeats until only dispersed charged gaseous analytes are left and drawn into the counter electrode (MS inlet) [103].

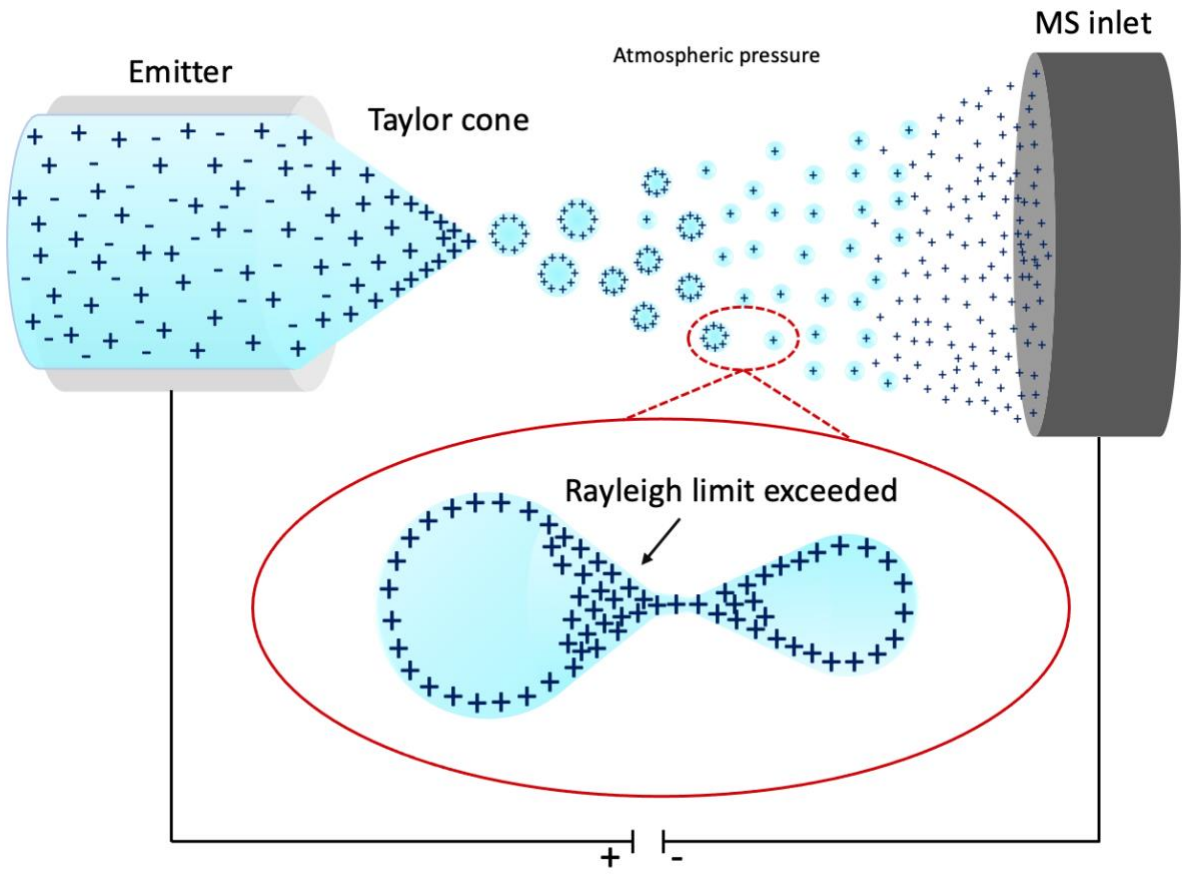

Figure 7. ESI in positive ion mode where the Taylor cone forms and emits larger droplets evaporating into smaller ones. The analytes end up as single gaseous ions due to the applied electric field across the pathway from the emitter to the MS inlet. The exceeding of the Rayleigh limit is also illustrated, in which smaller droplets are formed as the electrostatic forces dominate the surface tension of the droplet. The illustration was adapted from [97].

Nano-electrospray ionization

The nano-electrospray ionization (nESI) process is similar to that of ESI, but with a lower flow (nL/min scale). Due to the lower flow, there is no need for a nebulizing gas. Wilm *et al.* derived an equation relating the flow rate to the emission diameter of the tip of the Taylor cone [104]. The emission region of the tip of the Taylor cone will be smaller with a small flow rate. Hence, lower flow rates generate smaller primary droplets. Therefore, with nESI, the primary droplets can be as small as the smallest final droplets of ESI (200 nm diameter) [104]. This makes the nESI more sensitive than ESI as the ionization is more efficient due to the easier desorption of the analytes from the smaller droplets. Hence, more ions reach the MS inlet. Wilm *et al.* also describe the ion jet as shorter with nESI than with ESI, allowing the emitter to be set closer to the MS inlet, enhancing the sensitivity further [104]. The low flow in nESI is highly compatible with nLC.

1.4.2 Triple quadrupole mass analyzer

After the analytes are ionized and in the gas phase, the ions migrate into the mass analyzer inside the MS. The mass analyzer is where the ions are separated based on their *m/z*. Several mass analyzers exist (e.g., quadrupole, ion trap, orbitrap, Fourier-transform ion cyclotron resonance (FT-ICR), time-of-flight (TOF), and magnetic sector), but as the triple quadrupole was used in this thesis, only this will be discussed here.

The triple quadrupole MS (TQMS) is a tandem MS consisting of three compartments, often denoted Q1, q2, and Q3, each with four circular or hyperbolic rods [105]. Q1 and Q3 are mass analyzers, while q2 is a collision cell pressurized with an inert gas like N_2 or Ar to fragment the ions. A typical TQMS is illustrated in **Figure 8**. Five scan modes are available; full scan, precursor ion scan, product ion scan, neutral loss scan, and selected reaction monitoring (SRM), also called multiple reaction monitoring (MRM) [106]. The latter will be discussed in more detail below.

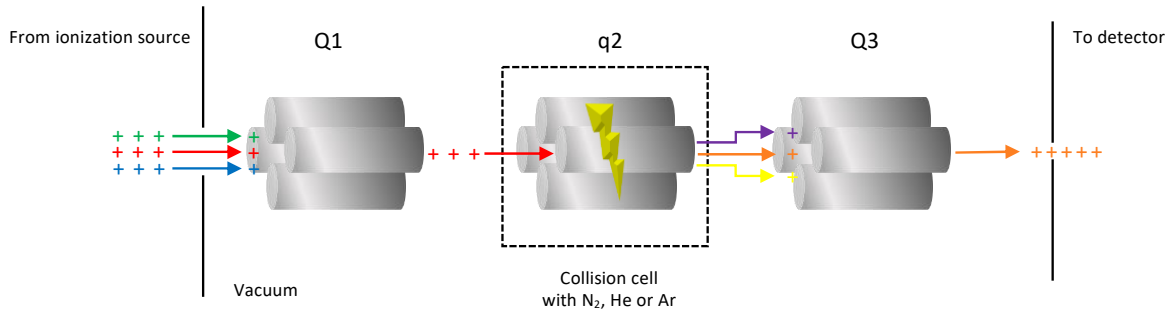

Figure 8. TQMS in SRM mode where one single ion is selected from Q1, fragmented in q2, and only one fragment ion is filtered through in Q3 and allowed to reach the detector. The illustration is adapted from [97].

Mass separation in Q1 and Q3 is achieved when applying a direct current (DC) voltage (U) and a radio frequency (RF) voltage (V) on the two rods contrary to each other. The U and V can be altered to ensure stable trajectories (ions not touching the rods) of the ions with the *m/z* values of interest. The other ions are eliminated when touching the rods and become neutralized [105]. The q2 cell is operated in an RF-only mode to allow stable trajectories of all entering ions.

Multiple reaction monitoring for increased selectivity

In MRM mode, Q1 and Q3 work as mass filters, where Q1 only filters through the selected precursor *m/z* of interest, q2 fragments the ions by the inert collision gas, and Q3 filters through the selected *m/z* fragments. The fragment giving rise to the highest signal is commonly used as the quantifier ion, and the fragment giving the second-highest signal is often used as a qualifier ion to confirm the presence of the analyte. The entire mass analyzer compartment is in a vacuum to ensure a free pathway for the migration of the ions, avoiding collision with other atmospheric gases. The MRM fragmentation pattern for derivatized 27-OHC is illustrated in **Figure 9**.

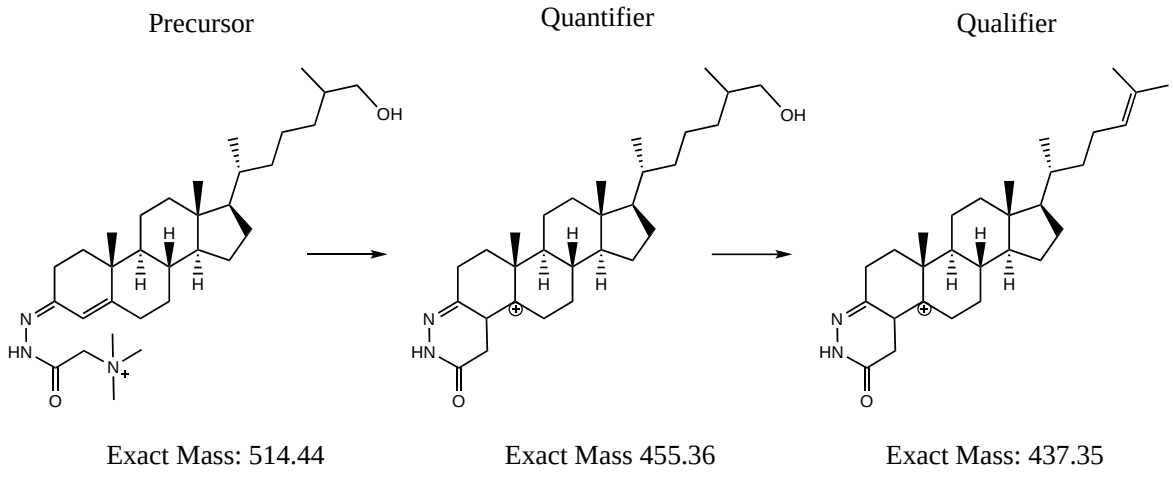

Figure 9. The fragmentation pattern of derivatized 27-OHC resulting in the quantifier- and qualifier-ions with *m/z* of 455.36 and 437.35, respectively. 22R-, 24S, and 25-OHC have identical fragment patterns [78, 88].

1.5 Liquid chromatography

Prior to detection with MS, separation of the oxysterol isomers is necessary. LC is a separation method used to separate molecules based on various separation principles [107]. The separation principles are based on the hydrophobicity, hydrophilicity, charge, and the size of the analytes. The most common separation principle is reversed phase (RP), suitable for analyte molecules with some hydrophobic segment. The SP in RP chromatography normally consists of fully porous silica particles with C18 alkyl chains attached to them (**Figure 10**). The MP consists of water, an organic modifier, and an acid or buffer for pH control.

1.5.1 Oxysterol selectivity: Reversed phase liquid chromatography

As side-chain oxysterols are neutral lipids, their structure is overall very hydrophobic (logP = ~7). Hence, the sterols are suited for RPLC, and a relatively high concentration of organic modifier is needed to elute them from the column.

In oxysterol quantification, RPLC with a C18 SP is the most common SP employed [63]. However, other SPs have been shown to provide better selectivity. Pataj *et al.* investigated a biphenyl SP and achieved baseline separation ($R_S \geq 1.5$) of 6 oxysterols, including 24S-, 25-, and 27-OHC, within 8 min [83]. Solheim *et al.* obtained baseline separation of 22R-, 24S-, 25-, and 27-OHC within 8 min with a core-shell phenyl-hexyl (PH) SP (**Figure 10B**) [92]. Compared to C18, the phenyl-based SPs offer π-π interactions in addition to hydrophobic interactions, giving increased selectivity for, e.g., aromatic compounds.

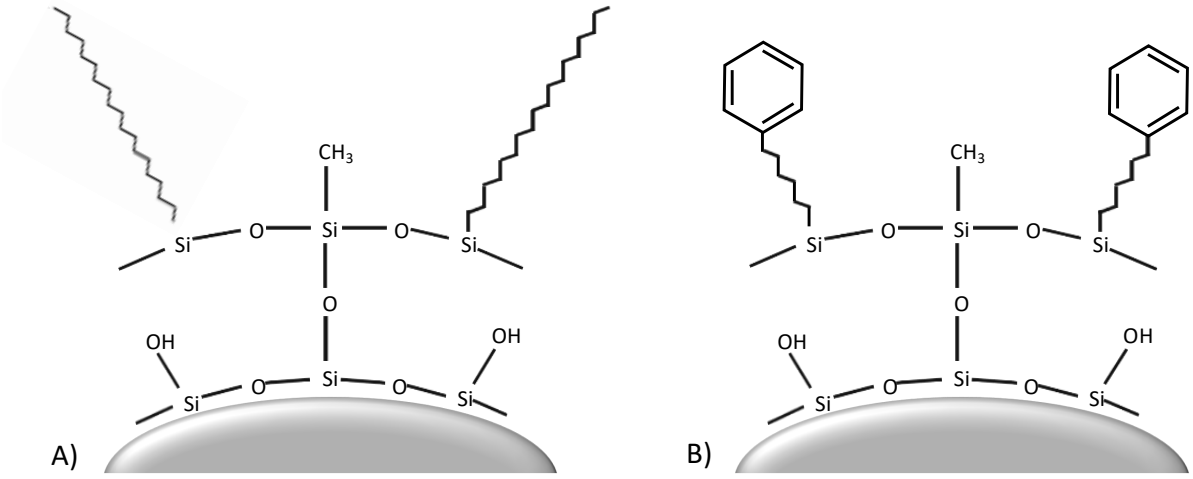

Figure 10. The SPs A) C18 (octadecyl) and B) PH (phenyl group attached to the hexyl chain). The illustration is adapted from [107].

1.5.2 Column performance

An important characteristic for evaluating column performance is the efficiency, expressed by the plate number N [107]. The number of plates was first described by Martin and Synge [108] and indicates the degree of band broadening in the column. The plate number is a theoretical value where each plate represents the equilibrium of the analyte between the MP and the SP; the more equilibria throughout a column, the sharper the peaks, and the better efficiency of the column [108]. The plate number is expressed by **equation 1**.

$$N = 16\left(\frac{t_R}{w_b}\right)^2 \qquad (eq.\,1)$$

Here t_R is the retention time of the analyte, and w_b is the peak width at the baseline. The equation parameters are illustrated in **Figure 11A**. If the peak is fronting, tailing, or partially separated, the peak width at half height can be used instead, as expressed in **equation 2**.

$$N = 5.54\left(\frac{t_R}{w_{0.5}}\right)^2 \qquad (eq.\,2)$$

Here t_R is the retention time of the analyte, and $w_{0.5}$ is the peak width at half height. The equation parameters are illustrated in **Figure 11A**.

According to the U.S. Food and Drug Administration's (FDA) "Validation of chromatographic methods", the number of plates should be > 2000 for conventional HPLC columns [109]. However, a well-packed HPLC column could have plate numbers as high as 20 000, also depending on the particle size.

However, very few chromatographic peaks are perfect Gaussian shapes. Most peaks are asymmetric due to secondary interactions, external column volume, and poor column packing. Peak asymmetry can be expressed by the asymmetry factor, A_s, expressed by **equation 3**.

$$A_s = \frac{b}{a} \qquad (eq.\,3)$$

Here a is the width left of half the vertical peak, and b the width right of half the vertical peak at 10% peak height. The equation parameters are illustrated in **Figure 11B**. Ideally, $A_S = 1$, then the peak has a perfectly symmetric Gaussian shape. If $A_S > 1$, the peak is tailing, and if $A_S < 1$, the peak is fronting. $A_S < 2$ is considered acceptable in conventional HPLC.

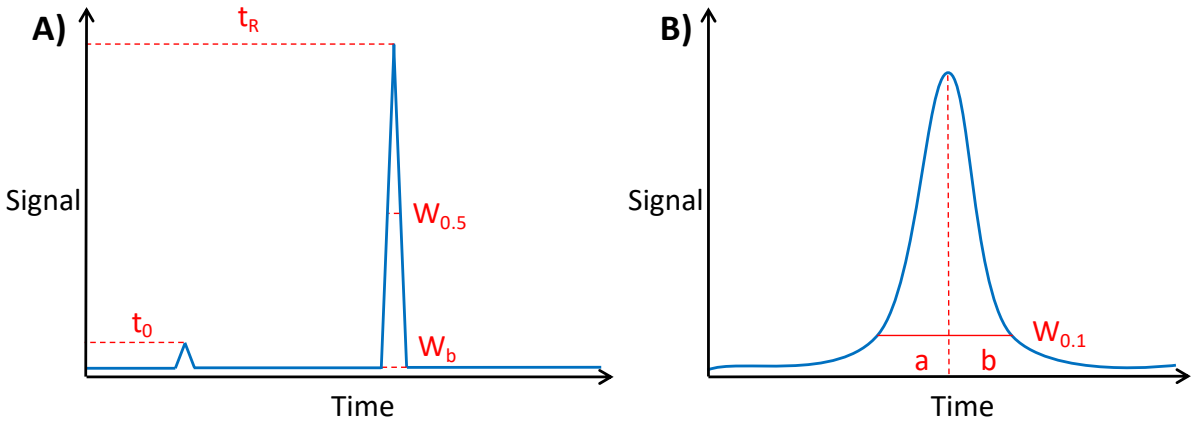

Figure 11. How the parameters A) t_M, t_R, w_b, and $w_{0.5}$ are extracted from a chromatogram to calculate the plate number and retention factor, and B) a and b is extracted at the peak width at 10% of the peak height to calculate the asymmetry of the peak.

The retention factor, k, expresses the time the analyte interacts with the SP compared to the time spent in the MP and is used to assess the repeatability of the columns. The retention factor is expressed by **equation 4**.

$$k = \frac{(t_R - t_M)}{t_M} \qquad (eq.\,4)$$

Here t_R is the retention time of the analyte, and t_M is the retention time of an unretained compound, like, e.g., uracil or thiourea on an RP SP.

As the retention of the analytes often is compared to those of standards, the retention factor is important to be repeatable between sample replicates within a column and between columns. The retention factor is also relevant when selecting a suitable trap column, since the trap column must provide a lower k than the analytical column to prevent additional band broadening. The retention factor is independent of flow rate and column dimensions [107]. **Figure 11A** illustrates how the parameters are extracted from the chromatogram.

1.5.3 Increased efficiency: smaller particles and core-shell silica particles

By reducing the column contributions to band broadening, the column efficiency increases. The band broadening is commonly expressed by the van Deemter equation (**equation 5**).

$$H = A + \frac{B}{u} + C * u \qquad (eq. 5)$$

Here H is the plate height, A represents the eddy dispersion, B the longitudinal diffusion, and C the resistance to mass transfer. The lower the plate height, the better the column efficiency. More details about band broadening within the column can be found in **chapter 7.1.2** in **Appendix**.

One way of enhancing the column efficiency is to decrease the particle size [110], reflected in a decrease of the eddy dispersion in the van Deemter equation. A reduction in particle size, however, result in higher backpressures compared to larger particles. Therefore, pumps and equipment suitable for handling the high pressures are needed, which can be a technical challenge [111, 112]. The instrumentation used for columns packed with small particles (typically sub-2 μm) is called ultra-high-performance liquid chromatography (UHPLC). Typical UHPLC pressure is up to 1400 bar [113].

The construction of the SP particle also plays a role in column efficiency. Fully porous particles (FPP) are the most common particle type used in HPLC today (**Figure 12A**). Core-shell particles, however, have gained popularity offering highly efficient separations at fast flow rates with relatively low backpressures [114]. Core-shell particles have a solid core surrounded by a porous shell and are illustrated in **Figure 12B**. A 2.7 μm core-shell particle with a 1.7 μm core and 0.5 μm porous shell could provide the same efficiency as a sub-2 μm fully porous particle with a backpressure close to that of a 3 μm fully porous particle [115]. The benefits with a solid core are many regarding decreased contributions to band broadening due to decreased eddy dispersion, longitudinal diffusion, and to some extent, resistance to mass transfer [116].

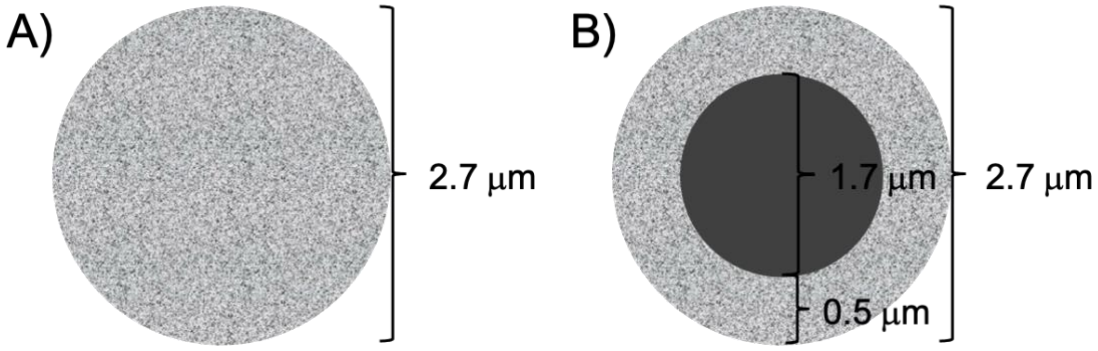

Figure 12. The intersection of A) an FPP and B) a core-shell silica particle with a porous shell surrounding the solid core, with examples of particle dimensions.

There will be a smaller number of pores with core-shell particles due to the solid core, which will decrease the amount of eddy dispersion due to shorter diffusion paths [117]. Core-shell particles may also deliver a more narrow particle size distribution than FPP (RSD of 5% vs. 15-20%), reducing eddy dispersion further [118]. Gritti *et al.* showed that the average linear velocity could be 10% faster near the wall compared to the denser bulk region of FPPs [119]. Predictions indicate that this phenomenon can be less significant for core-shell particles as they may provide a more dense wall region and, in general, have a more homogenously packed bed [116]. Radial heterogeneity in packing density can lead to significant contributions to eddy dispersion; in fact, about 70% of the band broadening contributions in UHPLC columns [116, 120].

Numerous and large pores will contribute to longitudinal diffusion. Again, since core-shell particles consist of less pore volumes than FPPs, less longitudinal diffusion may occur [115]. Packing density also plays a role here. The lower the packing density of the column, the larger the contribution from longitudinal diffusion since larger pore volumes between particles are available for the MP and analytes to diffuse into [116].

Reduction of resistance to mass transfer is also seen with core-shell particles. However, resistance to mass transfer is not the dominant cause of band broadening in HPLC in general. Guiochon and Gritti have shown that only modest gains are made in efficiency by reducing resistance to mass transfer with core-shell particles [121].

For the separation of the oxysterol isomers 22S-, 24R-, 25-, and 27-OHC, a column providing limited peak broadening is especially important as few differences in chemical properties produce closely eluting peaks.

1.5.4 On-line sample clean-up and preparation

In bioanalysis, attractive parameters to optimize are sensitivity and selectivity to enable the detection of low abundant analytes in complex biological samples [94]. The automatic filtration and filter backflushing (AFFL) system combined with a trap column is an on-line sample clean-up and preparation technique that enhances sensitivity, selectivity, and robustness of the chromatographic platform. The AFFL-system was first described by Svendsen *et al.* in 2011 [95] and included two pumps, a 10-port-2-position switching valve, and a filter (**Figure 13**). The sample is first loaded onto the system by the MP by pump 1 and through a filter that removes particulate matter. Next, the sample is introduced onto the trap column where the analytes are trapped, while the rest of the sample matrix and reagents are led to waste. When the 10-port valve is switched, the filter is backflushed, eluting the debris particles to waste. Simultaneously, the analytes from the trap column get eluted onto the analytical column. For an RP SP, it is favorable to load the sample onto the trap column with an aqueous MP to maximize the trapping of the analytes, hence avoid loss of the analytes during loading.

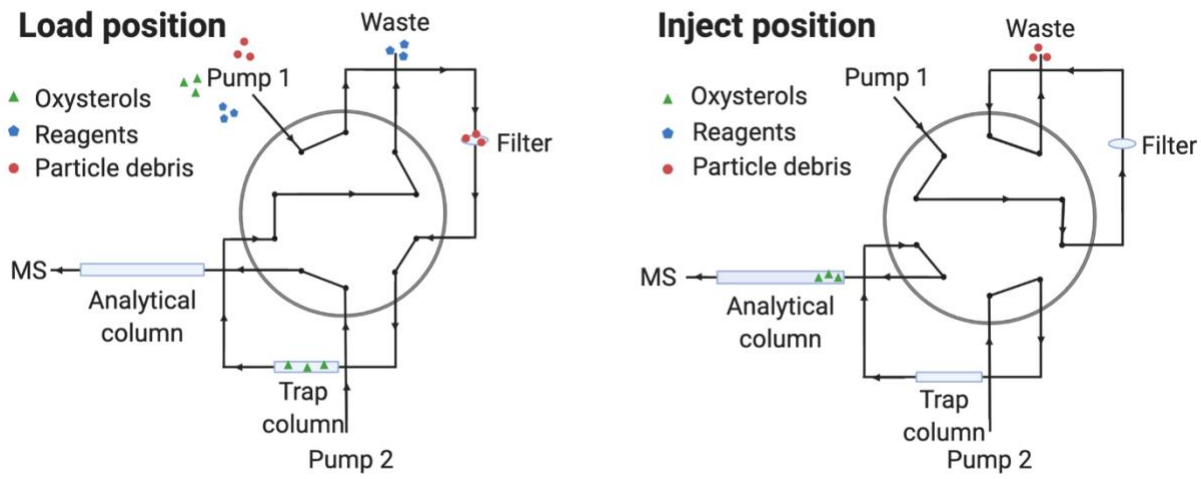

Figure 13. An AFFL-set-up combined with a trap column. The 10-port-2-position switching valve with the trap column and filter in both load and inject position. The filter is backflushed in inject-position to remove particle debris for easy sample clean-up. The illustration is adapted from [78].

The AFFL-system combined with a trap column enhances selectivity due to the isolation of the analytes on the trap column. Additionally, the robustness is enhanced due to less backpressure build-up since unwanted particles are removed by the filter between each injection. It is required

that the trap column contains an SP with less retention (smaller k) of the analytes compared to that of the analytical column. Less retention is important to ensure refocusing of the analytes on the analytical column, minimizing band broadening and peak tailing [94].

The AFFL-system combined with a trap column contributes to enhanced sensitivity by allowing large volume injection. Large volume injection increases the total number of analytes loaded onto the narrow analytical column, as the matrix is flushed to waste during loading [95]. Removal of reagents from derivatization is especially important before MS detection to keep ion suppression from the reagents at a minimum. Bioanalysis often contains a high number of samples, calling for high sample throughput. The automated AFFL-system allows high sample throughput by reducing the time consumption compared to off-line sample purification and preparation and by increasing the robustness of the platform.

1.5.5 Nano liquid chromatography enhances sensitivity

Nano liquid chromatography (nLC) enhances the sensitivity of the chromatographic platform. In nLC, the inner diameter of the LC column is downscaled, thereby increasing the sensitivity of the chromatographic system when using a concentration-sensitive detector such as ESI-MS [96]. A narrower column reduces the radial dilution of the analytes in the column, allowing more concentrated bands of the analytes to reach the detector, creating higher intensity signals, as illustrated in **Figure 14.** Radial dilution can be expressed by the dilution factor, D (**equation 6**) [122],

$$D = \frac{c_0}{c_{max}} = \frac{\varepsilon \pi r^2 (1 + k)\sqrt{2\pi LH}}{V_{inj}} \qquad (eq.\,6)$$

where c_0 is the analyte concentration in the sample, c_{max} is the analyte concentration at the detector, ε is the particle porosity, r is the radius of the inner diameter of the column, k is the retention factor, L is the column length, H is the plate height, and V_{inj} is the injection volume [107]. Hence, radial dilution is proportional to the square of the radius of the column, and miniaturization of the column ID allows more concentrated bands to reach the detector.

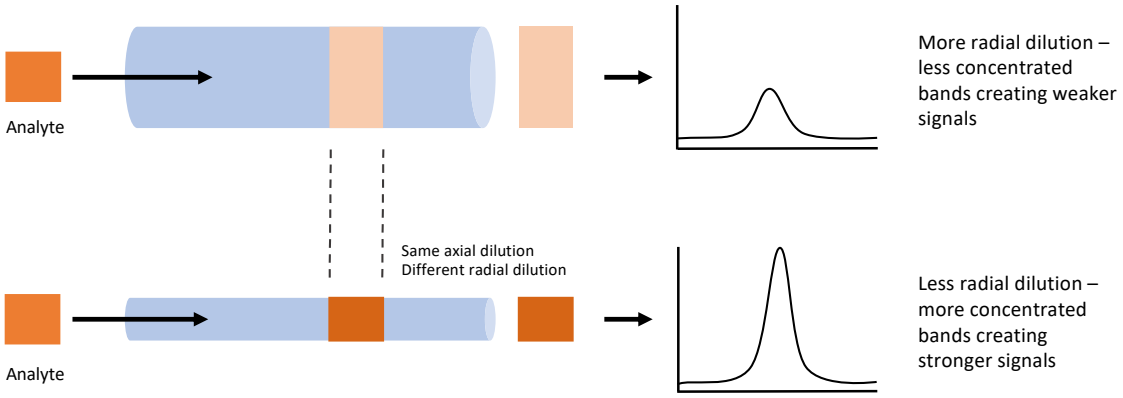

Figure 14. The effect of downscaling the inner diameter of a larger LC column (upper) to a narrower LC column (lower). The color intensity (orange) represents the concentration of the analyte. The illustration was adapted from [96].

The effect of downscaling on method sensitivity may be demonstrated by the downscaling factor, f, for columns with equal lengths and is expressed by **equation 7**.

$$f = \frac{r^2_{\text{large ID}}}{r^2_{\text{small ID}}} = \frac{D^2_{\text{large ID}}}{D^2_{\text{small ID}}} \qquad \text{(eq. 7)}$$

Here $r^2_{\text{large ID}}$ is the radius of the column with the larger ID, and $r^2_{\text{small ID}}$ is the radius of the column with the smaller ID. If a column is downscaled from 2.1 mm ID to 0.075 mm ID, the downscaling factor will be 784, hence, in theory, giving rise to a 784-fold increase in signal intensity when the same number of analytes are injected [123]. This enables trace-level detection of analytes in a sample of limited amount, such as oxysterols, which is a great advantage of using nLC compared to conventional LC [96]. The downscaling factor can be applied to all system parameters, including the flow rate and injection volume [124]. nLC also offers lower solvent consumption by lower MP flow rates (nL/min scale) which is economically and environmentally advantageous [96]. Downscaling to nLC columns also limits the injection volume. However, large volume injections can account for this by inserting a trap column in front of the analytical column [96].

Applying nLC in oxysterol determination is not well investigated. However, Røberg-Larsen *et al.* detected 24S-, 25-, and 27-OHC in the attomole range by connecting an AFFL-system and a trap column to a 100 μm ID column [78]. Vehus *et al*. detected oxysterols down to a zeptomole range using open tubular (OT) columns with 10 μm ID [125].

Although the sensitivity can be greatly enhanced operating at downscaled formats, some complications may occur. As all aspects of the chromatographic system are miniaturized, including tubings and connections, advanced technical experience is required to avoid extra-column volumes due to inadequate connections [96, 122]. Extra-column volumes in nLC could be detrimental as even marginal volumes have major effects on band broadening [111, 126]. Additionally, nLC columns are typically packed in fused silica capillaries requiring delicate handling and knowledge of the correct connections to be used, and coupling of these can be laborious. In general, a downscaled platform is more demanding to handle than a conventional LC platform.

Combining UHPLC- and core-shell particles with nLC

A great effort has been made to miniaturize LC, but not much effort has been made to miniaturize UHPLC [127]. UHPLC is found to perform better in miniaturized LC than in conventional LC, as issues regarding frictional heating within the column are reduced due to faster dissipation of the heat [96, 110, 128]. Frictional heating is induced when friction between the MP and the SP particles generates heat (due to the high flow rate and small SP particles). The friction results in radial and axial temperature gradients in the column, which can damage the separation power of the column [113, 129, 130]. On the other hand, the packing of core-shell particles in miniaturized LC has proven to be challenging [121, 126] as larger voids in the packed bed have been observed (especially at higher slurry concentrations), increasing the contributions to band broadening [131].

2 Aim of study

Simple and less invasive diagnostic tools for NAFLD are currently lacking. Hence, it is desired to discover biomarkers for the disease, and oxysterols are proposed as potential candidates. Liver organoids are a promising research model used for disease modeling and may provide enhanced recapitulation of the human *in vivo* NAFLD development. A highly sensitive analytical method for oxysterol quantification, in addition to an on-line sample clean-up and preparation, is needed to enable detection of the low abundant oxysterols in the small liver organoids (typically 1500-2000 cells per organoid). nLC columns can increase method sensitivity combined with a trap column for large volume injection.

The aim of this study was to investigate if an nUHPLC-MS platform using core-shell particles in in-house packed fused silica capillaries, combined with an on-line sample clean up in the form of an AFFL-system and a trap column (with a suitable SP), was suitable towards highly sensitive, efficient, and robust quantification of 22R-, 24S-, 25-, and 27-OHC in liver organoids. The developed method was to be used to investigate suitability for NAFLD biomarker detection. ***Figure 15*** *gives a visual illustration.*

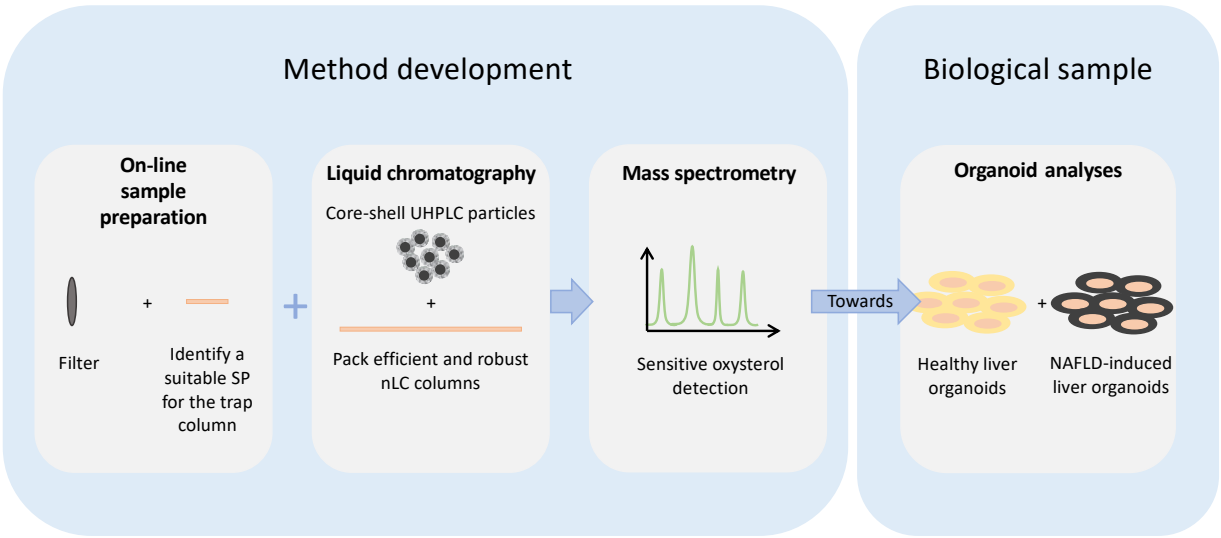

Figure 15. An overview of the aim of study.

3 Experimental

3.1 Chemicals

Acetonitrile (ACN, LC-MS grade), methanol (MeOH, LC-MS grade), HPLC-MS grade water, sodium hydroxide (NaOH), toluene (RG2025), and thiourea ≥ 99.0% (88810-100G) were purchased from VWR (Radnor, PA, USA). Isopropanol (LC-MS grade), formic acid (FA, HPLC-grade, 98%, and LiChropur LC-MS grade, ≥ 98%), Girard T reagent (99%), KH_2PO_4, acetic acid (glacial, 100%), 22R-OHC, 25-OHC, cholesterol-25,26,27-^{13}C (99%), and cholesterol oxidase from *Streptomyces* sp. were purchased from Sigma-Aldrich (Saint-Louis, MO, USA). The type 1 water was from a Milli-Q® Integral purification system from Merck Millipore (Burlington, MA, USA). The frit kit consisting of formamide and Kasil 1624 (potassium silicate/water 24/76 %) was from Next Advance (Troy, NY, USA). 24S-OHC, 27-OHC, 22R-OHC-d_7, 25-OHC-d_6, and 27-OHC-d_6 were purchased from Avanti Polar Lipids (Alabaster, AL, USA).

3.2 Columns and particles

The columns and particles used in this study are summarized in **Table 1**.

Table 1. The columns and particles used in this study. The particles used for in-house packed columns were collected from commercial columns and repacked in capillaries. The commercial columns were used as-is.

Producer	Name	Particles	Size	Dimensions	Serial no./part no.	Pore
Particles collected from columns for in-house packing						
ACE (Aberdeen, Scotland)	Ultracore	Super phenyl-hexyl	2.5 μm	150 x 2.1 mm	A174508/-	95 Å
ACE (Aberdeen, Scotland)	Ultracore	Super phenyl-hexyl	2.5 μm	150 x 2.1 mm	A226044/CORE-25B-1502U	95 Å
Phenomenex (Torrance, CA, USA)	Luna	Phenyl-hexyl	5 μm	30 x 4.6 mm	224976G/03A-4257-E0	100 Å
Commercial columns						
Septech (Ski, Norway)	HotSep Tracy	C4	5 μm	5 x 0.3 mm	-	300 Å
Septech (Ski, Norway)	HotSep Tracy	C8	5 μm	5 x 0.3 mm	-	300 Å
Septech (Ski, Norway)	HotSep Tracy	C18	5 μm	5 x 0.3 mm	-	300 Å
ACE (Aberdeen, Scotland)		C8	3 μm	150 x 0.1 mm	A133336/ACE-112-15001	100 Å

The commercial ACE Ultracore Super Phenyl-Hexyl (SPH) columns (150 x 2.1 mm ID, 2.5 μm) and the Phenomenex Luna Phenyl-Hexyl (PH) column (30 x 4.6 mm ID, 5 μm) were opened in one end, and the filter was removed. A pump pressure was exerted onto the column with a 0.25 mL/min flow rate with 100% MeOH, and the particles were collected in 1.5 mL microcentrifuge tubes (Eppendorf, Sigma Aldrich). The particles were dried using a Concentrator Plus from Eppendorf (Hamburg, Germany) and stored in the microcentrifuge tubes at room temperature.

The fused silica capillaries were from Molex (Lisle, IL, USA).

3.3 Solutions

3.3.1 Oxysterol and heavy cholesterol stock solutions

Stock solutions (100 μM) of 22R-OHC, 24S-OHC, 25-OHC, 27-OHC, 22R-OHC-d_7, 25-OHC-d_6, and 27-OHC-d_6 were prepared separately in-house by Associate Professor Hanne Røberg-Larsen in earlier studies by dissolving the received amount from the supplier in a specified volume of isopropanol. The 6 μM heavy cholesterol (cholesterol-25,26,27-^{13}C) stock solution was prepared in-house in a similar manner.

3.3.2 Oxysterol working solutions

Working solutions (WS) of the oxysterols (22R-OHC, 24S-OHC, 25-OHC, and 27-OHC) and their respective deuterated internal standards (ISs, 22R-OHC-d_7, 25-OHC-d_6, and 27-OHC-d_6) were prepared separately by diluting 100 μM stock solutions 100 000 and 66 666 times with isopropanol to 1 nM (A WS) and 1.5 nM (IS WS), respectively. The WSs were stored in the refrigerator (+ 5°C).

3.3.3 Oxysterol evaluation solutions

Evaluation solutions for the conventional UHPLC-MS platform

The evaluation solutions were prepared as summarized in **Table 2**. Additionally, 5 μL of 6 μM heavy cholesterol was added to each evaluation solution. The oxysterols were then derivatized as described in **chapter 3.4**.

Table 2. The volumes added of 1 nM A WS and 1.5 nM IS WS to achieve the various concentrations. The volumes represent the X- and Y-values in **Figure 16**.

C analyte (pM)	C IS (pM)	V A WS (μL)	V IS WS (μL)
50	200	37	100
100	200	74	100
200	200	148	100
300	200	222	100
400	200	296	100
500	200	370	100

Evaluation solutions for miniaturized LC-MS platform

The evaluation solutions were prepared as summarized in **Table 3**. Additionally, 5 µL of 6 µM heavy cholesterol was added to each evaluation solution. The oxysterols were then derivatized as described in **chapter 3.4**.

Table 3. The volumes added of 1 nM A WS and 1.5 nM IS WS to achieve the various concentrations. The volumes represent the X- and Y-values in **Figure 16**. Two different volumes and concentrations were used for the ISs.

C analyte (pM)	C IS (pM)	V A WS (µL)	V IS WS (µL)
13	50/100	10	25/50
27	50/100	20	25/50
54	50/100	40	25/50
81	50/100	60	25/50
108	50/100	80	25/50

3.3.4 Column evaluation solutions

Evaluation solution for efficiency testing of the in-house packed nLC columns

A stock solution of 1% toluene was prepared by diluting 100 µL of 100% toluene in 10 mL MeOH. A stock solution of 1 mg/mL of thiourea was prepared by diluting 25 mg thiourea to 25 mL MeOH. An evaluation solution of 0.1% toluene and 20 µg/mL thiourea was prepared by diluting 1 mL of toluene stock solution and 200 µL thiourea stock solution into 10 mL 50/43/7 H_2O/ACN/MeOH (v/v/v). The evaluation solution was stored in a refrigerator, and aliquots were taken out each day of column evaluation.

Evaluation solution for retention factor determination

To determine the retention factor, k of 25-OHC on 2.5 µm SPH and 5 µm PH columns, a 1 ng/mL 25-OHC evaluation solution was used. The 10 µg/mL 25-OHC evaluation solution prepared for direct injection as described in **chapter 3.5**, was diluted 10 000 times, by first diluting 10 µL 10 µg/mL 25-OHC to 10 mL 0.1% FA in MeOH, and then diluting 1 mL 10 ng/mL to 10 mL 0.1% FA in MeOH yielding a 1 ng/mL 25-OHC evaluation solution.

3.3.5 Cholesterol oxidase in phosphate buffer

A 50 mM phosphate buffer containing 0.03 mg/mL of the enzyme cholesterol oxidase was prepared by dissolving 952.5 mg KH_2PO_4 in 140 mL water. Cholesterol oxidase, 4.2 mg, was added to the solution and the buffer was pH adjusted to 7.0 with 1 M NaOH. The pH adjustment of the buffer was performed with a Titrino Plus 877 titrator with a pH meter from Metrohm (Herisau, Switzerland). Aliquots of 1250 µL were aliquoted into 1.5 mL microcentrifuge tubes from Eppendorf and stored at -80 °C.

3.4 Derivatization procedure

The oxysterol derivatization procedure is illustrated in **Figure 16**. After the addition of the WSs and heavy cholesterol into the microcentrifuge tubes, the evaluation solutions were evaporated into dryness by a Concentrator Plus and resolved in 20 µL isopropanol. Next, 200 µL of 50 mM phosphate buffer containing 0.03 mg/mL cholesterol oxidase was added, and reaction took place for 1h at 37 °C with slow stirring in either a PHMT PSC-20 Thermoshaker from Grant Instruments (20x2.0 mL) (Cambridge, UK) or stirring with a Hula Dancer vortex mixer from IKA (Staufen, Germany) before incubation in a drying cabinet from Skala (Oslo, Norway). A derivatization reagent was prepared by dissolving 15 mg Girard T reagent in 500 µL MeOH and 15 µL glacial acetic acid. The masses and volumes needed for the reagent were multiplied by the number of evaluation solutions to be made, and a large mixture was prepared. Aliquots of 515 µL of the mixture were added to each evaluation solution, and the reaction took place overnight in the dark at room temperature before transferring the solutions to microvial-autosampler vials (0.3 mL) with screw caps from VWR International AS.

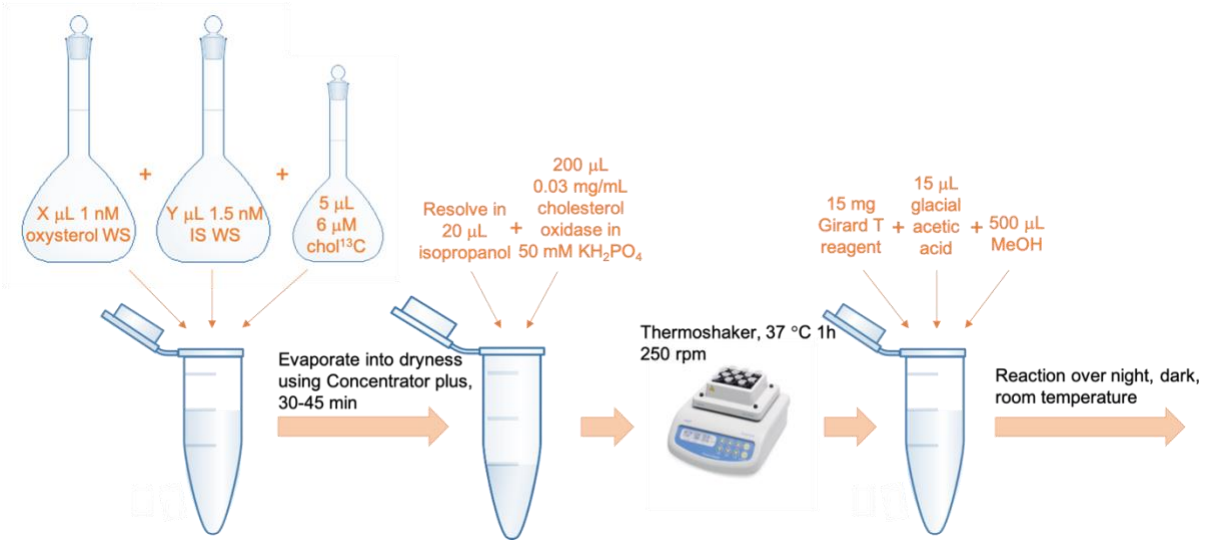

Figure 16. The oxysterol derivatization process with Girard T reagent. The X- and Y-volumes are summarized in **Table 2** and **Table 3.** The image of the Thermoshaker is retrieved from the supplier's web page [132].

3.5 Off-line solid phase extraction procedure

Off-line solid phase extraction prior to direct injection of oxysterols

25-OHC, 25-OHC-d_6, and 22R-OHC-d_7 were prepared in 10 µg/mL, 10 µg/mL and 2 µg/mL (smaller concentration due to lack of stock solution material) evaluation solutions, respectively. Off-line SPE was performed to remove the derivatization reagent before direct injection. Oasis HLB Prime SPE cartridges from Waters (Milford, MA, USA) were used and did not need washing or conditioning before the addition of the evaluation solution. 730 µL of 10 µg/mL 25-OHC, and 25-OHC-d_6, and 730 µL of 2 µg/mL 22R-OHC-d_7 evaluation solution were added to an SPE cartridge each. The oxysterols were eluted with 1 mL MeOH before evaporation into dryness and resolving in 730 µL 0.1% FA in MeOH. The off-line SPE procedure is illustrated in **Figure 17**.

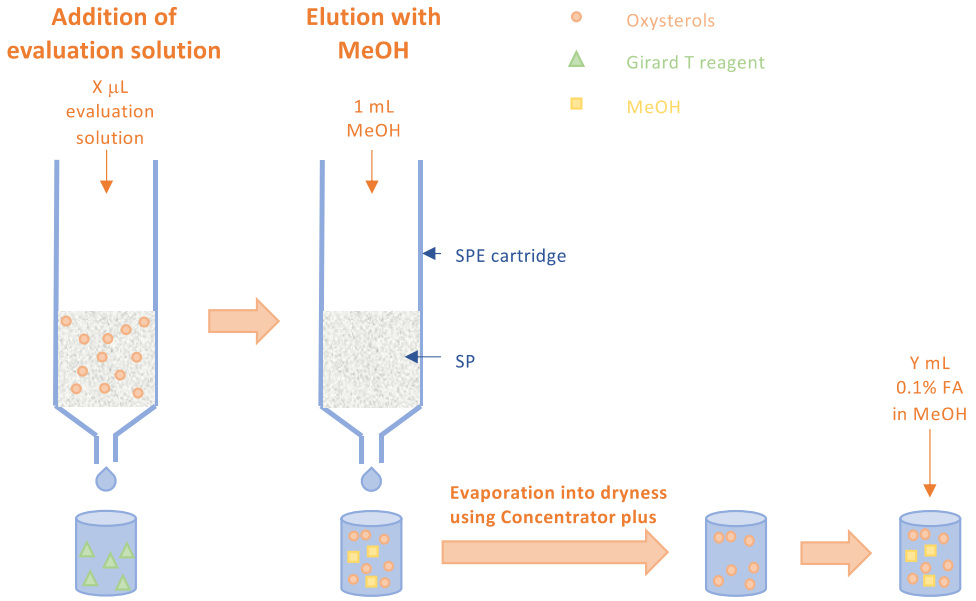

Figure 17. The off-line SPE procedure using Oasis HLB Prime SPE cartridges from Waters. The SPE cartridges did not need conditioning or washing before the addition of the evaluation solution. The X- and Y-volumes depends on the end-concentration of interest.

Off-line SPE before investigation of extra-column volume band broadening

Off-line SPE was performed on a 500 pM 22R-OHC, 24S-OHC, 25-OHC, and 27-OHC and 200 pM 22R-OHC-d_7, 25-OHC-d_6, and 27-OHC-d_6 evaluation solution. The same procedure as described in **Figure 17** was used, and both X and Y volumes were 300 µL to end up at the same concentration of 500 pM.

3.6 In-house packing procedure for nLC columns

The packing of the nLC columns was performed using the packing procedure developed by Berg *et al.* [133]. The in-house packing station consisted of a pressure bomb using nitrogen gas to exert pressure (approximately 150-200 bar) onto the capillary for packing of the particles, as illustrated in **Figure 18**.

3.6.1 Frits

A frit was made at the outlet of the fused silica capillaries before the column packing to contain the particles. A "Frit Kit" consisting of formamide and Kasil 1624 (a potassium silicate) was used. 2 μL formamide and 6 μL Kasil 1624 were mixed well in a microcentrifuge tube with a pipette tip. Fused silica capillaries of 75, 100, or 180 μm ID were cut to a ~30 cm length and placed in the frit solution for the capillary forces to pull the solution into the capillary. The frits were polymerized in a GC oven from Fisons Instruments (Ipswich, UK) at 100 °C overnight. The frit was examined by a microscope from Motic (Xiamen, China) to confirm its presence and was cut to ~1 mm.

3.6.2 Column packing

Before packing the particles, the capillaries were flushed with 100% ACN or acetone for washing. A slurry was made by adding 30 mg particles in 1 mL solvent in a 1.5 mL glass vial (30 mg/mL slurry). The slurry solvent were 80/20 ACN/H_2O (v/v), 90/10 ACN/H_2O (v/v), or 100% acetone. The slurry was placed in an ultrasonic bath from ATU Ultrasonidos (Valencia, Spain) for approximately 10 min to prevent the suspended particles to sediment. Packing with magnetic stirring was employed, where a small magnet (3x3 mm) from VWR was added to the vial. The capillaries were placed in the bomb chamber top-cap and attached through a stainless steel (SST) nut and vespel/graphite (85/15) ferrule (350 µm ID, in-house opened to 370 µm ID) from VICI Valco Instruments Co. Inc. (Schenkon, Switzerland), see **Figure 18**. The capillaries were placed in the vial with the slurry, and the bomb chamber top-cap was attached to the bottom part and placed on a Topolino magnetic stirrer from IKA (Staufen, Germany). Nitrogen gas (4.0 quality (99.99%)) from Nippon Gases Norge AS (Oslo, Norway) was exerted on the capillaries for approximately 30-120 min to obtain a ~15 cm packed bed depending on the slurry solvent used. The columns were visually inspected by a microscope.

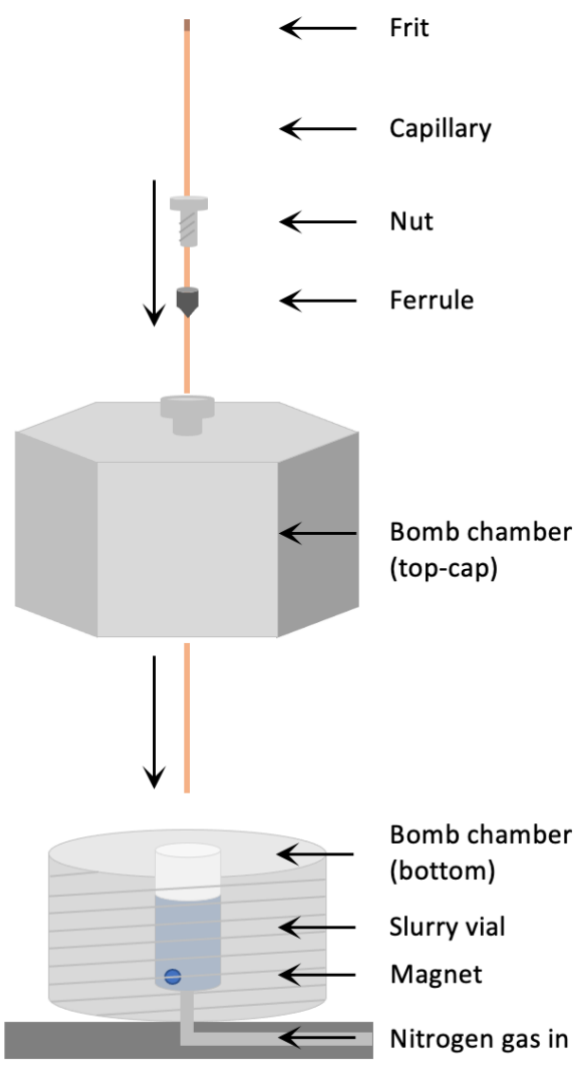

Figure 18. The in-house pressure bomb system used to pack the nLC columns. The illustration is adapted from [133].

An EASY-nLC 1200 pump from Thermo Fisher Scientific (Waltham, MA, USA) was used to deliver a 400-900 nL/min flow rate of 80/20 ACN/water (v/v) for ~30 min to flush the column after packing to allow the particles to settle.

3.7 Instrumentation

3.7.1 Conventional UHPLC-MS platform

A conventional UHPLC-MS platform with an on-line sample preparation and clean-up (AFFL-system and trap column) system was used as described by Solheim *et al.* [92]. The platform is described in more detail in **Figure 40** in **chapter 7.2** in **Appendix**.

3.7.2 nLC-UV one-column system for column testing

The nLC-UV system used for nLC column performance testing is illustrated in **Figure 19**. An EASY-nLC 1200 pump was used to deliver 70/30 ACN/H_2O (v/v) isocratic with a flow rate of 450 and 600 nL/min. The manual injection was performed using a Cheminert microvolume 4-port-2-position injection valve with a 50 nL sample loop and an SST fill port (1/16") from VICI Valco Instruments Co. Inc. Sample injection was done using a 25 µL syringe from Hamilton (Bonaduz, Switzerland). A WellChrom K-2600 UV-detector from Knauer (Berlin, Germany) was used operating at a 254 nm λ. The TotalChrom Navigator software from PerkinElmer (Waltham, MS, USA) was used for data acquisition.

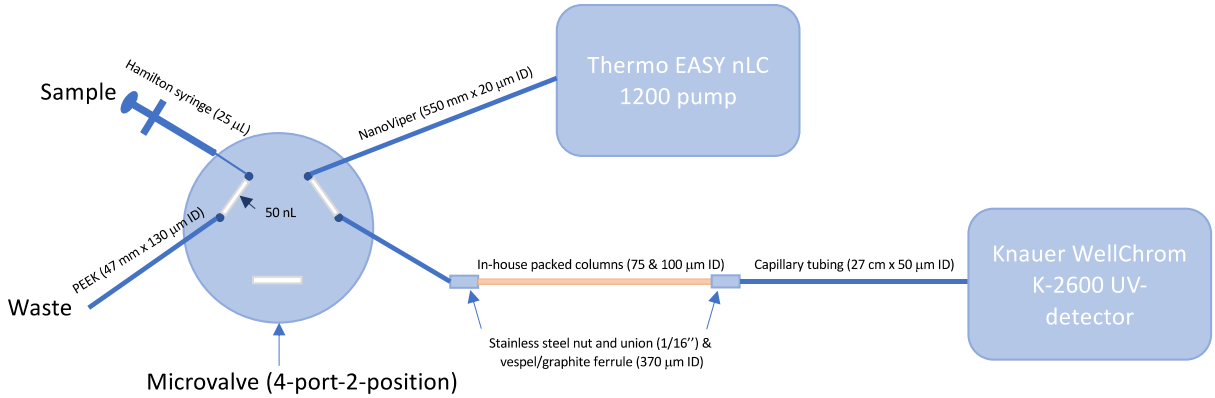

Figure 19. The nLC-UV system used to perform column performance testing. The microvolume 4-port-2-position injection valve contained three tracks (in white). In inject position, the rotor track (50 nL) between the sample and waste was filled with evaluation solution, and excess was directed to waste. In load position, the valve was switched, putting the track with sample between the pump and the nLC column. The isocratic flow delivered from the pump flushed the evaluation solution from the track and onto the analytical column. The injection volume was 50 nL, as the volume of the rotor track was 50 nL.

3.7.3 nLC-MS one-column platform for column testing (Platform I)

The nLC-MS set-up used to test the retention factor of 25-OHC on the 2.5 µm SPH and 5 µm PH particles- and the extra-column volume band broadening is illustrated in **Figure 20.** An EASY-nLC 1200 pump was used to deliver the isocratic flow rate. An evaluation solution was manually injected with a 25 µL syringe from Hamilton through an SST fill port (1/16") in the 4-port-2-switch injector valve with a sample loop of 50 nL (injection volume). MS tune settings and parameters are described in **Table 4** and **Table 13**, respectively. The detection was done with the TSQ Quantiva Triple Quadrupole MS from Thermo Scientific with a nanospray flex ion source.

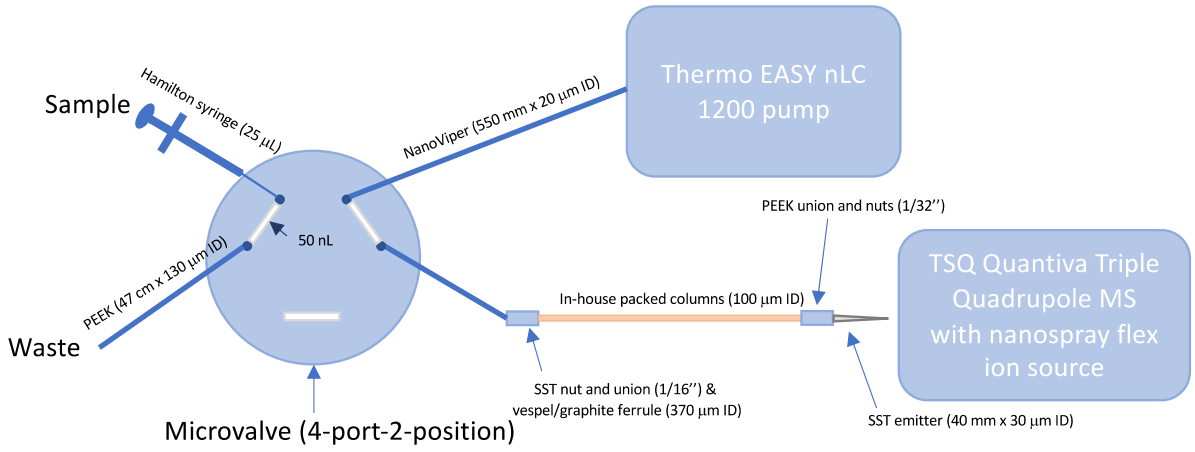

Figure 20. The nLC-MS platform (Platform I) used for retention factor- and extra-column volume band broadening testing. The nLC-MS set-up resembles the nLC-UV system shown in **Figure 19**. However, an emitter was coupled at the column outlet, and the detector was exchanged with a TSQ Quantiva Triple Quadrupole MS.

3.7.4 Direct injection for MS parameter optimization

To optimize MS parameters, direct injection on a TSQ Quantiva Triple Quadrupole MS with a HESI-source was performed. About 300 µL of the 10 µg/mL 25-OHC evaluation solution was filled into a 500 µL syringe from Hamilton, and the syringe was placed in a Fusion 101 syringe pump from Chemyx Inc. (Stafford, TX, USA) connected to the MS. A 5 µL/min flow rate was applied, while the MS was operated in full scan. The precursor *m/z* was manually chosen from the full scan and added to the TSQ Quantiva Tune Application software (Thermo Scientific). Optimization options in the software extracted the optimized quantifier and qualifier *m/z*

transitions and their respective optimized collision energies in a report. The report data was added to the instrument method in Xcalibur (Thermo Scientific). The procedure was repeated for both the 25-OHC-d_6- and 22R-OHC-d_7-evaluation solutions.

3.7.5 nLC-MS two-column platform (Platform II)

The initial nLC-MS platform with the implemented trap column and AFFL-system built in this study is illustrated in **Figure 21**. The platform is described in more detail below. The injection volume was 5 µL.

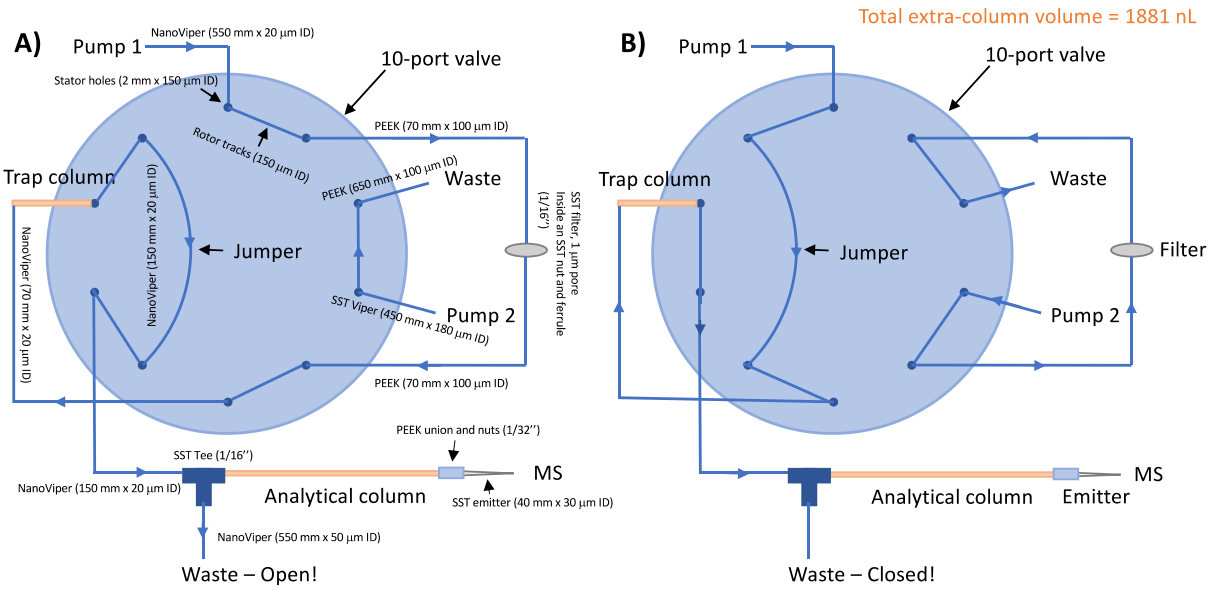

Figure 21. The initial nLC-MS platform (Platform II) with the implemented trap column and AFFL-system in both A) inject position and B) load position.

Mass spectrometer TSQ Quantiva Triple Quadrupole

The MS was a TSQ Quantiva triple quadrupole and was equipped with a nanospray flex ion source (nESI). The position of the SST emitter (40 mm x 30 µm ID, from Thermo Scientific) outlet was adjusted with the XYZ-manipulator on the ion source to about 3-5 mm away from the MS-inlet. The MS tune settings are summarized in **Table 4** and were held constant throughout the whole study. As no sheath-, auxiliary-, or sweep-gas is used in nESI, these values were not relevant. *m/z* transitions for qualifier and quantifier ions and their respective collision energies in MRM mode were optimized as described in **chapter 4.3** (and the values are summarized in **Table 13**). The Xcalibur software was used for creating instrument methods,

sequence setup, and data acquisition, and handling. The TSQ Quantiva Tune Application software was used to control the MS.

Table 4. The MS tune settings held constant throughout the study.

MS tune settings	
Mode	Positive
Spray voltage (V)	2200
Ion transfer tube temperature (°C)	310
CID (mtorr)	1.5
Q1 resolution (FWHM)	0.7
Q3 resolution (FWHM)	0.2

Pumps

An EASY-nLC 1200 pump was used as the autosampler and loading pump (Pump 1 in **Figure 21**), while a Hitachi L-7100 HPLC pump from Merck (Kenilworth, NJ, USA) was used for backflushing the filter (Pump 2). The EASY-nLC 1200 pump was an nUHPLC pump that could deliver flow rates in the nL-scale and withstand pressures up to 1200 bar. The MP inlets did not have built-in degassers calling for degassing of the MPs before pump-introduction. The Hitachi L-7100 HPLC pump was a regular HPLC pump equipped with one MP inlet able to deliver a flow rate of 1 μL/min-10 mL/min. A flow rate of 0.1 mL/min was used to backflush the filter.

10-port valve, filter, trap column, and attached tubings

To build the on-line trap column and AFFL-system in the nLC-MS platform, the trap column and filter were assembled in a Cheminert 10-port-2-position valve (1030 bar, C82X-6570, 20I-1569C) from VICI Valco Instruments Co. Inc. The 10-port valve was equipped with a CapLC selector valve from Waters for automatic switching. An SST 1 μm pore filter (part no.: 1SR1-10) from VICI Valco Instruments Co. Inc. was inserted into an SST union (1/16”, 150 μm ID), and the union was connected to polyether ether ketone (PEEK)-tubings (70 mm x 100 μm ID) from IDEX (Lake Forest, IL, USA) on each side with SST-nuts (1/16”) and -ferrules (1/16”). A PEEK-tubing (650 mm x 100 μm ID) was used as waste-tubing for the backflushing of the filter and was connected to the 10-port-valve with an SST-nut (1/16”) and -ferrule (1/16”). The pump used for backflushing of the filter was connected to the 10-port-valve with an SST fingertight Viper from Thermo Scientific (550 mm x 180 μm ID).

For the connection of the trap column, direct-connect 360 μm FS tubing UHPLC-Fittings (1/16", 1700 bar) from VICI Valco Instruments Co. Inc., from now on termed UHPLC-connections, were used on each side of the column. The UHPLC-connections are illustrated in **Figure 22**. All tubings assembled in the 10-port-valve was NanoViper Zero Dead Volume Fingertight Fitting (20 μm ID) in lengths of either 150, or 70 mm, from now on termed nanoViper, from Thermo Fisher Scientific. The narrowest nanoVipers available (20 μm ID) were purchased to minimize the system extra-column volume. The inlet of the trap column was attached to a nanoViper (70 mm x 20 μm ID) through an SST Viper-union with a UHPLC-connection, and the nanoViper was inserted into the 10-port-valve. The outlet of the trap column was connected to the 10-port-valve with a UHPLC-connection.

A nanoViper (150 mm x 20 μm ID) was used as a "jumper" to connect the trap column to the analytical column during loading. A nanoViper (150 mm x 20 μm ID) was coupled from the 10-port-valve to a 150 μm bore SST tee (1/16"), as shown in **Figure 21**. The analytical column was connected to the outlet of the SST tee with a UHPLC-connection. The outlet of the analytical column was connected to an SST emitter from Thermo Fisher Scientific (40 mm x 30 μm ID) through a PEEK-union with PEEK-nuts (1/32") both on the analytical column and the emitter. Both the outlet of the analytical column and the emitter wore PEEK-sleeves (1/32") for grip. A nanoViper (550 mm x 55 μm ID) was connected in the last inlet of the SST tee to the waste valve on the EASY-nLC 1200 pump. A Butterfly Portfolio Heater (15 x 4 cm) combined with a Column Heater Controller for heating of the analytical column was purchased from MS Will (Aarle Rixtel, Netherland) and is depicted in **Figure 33**.

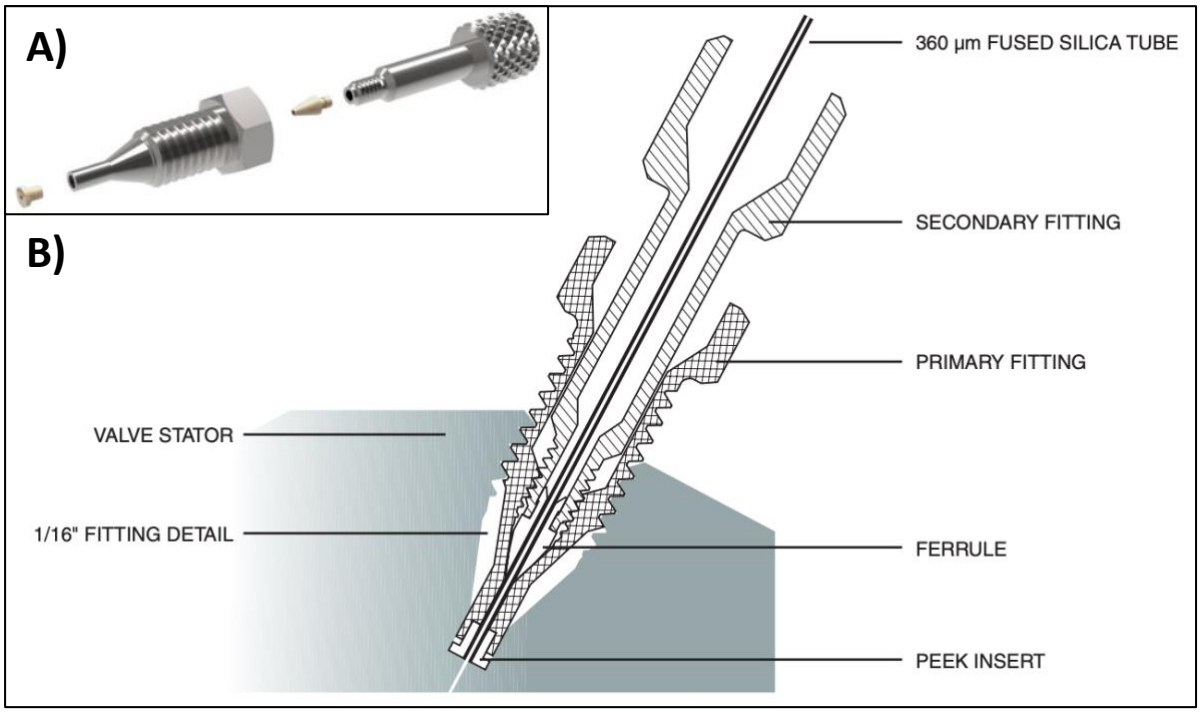

Figure 22. A) A photo of the UHPLC-connections and B) a sketch of the UHPLC-connections with names on the different parts. The UHPLC-connection is compatible with fused silica columns with a 360 µm OD and consists of two main parts – the primary and the secondary fitting. The two fittings are screwed loosely together, and the fused silica column is inserted into the two fittings until it extends beyond the PEEK-insert. Next, the fitting assembly is inserted into the fitting detail (1/16" e.g., a 10-port-valve), and the column is pulled slightly out and pushed back in to assure that the column is bottomed out in the fitting detail. The primary fitting is finger tightened, still making sure that the column is bottomed out. Finally, the secondary fitting is tightened for additional gripping force. The PEEK-ferrule and -insert will tighten around the fused silica column and ensure grip. A) is retrieved from the vendors web page [134], and B) is retrieved from the vendor's manual of the UHPLC-connections [135].

3.7.6 nLC-MS two-column platform (Platform III)

The nLC-MS platform with a redesigned trap column and AFFL-system (Platform III) for extra-column volume reduction is similar to the platform illustrated in **Figure 21**. However, the platform now included changing the IDs of the PEEK-tubings on both sides of the filter from 100 µm ID to 64 µm ID and removing one nanoViper (150 mm x 20 µm ID), four stator holes, and two rotor tracks during loading. The injection volume was 5 µL. The platform is illustrated in **Figure 23**.

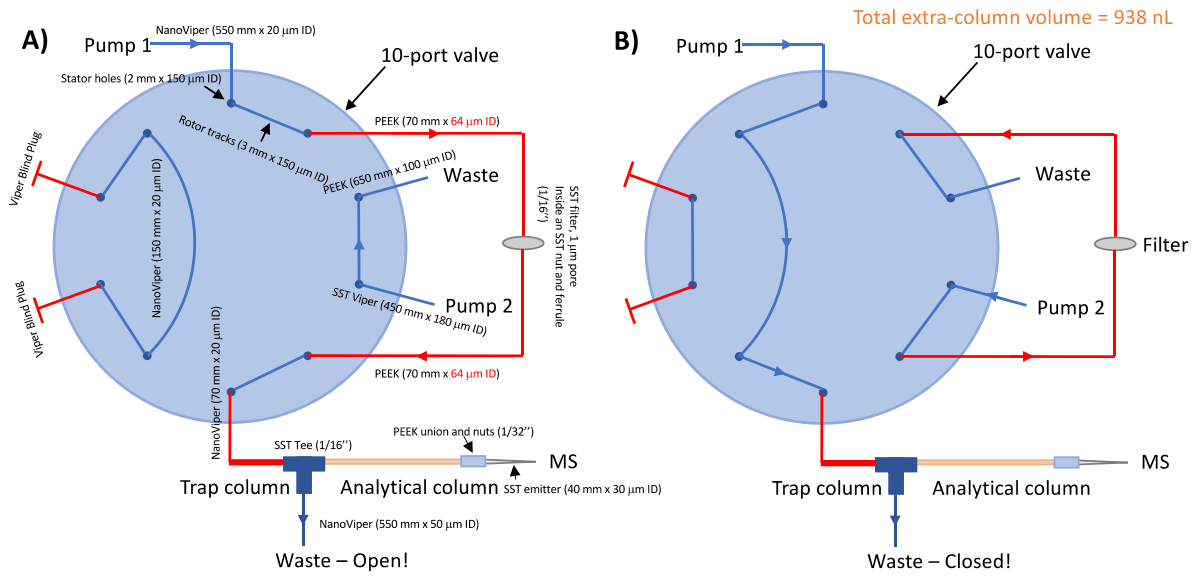

Figure 23. The nLC-MS platform (Platform III) with alterations in extra-column volume compared to **Figure 21** in both A) inject position and B) load position. The alterations are shown in red.

As illustrated, the outlet of the trap column was now connected directly to the SST tee (1/16"). A nanoViper (150 mm x 20 µm ID) was still used as a "jumper", but now connected the EASY-nLC 1200 pump (Pump 1) directly to the trap- and analytical column when the filter was switched for backflushing (load position). The redesign eliminated two inlets in the 10-port-valve, and hence, two viper blind plugs were inserted into these inlets. The entire platform is illustrated in **Figure 24,** also with real-life pictures of the couplings of the trap column and filter.

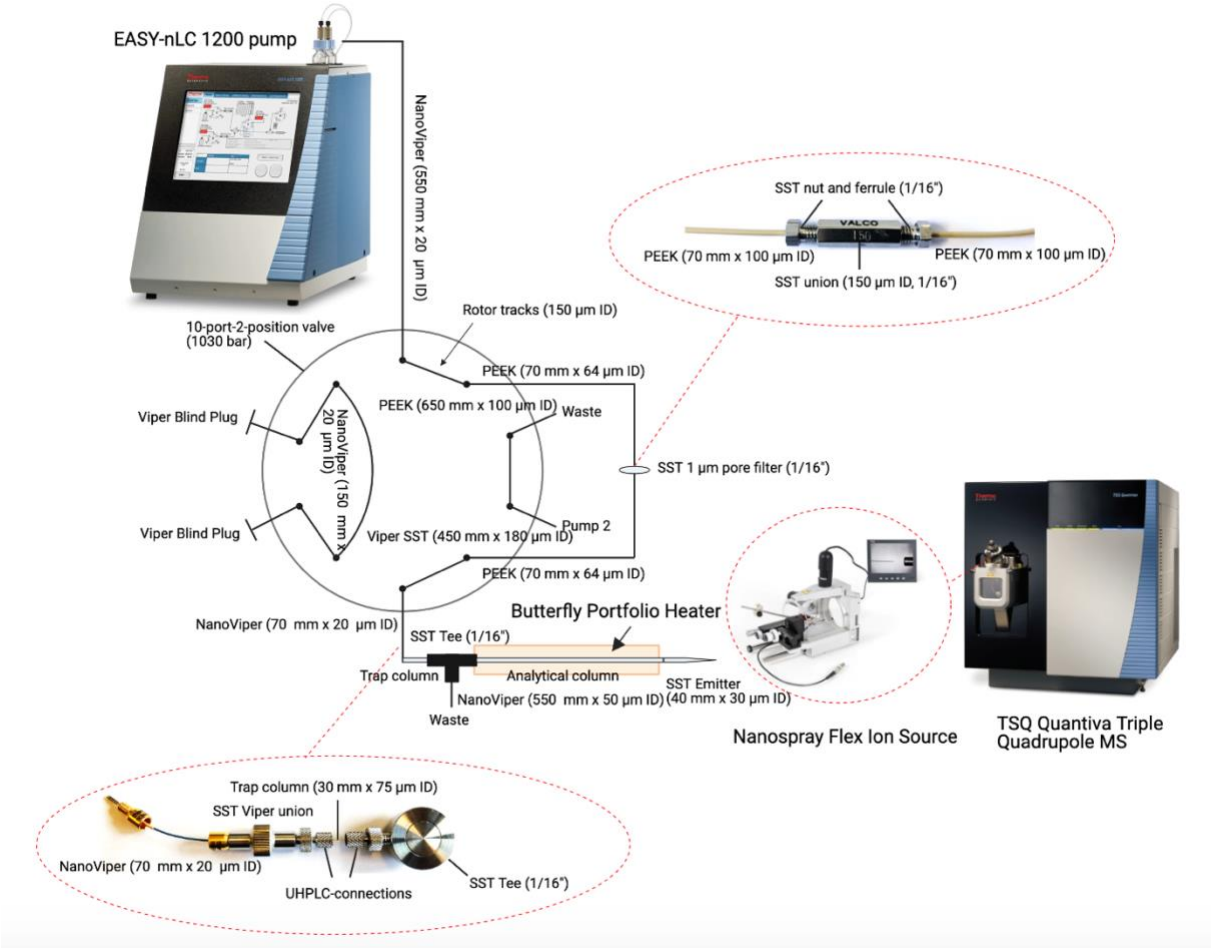

Figure 24. The final AFFL-trap-column-nLC-nESI-TQMS platform (Platform III) with dimensions and materials of the filter, emitter, tubings, and connections. Real-life images of the trap column and filter and respective couplings are also shown in the red dotted circles. Images of the EASY-nLC 1200 pump, nanospray flex ion source, and TSQ Quantiva Triple Quadrupole MS were retrieved from the supplier's web page [136-138].

3.7.7 nLC-MS two-column platform with commercial columns (Platform IV)

The nLC-MS platform with the commercial trap- and analytical column is illustrated in **Figure 25**. The injection volume was 5 µL.

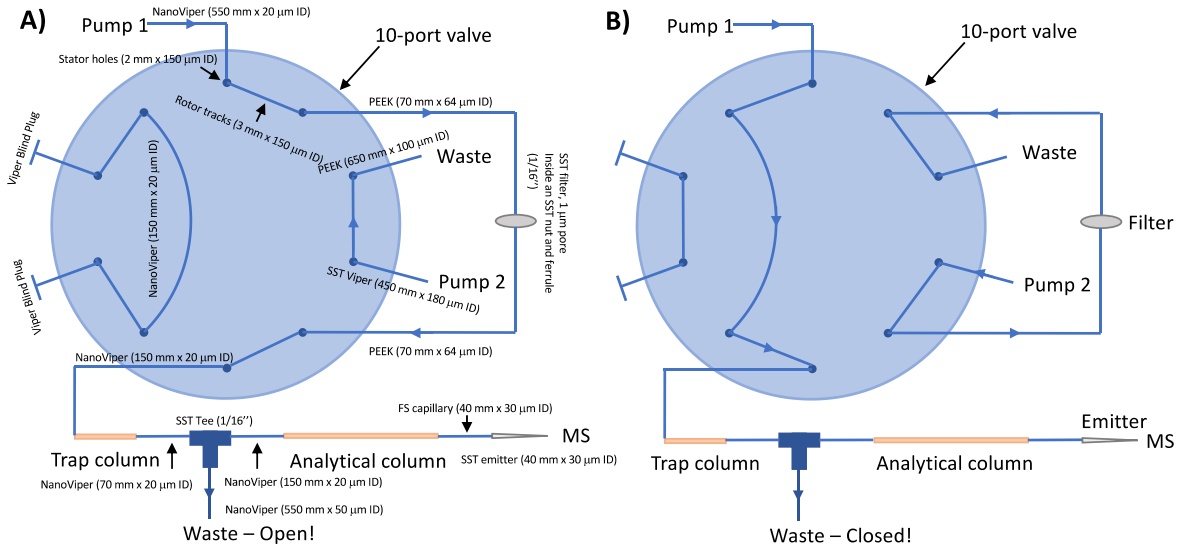

Figure 25. The nLC-MS two-column platform (Platform IV) for the commercial trap- and analytical columns in both A) inject position and B) load position.

3.7.8 Scanning electron microscope

The scanning electron microscope (SEM) used was a SU-8320 model from Hitachi (Tokyo, Japan). Preparation regarding research for appropriate settings was performed in advance and brought along when taking the images, but the SEM itself was operated by trained personal.

4 Results and discussion

The aim of this study was to develop an LC-MS method that enables the determination of trace levels of oxysterols in liver organoids combined with on-line sample preparation and clean-up. The already existing in-house analytical chromatographic method did not provide sufficient sensitivity. Therefore, a highly sensitive nLC method with an nESI and a TSQ triple quadrupole MS was to be developed.

The work was divided into four work packages, as illustrated in **Figure 26**. First, preliminary experiments on method evaluation on the current chromatographic method are discussed, followed by the packing and evaluation of the nLC columns before MS parameter optimization. Lastly, the development of the miniaturized nLC-MS platform with an on-line sample preparation and clean-up is presented.

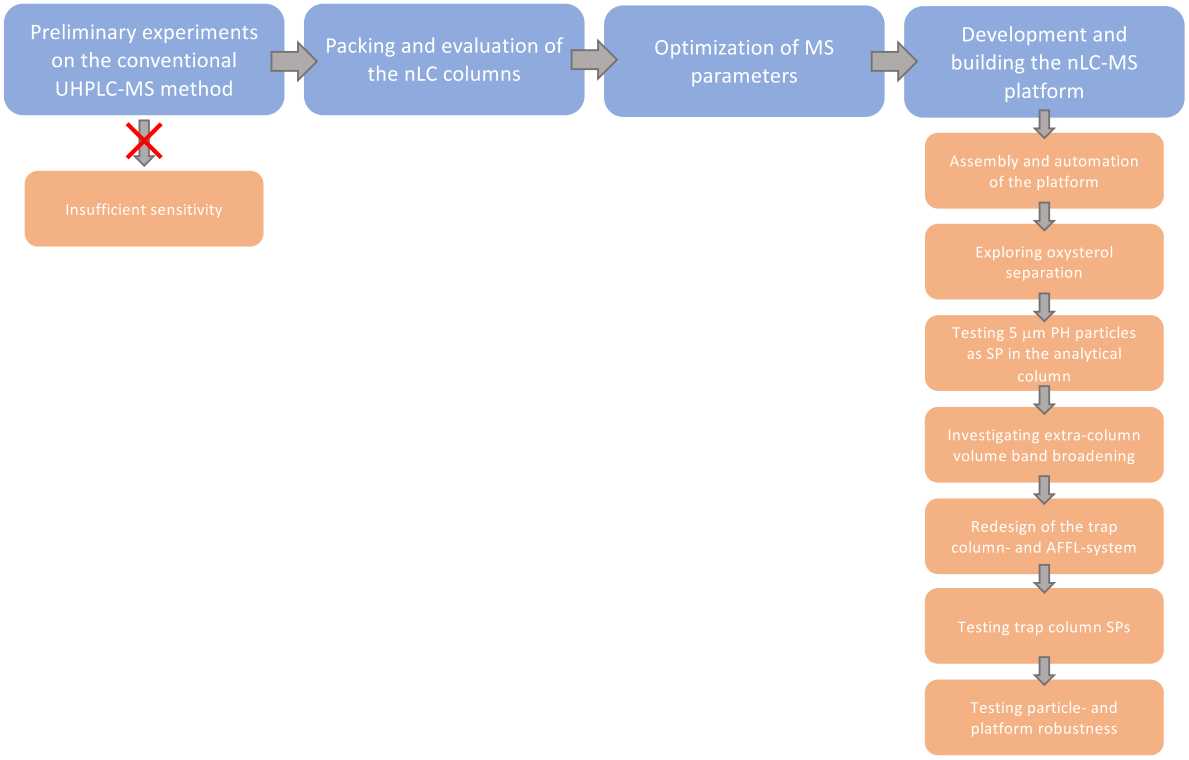

Figure 26. A flow chart of the progress of the study.

4.1 Preliminary experiments with the current analytical method

The established method for oxysterol quantification with the conventional UHPLC-MS set-up (the platform is described in **chapter 7.2**) was evaluated to investigate if it was fit for purpose regarding analytical sensitivity. The method had been developed and optimized by the research group of Bioanalytical chemistry at the Department of Chemistry, UiO, led by Associate Professor Hanne Røberg-Larsen. Eurachem's guidelines were used to perform the method evaluation [139].

Oxysterols are low abundant in biological systems, which requires high analytical sensitivity for quantification. Based on the work of Røberg-Larsen *et al*., where 19 fmol (130 amol injected on column) of 25-OHC was quantified per 10 000 pancreatic cancer cells [78], it was estimated that oxysterol levels in 50 liver organoids (~80 000 cells) were in the low-fmol range, assuming the abundance of oxysterols in liver organoids is equal or lower. Cancer cells typically have higher oxysterols concentrations than healthy cells, leaving the possibility of even lower oxysterol levels in healthy organoids. A goal is to reduce the number of liver organoids necessary, increasing the need for enhanced sensitivity further.

Evaluation solutions of 50, 300, and 500 pM 22R-, 24S-, 25-OHC, and 27-OHC were analyzed to obtain data for the S/N on the conventional platform. The evaluation solutions were prepared from WSs prepared by me (2020) and Ph.D. Alex Websdale (2019). The S/N were compared against data of the same concentration range obtained by another researcher (2018). The S/N are presented in **Table 5**. The S/N ratios were small for all evaluation solutions, and the highest concentration of 500 pM was not sufficient for detection, indicating that the sensitivity of the TSQ Vantage MS had been lost compared to 2018. The raw data for S/N are found in **chapter 7.5.1** in **Appendix**. Further preliminary experiments for method evaluation not included here are discussed in **chapter 7.1.2** in **Appendix**.

Table 5. The average S/N for evaluation solutions of 25-OHC. 25-OHC was used as an example, but none of the oxysterols provided sufficient sensitivity. ND = not detected (S/N < 3).

	S/N for 25-OHC		
	2020	**2019[1]**	**2018[2]**
50 pM	ND	ND	3
300 pM	ND	ND	22
500 pM	ND	ND	73

1) Prepared by oxysterol-research collaborator Ph.D. Alex Websdale (University of Leeds), 2) Prepared by Associate Prof. Hanne Røberg

Thus, the preliminary experiments showed that the conventional UHPLC platform (2.1 mm ID LC column) coupled to the TSQ Vantage MS did not fulfill the acceptable criteria for sensitivity needed for quantification of oxysterol levels in the liver organoids. Therefore, a miniaturized and highly sensitive nLC-MS system (50-100 µm ID LC columns) had to be developed.

4.2 Packing of the nLC columns

Downscaling of the LC column ID was approached to enhance the sensitivity. Columns in the nano format packed with 2.5 μm Super Phenyl-Hexyl (SPH) particles, as previously shown to give baseline separation of 22R-, 24S-, 25-, and 27-OH [92], were not commercially available and had to be packed in-house. nLC columns with C8 and C18 SP are commercially available but do not provide as good selectivity for the oxysterols as the SPH. An SP suitable as a trap column compatible with the 2.5 μm SPH particles also needed to be identified.

4.2.1 Evaluation of the in-house column packing process

The packing of nLC columns is an art of itself and requires research and experience to achieve a well-packed bed for great column performance [116]. The packing procedure was based on the procedure proposed by Berg *et al.* [133] with the set-up as described in **chapter 3.6**. Eighteen nLC columns with different IDs and slurry solvents were packed and evaluated.

To achieve a column with great performance, it is important to create a stable packed bed so contributions from eddy dispersion and longitudinal diffusion are minimized [116, 131]. To achieve a stable packed bed, a homogenous slurry suspension is essential, according to Capriotti *et al*. [118], and the correct viscosity of the slurry solvent is crucial to obtain a stable slurry. Low viscosity is mentioned as both an advantage and a disadvantage in the literature [118]. It can ensure a fast packing speed but also a high sedimentation velocity of the particles in the slurry, resulting in heterogeneous or loosely packed beds [140]. If a shorter column is packed, low viscosity may be favorable to achieve fast packing, hence avoiding particle sedimentation. Choosing the correct slurry solvent is also important to ensure that the particles move independently to avoid particle aggregation [118]. Particle aggregation is important to avoid as the packing can be slowed down, clog the column, and result in a very inhomogeneous packed bed. Sonication of the slurry before packing and magnetic stirring during the entire packing process are ways to maintain a stable suspension. Heat is also mentioned in the literature as applicable to slow down the sedimentation of the particles but was not used here [118]. Since the nature of particles is to settle, a fast-packing process is desired (30-45 min).

Berg *et al.* packed core-shell C18 particles suspended in various solvents, and the binary solvent 80/20 ACN/H_2O (v/v) gave the quickest packing (~25 cm in 1 hour) in combination with the best peak capacity. Therefore, 80/20 ACN/H_2O (v/v) was also chosen as a slurry solvent in this study. With the desired length of the packed bed being 15 cm (considered semi-long), a solvent with even lower viscosity was also tested, namely 90/10 ACN/H_2O (v/v). Lastly, 100% acetone was tested, as Fanali *et al.* showed a homogenous suspension of core-shell PH particles in acetone [141, 142]. Fused silica capillaries were packed with the 2.5 μm SPH particles with 75 μm and 100 μm IDs to explore the column performance.

The slurry concentration should not be too diluted or too concentrated. The former may result in low packing efficiency (e.g., 3 mg particles/mL slurry), and the latter may cause aggregation of the SP particles, clogging the column (e.g., 100 mg particles/mL slurry) [143]. A high slurry concentration is two-fold. It can ensure particle agglomeration yielding a densely packed bed and a great column efficiency [143, 144], or result in large voids in the packed bed, reducing the column efficiency [131]. Thus, a compromise must be found, according to Gritti *et al.* [145]. Therefore, a slurry concentration of 30 mg particles/mL was held constant as proven by Berg *et al*. to give sufficient density of the packed bed for core-shell particles [133]. Three replicates of each solvent (80% ACN, 90% ACN, and 100% acetone) for both column dimensions (75 and 100 μm ID) were packed, giving a total of 18 columns.

The packing time was unpredictable and had large variations and is summarized in **Table 6**. This resulted in some differences in the length of the packed bed, as shown in **Table 7**. The slurry solvent with the highest viscosity (viscosities in **Table 8**), namely 80% ACN, proved to pack the fastest for both IDs, contrary to what literature suggested about the highest viscosity slurry expected to pack slowest.

Table 6. The average packing time (n=3) for ~15 cm packed bed with 80% ACN, 90% ACN, and 100% acetone.

	Time for ~15 cm packed bed (min)	
Slurry solvent	**75 μm ID**	**100 μm ID**
80/20 ACN/H_2O (v/v)	~60	~60
90/10 ACN/H_2O (v/v)	~115	~80
100% acetone	~110	~110

Table 7. The lengths of the packed bed in the in-house packed nLC columns.

The length of the packed bed (cm)			
	Replicate	**100 µm**	**75 µm**
80% ACN	1	14.2	15.5
	2	15.2	13.1
	3	15.5	15.0
90% ACN	1	14.3	11.6
	2	15.2	15.4
	3	14.3	15.2
100% acetone	1	11.8	15.4
	2	15.4	15.4
	3	15.5	15.2

Table 8. The viscosities of the slurry solvents used.

Slurry viscosity (mPA*s at 25 °C)		
80/20 ACN/water (v/v)	=	0.52
90/10 ACN/water (v/v)	=	0.46
100% acetone	=	0.30

Occasionally, the particles had not been packed, and the capillary was eliminated or given a second attempt. Slow packing can occur due to particle sedimentation during packing or evaporation of slurry solvent during packing preparations leading to an altered slurry viscosity and concentration. Additionally, the slurry was not always sonicated between each column packing, which increased the possibility for particle sedimentation, which could also be why the particles had not packed. This showed that sonication should always be performed between each column packing. Additionally, the capillaries were depressurized instantaneously when the N_2-gas was switched off, which led to a great pressure drop pulling the lastly packed particles out of the column and possibly created voids in the packed bed. The pressure valve should hence have been opened more carefully to slow down the depressurization. The fast depressurization may also have caused variations in the packing time needed for a 15 cm packed bed.

During the thesis, it was discovered that it was possible to manually slow down the depressurization of the pressure bomb system after packing, which reduced the pullback of the particles within the column, making the packing procedure more efficient. A 17-19 cm of packed bed was achieved only within 30 min.

To conclude, there were challenges during the packing, showing variability in both time and length, and some replicates did not pack at all. Finally, 18 columns with 75 and 100 μm IDs were successfully packed and ready for performance testing.

4.2.2 Evaluation of the column performance

The plate number, asymmetry, and retention factor of the test compound toluene were tested for all 18 columns. During column performance testing, the operating conditions must be optimal to avoid additional contribution to performance impairment outside the column. External column factors comprise volumes like tubings, connections, pump, valves, and detector [146]. Toluene was used as a model compound as it is commonly used to test hydrophobic interactions in RP column performance testing, and thiourea was used to establish t_M. The operating conditions are summarized in **Table 9,** and the nLC-UV set-up used for column performance testing is described in **chapter 3.7.2**.

Table 9. The operating conditions held constant during the column performance testing.

Operating conditions	
Injection volume	50 nL
Injector	Manual 4-port-2-position
Flow rate	450 nL/min (75 μm ID columns) 600 nL/min (100 μm ID columns)
MP composition	70/30 ACN/H_2O (v/v)
Column temperature	Ambient
Detector	UV at λ = 254 nm Flow cell volume = 15 nL
Evaluation solution	0.1% toluene and 20 μg/ml thiourea in 50/43/7 H_2O/ACN/MeOH (v/v/v)

Plate number

The evaluation of the plate number was performed with isocratic elution at a constant temperature. With self-packed nLC columns, lower plate numbers compared to conventional HPLC columns are expected.

Table 10 shows the average plate numbers obtained from the evaluation. The plate number for 0.1% toluene was ranging from 711-4856 across all 18 columns. In general, the intra-column relative standard deviation (RSD) was acceptable (< 9%), while the variation between the columns was between 6-21%, except for the extreme deviations in 100 μm ID columns packed with both 80% and 90% ACN (difference and inter-column RSD of 147% and 47%, respectively).

One column was excluded from the project (100 μm ID, 80% ACN) due to issues with the injector switching during evaluation. The remaining two replicates had a difference of 147%, making it difficult to draw any conclusions on the performance. The raw data used for plate number calculations are included in **Table 18** in **chapter 7.5.3** in **Appendix**.

Table 10. The average plate number (n=9) of toluene with both intra- and inter-column variations.

Column	N	Intra-column RSD (%)	Difference (%)
80% ACN, 100 μm	$2.8*10^3$	0.9-5.1	147
		Intra-column RSD (%)	**Inter-column RSD (%)**
90% ACN, 100 μm	$2.7*10^3$	4.9-6.9	47
100% acetone, 100 μm	$1.8*10^3$	5.3-6.8	16
80% ACN, 75 μm	$1.3*10^3$	3.7-6.0	5.5
90% ACN, 75 μm	$0.9*10^3$	3.5-8.8	17
100% acetone, 75 μm	$1.8*10^3$	4.8-6.0	21

No significant differences were observed in the plate numbers between the slurry solvents in the 100 μm ID columns, making it difficult to draw a conclusion of the highest plate number exclusively based on the slurry solvent. However, 100% acetone gave much less inter-column variation than 80% and 90% ACN.

Interestingly, in the columns with an ID of 75 μm, 100% acetone gave significantly higher plate numbers than 80% ACN, and 80% ACN gave significantly higher plate numbers than 90% ACN. Hence, 100% acetone appears to deliver the highest plate number (N = $1.8*10^3$) in

columns with an ID of 75 μm. This agrees with what Fanali *et al.* state about acetone creating a stable slurry suspension and a stable packed bed [141]. Compared to the 100 μm ID columns, the best 75 μm ID column did not provide significantly lower plate numbers. Significance tests were calculated using a two-tailed t-test at a 95% confidence interval, and an example of a t-test calculation is shown in **chapter 7.4** in **Appendix**.

Fanali *et al.* packed 15 cm 75 and 100 μm ID columns with 2.6 μm core-shell PH particles and achieved plate numbers of about ~12 400 and ~14 400 plates, respectively [141]. This is significantly higher than the plate numbers obtained in this thesis. Fanali *et al.* also reported lower inter-column plate height variation of 5-10%, indicating that the packing procedure requires technical experience.

The testing conditions were sub-optimal to give representative values for the column performances. This could be improved by decreasing extra-column volume and using a detector with a smaller flow cell. Extra-column volumes in the actual columns could be reduced by straighter column cuts, or filing of the column ends since irregularities leave extra-column volume inside the fittings. Lastly, shorter nLC tubings and zero-extra-column-volume fittings are also expected to decrease extra-column volume. As some refocusing of the analytes did occur in the column due to lower concentration of the organic modifier in the sample compared to the MP composition, reduction of the extra-column volume after the column (detector flow cell) would be most significant to reduce performance impairment.

Polymerization of the frit was also an issue. Occasionally, the entire frit did not polymerize and looked axially and radially inhomogeneous. Frits are known to contribute to band broadening [147, 148], especially in shorter columns (≤ 15 cm) packed with sub-3 μm core-shell particles with early eluting compounds ($k < 2$) [149, 150]. Therefore, an uneven frit distribution would expectably increase band broadening further.

To summarize, 100% acetone in both 75 and 100 μm ID columns resulted in the highest number of plates or the lowest inter-column variations within its column dimension, respectively. Therefore, these were further considered for the final method.

Peak shape – Asymmetry

The average asymmetry factors obtained are presented in **Table 11**. Asymmetry was apparent for all the columns and ranged from 3.1 to 5.9. Acceptable values for A_S are considered to be ≤ 2 in conventional HPLC, indicating that the tested columns did not meet the standards. However, higher A_S is expected for self-packed nLC columns. The 100 µm ID columns packed with 90% ACN and 100% acetone and 75 µm ID columns packed with 100% acetone had the lowest asymmetries of 3.1, 3.7, and 4.4, respectively. Again, better-suited zero-extra-column-volume fittings, better cutting, and filing of the column ends, and smaller flow cell volume in the detector could potentially have improved the symmetry. An example chromatogram is shown in **Figure 27**.

Table 11. The average asymmetry factor (n=9) of toluene with both intra- and inter-column variations.

Column	A_S	Intra-column RSD (%)	Difference (%)
80% ACN, 100 µm	4.6	2.5-3.4	37
		Intra-column RSD (%)	**Inter-column RSD (%)**
90% ACN, 100 µm	3.1	1.1-1.6	29
100% acetone, 100 µm	3.7	2.3-3.2	11
80% ACN, 75 µm	5.9	1.0-3.4	15
90% ACN, 75 µm	5.3	1.2-3.7	9.1
100% acetone, 75 µm	4.4	1.0-3.1	4.6

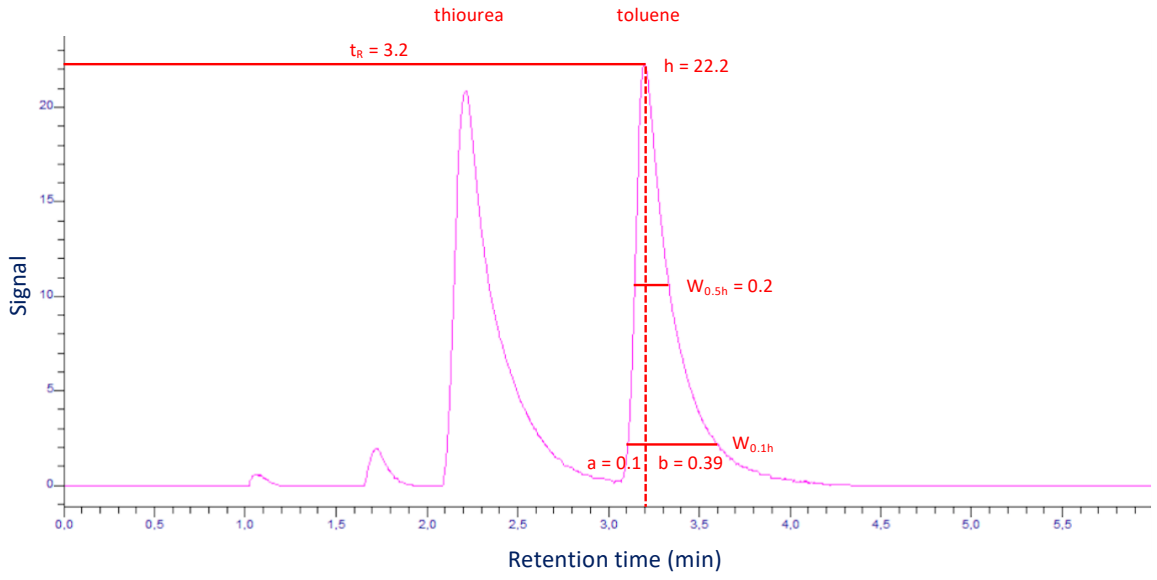

Figure 27. A chromatogram of thiourea and toluene from a 100 µm ID column packed with 100% acetone as slurry solvent illustrates how the values were extracted to calculate the plate number and asymmetry.

For the 100 μm ID columns, it was found that packing with 90% ACN and 100% acetone gave significantly lower asymmetry than 80% ACN, but 90% ACN was not significantly more symmetric than 100% acetone. For the 75 μm ID columns, 100% acetone gave significantly lower asymmetry than both 80% and 90% ACN, but 80% ACN did not give significantly lower asymmetry than 90% ACN. For comparison, both 90% ACN and 100% acetone in 100 μm ID gave significantly lower asymmetry than 100% acetone in 75 μm ID. The raw data for asymmetry calculations can be found in **Table 19** in **chapter 7.5.3** in **Appendix**

To sum up, columns packed with 90% ACN in 100 μm ID and 100% acetone in both the 75 μm and 100 μm ID columns had the lowest asymmetry and were further considered for the final method.

Retention factor

The inter- and intra-column variabilities of the retention factor are valuable parameters to use when assessing the repeatability of the column performance. The retention factor is independent of column dimensions and should therefore be similar in all 18 columns. **Table 12** shows data for the average retention factor, including the intra- and inter-column variation. The highest intra-column variation was 2.3%, which is considered acceptable. Inter-column variability was lowest for 80% ACN in both the 75 μm and 100 μm ID columns with an RSD of 8.5% and 3.6%, respectively. However, inter-column variabilities were generally high across the other columns, especially compared to the figures reported by Fanali *et al.* of 5-10% RSD [141]. This shows that well packing of the core-shell particles in nLC columns is difficult to reproduce by less experienced operators. Large variations can also be due to the pump failing to deliver the correct flow consistently. The raw data for retention factor calculations can be found in **Table 20** in **chapter 7.5.3** in **Appendix**.

Table 12. The average retention factor (n=9) of toluene with both intra- and inter-column variations.

Column	k	Intra-column RSD (%)	Difference (%)
80% ACN, 100 μm	0.43	0.4-2.3	6.0
		Intra-column RSD (%)	**Inter-column RSD (%)**
90% ACN, 100 μm	0.34	0.4-1.5	20
100% acetone, 100 μm	0.37	0.3-1.8	29
80% ACN, 75 μm	0.31	0.6-1.3	8.5
90% ACN, 75 μm	0.27	0.9-1.4	26
100% acetone, 75 μm	0.31	0.3-1.2	15

To summarize the retention factor data, generally high inter-column variations confirm that packing core-shell particles in nLC columns is challenging.

To conclude the column performance study, the columns were difficult to reproduce, and there was no obvious trend on column performance solely based on slurry solvent or column ID. Furthermore, the packing procedure seemed sensitive to external factors; therefore, the efficiency was not tested on later packed columns. However, 90% ACN (100 μm ID) and 100% acetone (both 75 and 100 μm ID) performed best regarding plate number, asymmetry, and retention factor variability. Based on these results and the fact that a smaller ID gives better

sensitivity enhancement due to the downscaling effect, the 75 μm ID column packed with 100% acetone as slurry solvent was selected for further use.

4.2.3 Evaluation of the in-house packed 5 μm phenyl-hexyl particles being suitable as stationary phase in the trap column

For successful on-line sample clean-up, a suitable trap column SP had to be identified. Fully porous 5 μm PH particles were proposed as suitable for trap columns, being the same SP as the analytical column but with a larger particle size. However, the 5 μm particles are fully porous (vs. core-shell particles), which may yield a larger surface area for retention. A lower retention factor for the trap column is necessary to ensure refocusing of the analyte in the analytical column and proper elution of the analytes off the trap column with the MP optimal for separation on the analytical column. The retention factors for the trap- and analytical columns were compared to determine whether the 5 μm particles were suitable as trap column particles.

A 100 μm ID column was packed with the 5 μm fully porous PH particles in 100% acetone. An average retention factor for toluene of 0.54 (RSD 8.8%) was obtained, which was greater than the retention factor of all the columns packed with 2.5 μm particles ($k < 0.44$). A trap column packed with 5 μm PH particles was hence not suitable for the nLC platform. The set-up for testing is described in **chapter 3.7.2**, and the raw data are summarized in **Table 21** in **chapter 7.5.4** in **Appendix**.

The retention factor was also tested with oxysterols, as these may have different interactions with the SP and hence, were more relevant for comparison. A 1 ng/mL 25-OHC evaluation solution was used for testing with MS-detection (as Girard T-tagged oxysterols do not have UV-absorbance), resulting in a lower retention factor on the 5 μm PH particles than for the 2.5 μm SPH particles (1.1 and 4.1, respectively), suggesting that the 5 μm PH particles were suitable for the specific purpose of oxysterol quantification. Platform I (described in **chapter 3.7.3**) was used for the testing, and the raw data are summarized in **Table 22** in **chapter 7.5.4**. in **Appendix**.

To conclude, the 5 μm PH particles were suspected to be well-suited in trap columns for oxysterols as 25-OHC had a lower retention factor on the columns packed with these particles compared to columns packed with the 2.5 μm SPH particles.

4.3 Optimization of mass spectrometer parameters

The development of a miniaturized LC-MS platform involved using a different MS than in the conventional UHPLC-MS method, and MS parameter optimization had to be performed on the TSQ Quantiva triple quadrupole MS. Optimized MS-transitions for both quantifier and qualifier ions were determined along with the respective collision energies. Only one compound from each mass was selected as precursor ions (derivatized 25-OHC (10 μg/mL), 25-OHC-d_6 (10 μg/mL), and 22R-OHC-d_7 (2 μg/mL)) for direct injection. The optimized values are summarized in **Table 13**. It was assumed that 22R-, 24S-, and 27-OHC would have the same fragmentation pattern and collision energies as 25-OHC and that 27-OHC-d_6 would have the same fragmentation pattern and collision energies as 25-OHC-d_6. The set-up used for the optimization is described in **chapter 3.7.4**.

Table 13. The optimized quantifier and qualifier MS-transitions for 25-OHC, 25-OHC-d_6, and 22R-OHC-d_7 and the respective collision energies.

Compound	Ion type	Transition	Collision energy
25-OHC	Quantifier	514.5 → 455.410	35
	Qualifier	514.5 → 437.398	40
25-OHC-d_6	Quantifier	520.5 → 461.445	35
	Qualifier	520.5 → 443.398	39
22R-OHC-d_7	Quantifier	521.5 → 462.418	37
	Qualifier	521.5 → 434.443	35

4.4 Miniaturization of the chromatographic platform

4.4.1 Assembly and automation of the nLC-MS platform

The in-house packed analytical and trap column (2.5 μm SPH particles packed with 100% acetone in 17 cm x 75 μm ID and 5 μm PH particles packed with 100% acetone in 9 cm x 180 μm ID, respectively) were assembled in Platform II as described in **chapter 3.7.5**. The 10-port-valve-set-up was inspired by Brandtzaeg *et al*. [151], but with the jumper positioned, so that backflushing of the trap column was avoided. The trap column only had a frit at the outlet of the column, and the backflushing would potentially flush the particles out of the column.

Developing a properly functioning miniaturized chromatographic platform required several parameters and technical issues to be settled. First, a pump able to deliver sufficiently low flow rates in the nL/min-scale and an autosampler capable of delivering sufficiently low enough injection volume in the nL-μL scale were desired. Second, the system had to be connected with downscaled tubings and connections to fit the downscaled columns. Hence, the narrowest nanoVipers available (20 μm ID) were purchased to minimize the extra-column volume. Lastly, appropriate connections had to be identified for the UHPLC-platform to run smoothly at pressures up to ~1000 bar. Regular SST-ferrules withstand the high backpressures but will break the fragile fused silica capillaries when assembled, while vespel/graphite ferrules are compatible with the fused silica capillaries but are not able to withstand the higher backpressure (< 450 bar) associated with UHPLC. New direct-connect 360 μm FS tubing UHPLC-Fittings (UHPLC-connections), compatible with both fused silica capillaries and withstanding UHPLC backpressures up to 1700 bar, were therefore tested. The UHPLC-connections are illustrated in **Figure 22**.

Automation

The goal of building an automated platform required the 10-port valve, EASY-nLC 1200 pump, and the TSQ Quantiva triple quadrupole MS to communicate. The pump was coupled to the MS with cables in “Start In” and “Ground inlets” on the MS to initiate the MS-scanning when a programmable signal was sent from the pump when the gradient started. Additionally, the 10-port valve was equipped with an automatic selector valve for automatic switching with cables in “Injection Hold” and “RO/IH” outlets on the MS. The valve switched when a programmable constant signal was received from the MS (signal programmed through the instrument method

in the Xcalibur software), such that the filter could be backflushed (remove particle debris) after loading.

A 10-port-2-position valve able to withstand a high backpressure (1000 bar) was used. Incompatibility between the 10-port valve and the automatic selector valve for automatic switching was identified when the rotor in the 10-port-valve "centered" between positions during injections. It was suspected the 10-port valve had slow rotors to withstand high pressures, causing a mismatch with the automatic selector valve. Therefore, the automatic selector valve was substituted with one compatible with high-pressure 10-port valves (1000 bar), which solved the issue. With this alteration, a fully automated nLC-MS-platform was successfully built.

4.4.2 Technical challenges and troubleshooting

The AFFL-trap-column-nUHPLC platform required several narrow nanoVipers (10-50 μm ID) coupled to the 10-port valve matching the nL/min-flow. Identifying leakages in these connections was especially challenging and laborious, as the amount of leakage was hardly visible. Air bubbles, known to disrupt stable backpressures, were also challenging to eliminate from the platform, highlighting the importance of proper off-line degassing. The EASY-nLC 1200 pump does not have a built-in degasser, and therefore, degassing (e.g., He-gas or sonication) had to be performed beforehand.

For the reasons mentioned above, technical challenges are highly associated with the assembly and development of an nLC platform. Moreover, combining nLC with UHPLC-particle-columns only increased the challenges as the higher backpressures required special pumps, valves, tubings, and connections.

Conventional HPLC-connections of SST or vespel/graphite had to be replaced by special UHPLC-connections for the fused silica trap- and analytical column to withstand the high backpressure. The UHPLC- connections required delicate handling, as they would be worn out if tightened too hard. However, it was discovered that the UHPLC-connections could be drilled open after being too tight and were hence found to be reusable and a well-suited option for coupling fused silica columns. The connections were also compatible with Viper-unions for an easy zero-extra-column-volume connection together with a nanoViper, as seen in the real-life image of the coupling of the trap column in **Figure 24.** Additionally, considering how the trap

column was connected directly to the 10-port valve with the UHPLC-connection (illustrated in **chapter 3.7.5**), the trap column easily broke when assembled. This resulted in laborious method development as new trap columns had to be packed.

To sum up, nLC combined with UHPLC-backpressures was time-consuming and required special technical skills of the operator achieved over time through experience. Additionally, the new UHPLC-connections were found to be well-suited for their purpose and eventually satisfactory for easy handling and connection, and withstood the high backpressure without creating leakages.

4.4.3 Development and assessment of the oxysterol separation

The nLC-MS platform (Platform II) was assembled, and evaluation solutions with the analytes 22R-, 24S-, 25-, and 27-OHC (concentration range of 13-108 pM each), and the ISs 25-OHC-d_6, 27-OHC-d_6, and 22R-OHC-d_7 (50 or 100 pM each) were used to investigate the separation of the oxysterol isomers. The nLC-MS set-up used for the testing of the oxysterol separation is described in **chapter 3.7.5**. **Figure 28** presents an overview of how the sterol separation was approached, including what steps resulted in improved separation.

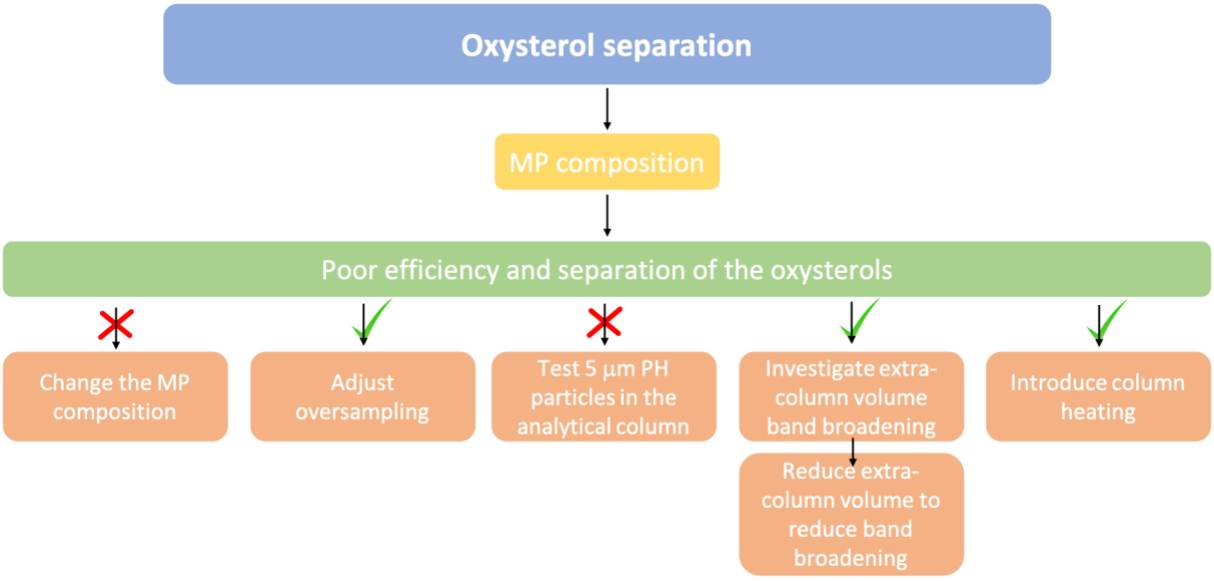

Figure 28. A flow chart showing the overview of how sterol separation was approached, including what steps resulted in an improvement in separation. The testing of the 5 µm PH particles in the analytical column is found in **chapter 7.3.2** in **Appendix**.

Mobile phase composition determination

As the miniaturized LC-platform used a binary pump (2 MP inlets) while the conventional UHPLC-platform used a quaternary pump (4 MP inlets), the organic modifiers (ACN and MeOH) of the MP had to be merged into MP B to achieve the desired composition of 57/33/10 water/ACN/MeOH (v/v/v) from the conventional method. The MP B also had to contain at least 5% water due to pump requirements. The MP A, used by the pump as default for sample loading onto the trap column, contained no organic modifier to maximize the trapping efficiency of the sterols during loading. Hence, MP A consisted of 0.1% FA in water, and MP B consisted of 0.1% FA in 72/23/5 ACN/MeOH/water (v/v/v), which would match the desired composition when a 55/45 MP A/B elution was run. These are the MPs used further unless otherwise are stated.

A 5-95% B gradient over 25 min at a 500 nL/min flow rate was used as a starting point for elution optimization. This gradient resulted in coelution of the oxysterols and ISs at ~22 min, as shown in **Figure 29**. Calculations revealed that the coelution occurred at ~84% B. Isocratic elution of a lower %B, namely 60%, was tested to improve separation but without success (results not shown). MP B was systematically decreased by 5% while achieving the best separation at 45% B, as shown in **Figure 30A** and **Figure 30C**. This matches the MP composition used in the conventional UHPLC method. The flow rate was held constant at 500 nL/min with a pressure of ~410 bar.

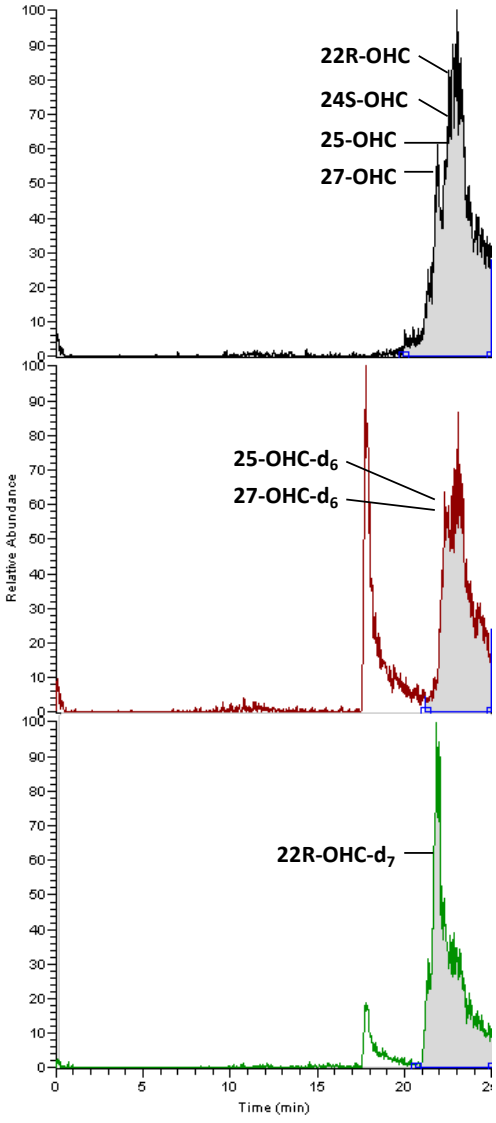

Figure 29. EIC of 0.54 fmol 22R-, 24-S, 25-, and 27-OHC, and 0.5 fmol 25- and 27-OHC-d_6 and 22R-OHC-d_7 when a 5-95% B gradient was run on Platform II with a 2.5 µm SPH (170 mm x 75 µm ID) analytical column and a 5 µm PH (90 mm x 180 µm ID) trap column at ambient temperature.

Separation of the compounds was complicated by very broad peaks, which increased the need for further separation. Analysis time of 50 min was also considered too high. To enhance separation further without increasing the analysis time, 43% B with a 750 nL/min flow rate was tested. However, the separation remained the same, and the analysis time increased by 10 min. Increasing the flow rate naturally also increased the backpressure to ~630 bar, almost reaching the upper-pressure limit at 690 bar (pressure limit set by the 10-port-valve), limiting the method to a ~750 nL/min flow rate. Although the peaks were very broad, the system at least provided a high level of sensitivity, as 0.54 fmol of the oxysterols gave high-intensity signals.

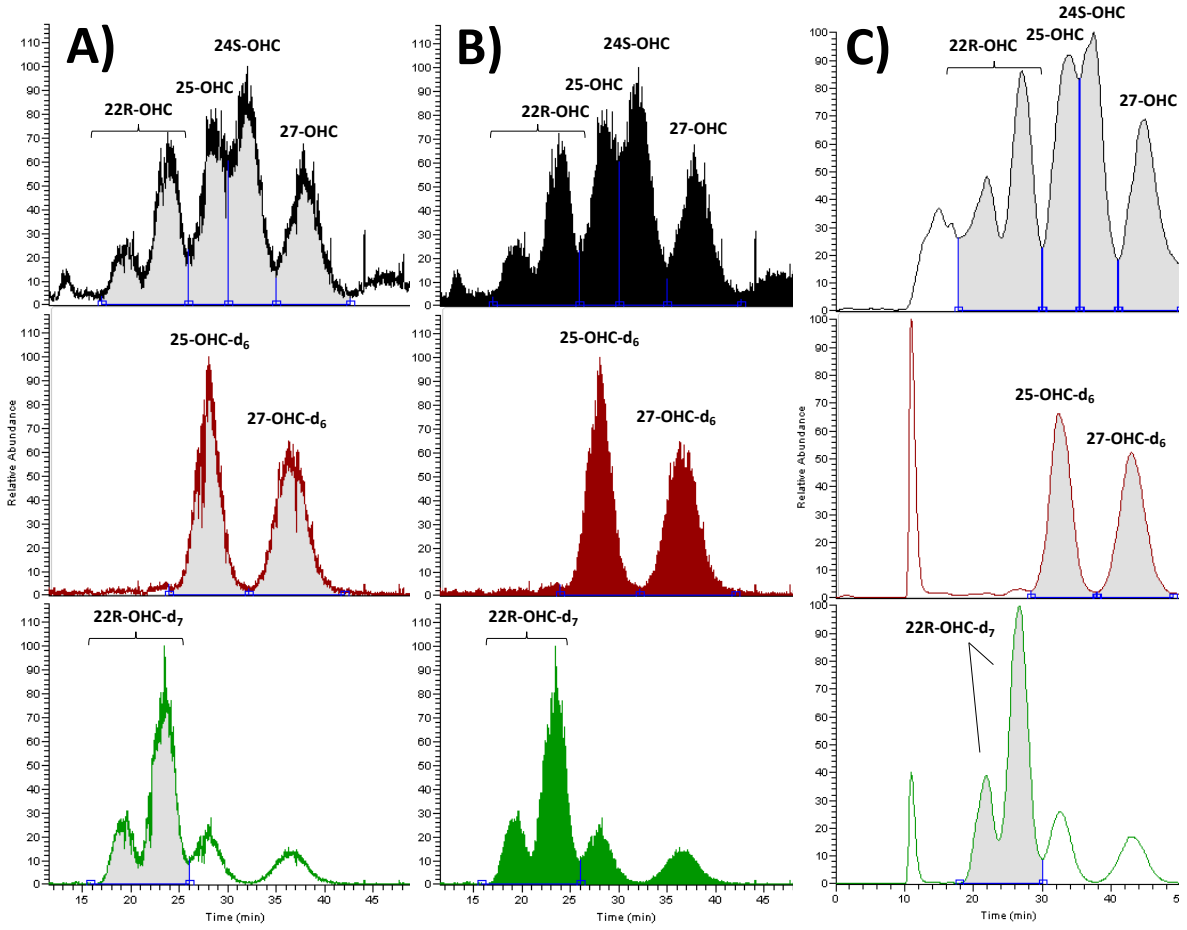

Figure 30. EIC of 0.54 fmol 22R-, 24S-, 25-, and 27-OHC and 0.5 fmol of the ISs 25-OHC-d_6, 27-OHC-d_6 and 22R-OHC-d_7 A) eluted with 55/45 MP A/MP B (MP A: 0.1% FA in water and MP B: 0.1% FA in 72/23/5 ACN/MeOH/water (v/v/v)) at a 500 nL/min flow rate on Platform II with a 2.5 µm SPH (170 mm x 75 µm ID) analytical column, and a 5 µm PH (90 mm x 180 µm ID) trap column at ambient temperature. B) Same as the chromatogram in A), but with a "stick"-display showing the oversampling as each "stick" (cannot be seen) represents one data point. As the entire chromatogram is shaded, it demonstrates that too many data points are generated over each peak. C) Smoothened peaks after cycle time and chrom. filter was adjusted in the instrument method to more suitable values for broad peaks. The same conditions as described in A) were used.

To obtain the same linear velocity in the downscaled method as in the conventional UHPLC-MS method (column ID: 2.1 mm), the flow rate should be 890 nL/min. However, a flow rate of 890 nL/min would exceed the upper-pressure limit of 690 bar. The conventional method additionally uses a column oven temperature of 55 °C, which decreases the viscosity of the MP and hence, decreases the backpressure allowing higher flow rates. The nLC column was operated at ambient temperature giving limitations regarding the linear flow rate compared to that of the conventional UHPLC method.

To conclude, at this point, the best separation of the oxysterols and the ISs on the 2.5 µm SPH particle column was obtained with a 55/45 MP A/MP B composition at a flow rate of 500 nL/min. However, peak broadening was a challenge.

Oversampling

The peaks in the chromatograms were very "noisy", indicating MS oversampling (generating too many data points over each peak). Ideally, 15-20 data points should be generated across each peak, and the cycle time should be adjusted accordingly. Hence, with several minutes' broad peaks, fewer data points should be generated per min. The oversampling is shown in the stick-format chromatogram in **Figure 30B**. The cycle time and chrom. filter were adjusted in the instrument method to 6 and 135, respectively. **Figure 30C** shows the chromatogram after the adjustment, showing improvements in peak noisiness.

Changing the organic modifier in the MP

As the separation of the oxysterols had to be enhanced, removing the ACN and increasing the amount MeOH in the MP's was tested, as Røberg-Larsen *et al.* successfully separated 22R-, 24S-, 25-, and 27-OHC with both isocratic 95% MeOH and gradient 75-90% MeOH over 25 min (on a C18 SP, however) [78, 152].

The MP B was changed to 0.1% FA in 95/5 MeOH/water (v/v), and a 5-95% B gradient over 30 min at a 500 nL/min flow rate was used as a starting point. Coelution was observed at 30 min, and 80% isocratic B was further tested without successful separation (results not shown). The MP B was systematically decreased by 5% until the best separation was obtained at 70% B (**Figure 31**). The analysis time was 60 min, not providing sufficiently low analysis time, combined with still poor separation. Different gradients were also tested without success.

Thus, the MP B consisting of only MeOH was not further investigated due to insufficient oxysterol separation.

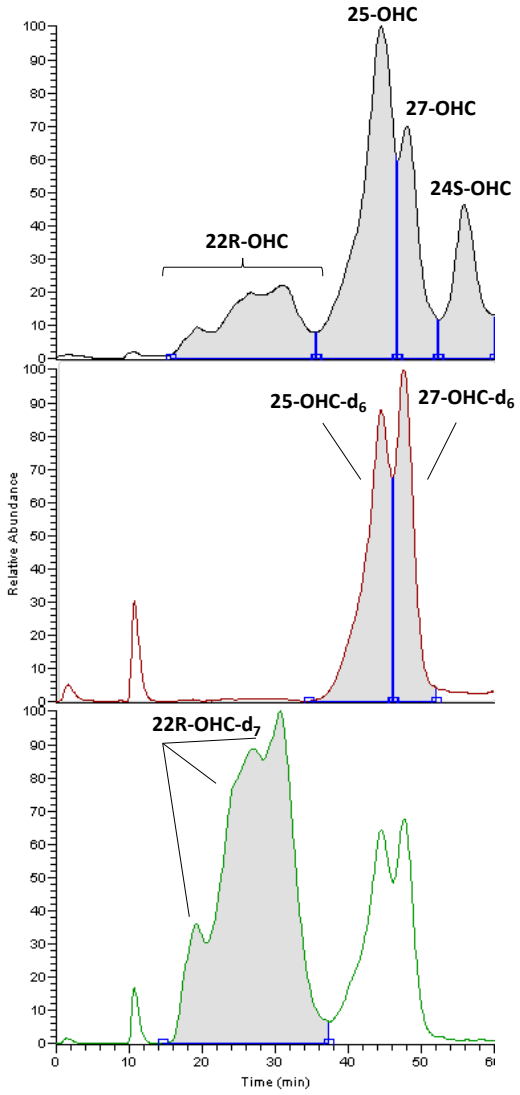

Figure 31. EIC of 0.54 fmol 22R-, 24-S, 25-, and 27-OHC, and 0.5 fmol 25- and 27-OHC-d_6 and 22R-OHC-d_7 when isocratic 70% B was run on Platform II with a 2.5 µm SPH (170 mm x 75 µm ID) analytical column and a 5 µm PH (90 mm x 180 µm ID) trap column at ambient temperature.

Additional experiments were made but did not improve the separation efficiency. The experiments are included in **chapter 7.3.2** in **Appendix**.

Investigating extra-column volume band broadening

As the peaks obtained were very broad at this point, and the platform consisted of many tubings and connections, it was desired to determine whether it was the column or the extra-column platform parts that provided most of the band broadening. Hence, direct injection onto the analytical column was explored. To remove Girard T-reagent, SPE was performed off-line on a 500 pM derivatized 22R-, 24S-, 25-, and 27-OHC and 200 pM 25-, and 27-OHC-d_6, and 22R-OHC-d_7 evaluation solution and injected directly onto the analytical column, surpassing possible extra-column volumes. With isocratic elution of 45% B and a 500 nL/min flow rate on a newly packed column, the efficiency, separation, and analysis time (25 min) were improved, as illustrated in **Figure 32A**. This confirmed that a lot of the band broadening happened outside of the column. The nLC-MS set-up used was Platform I and is described in **Figure 20** in **chapter 3.7.3**.

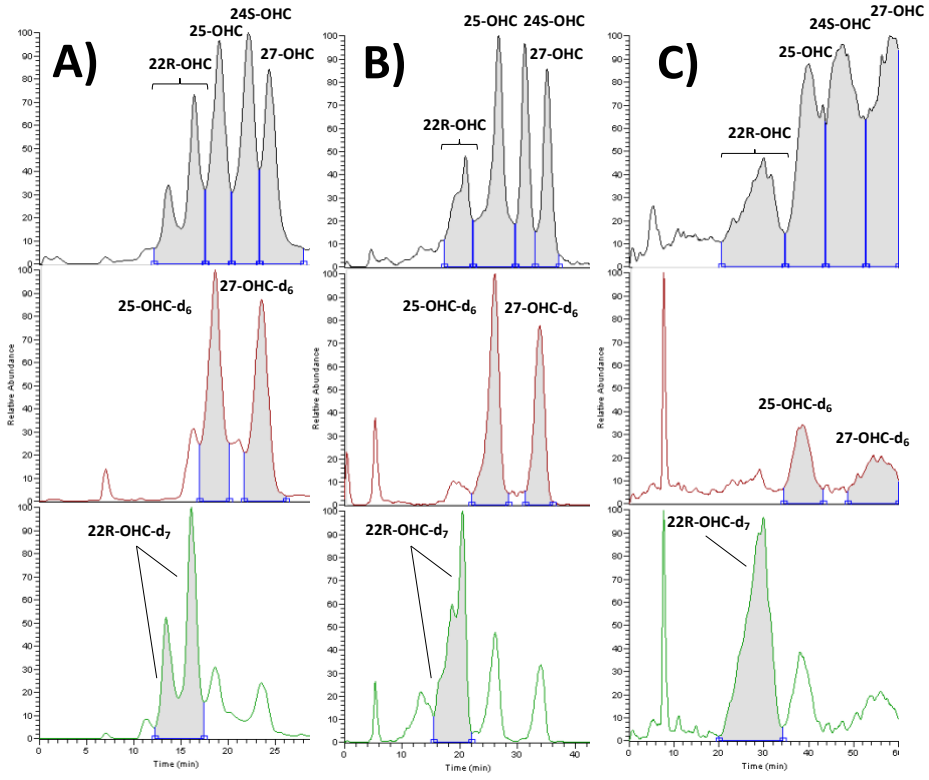

Figure 32. EIC of 0.54 fmol of the oxysterols using a 2.5 µm SPH column (165 mm x 75 µm ID) A) without the extra-column platform parts (Platform I) with 55/45 MP A/MP B (MP A: 0.1% FA in water and MP B: 0.1% FA in 72/23/5 ACN/MeOH/water (v/v/v)) at a 500 nL/min flow rate at ambient temperature, B) without the extra-column platform (Platform I) at the optimized conditions of 61/39 MP A/MP B (MP A: 0.1% FA in water and MP B: 0.1% FA in 72/23/5 ACN/MeOH/water (v/v/v)) at an 890 nL/min flow rate and 55 °C column temperature, C) with the extra-column platform (Platform II) connected including the 5 µm PH trap column (90 mm x 180 µm ID) under the same conditions described in B).

Introducing the Butterfly Portfolio Heater for nLC column heating

Column efficiency can be increased by increased column temperature, with the bonus of allowing higher flow rates (as the heat decreases the MP viscosity, decreasing the backpressure). Column temperature was already exploited in the conventional UHPLC-MS platform (55 °C).

In the nLC platform, the column was directly coupled to the emitter of the ion source, and heating was hence technically challenging. Therefore, specialized equipment in the form of the Butterfly Portfolio Heater (**Figure 33**) was purchased, compliant with the nLC column lying inside the nESI source (**Figure 33C**). The heater would possibly allow the same linear velocity (890 nL/min) as in the conventional UHPLC-MS platform.

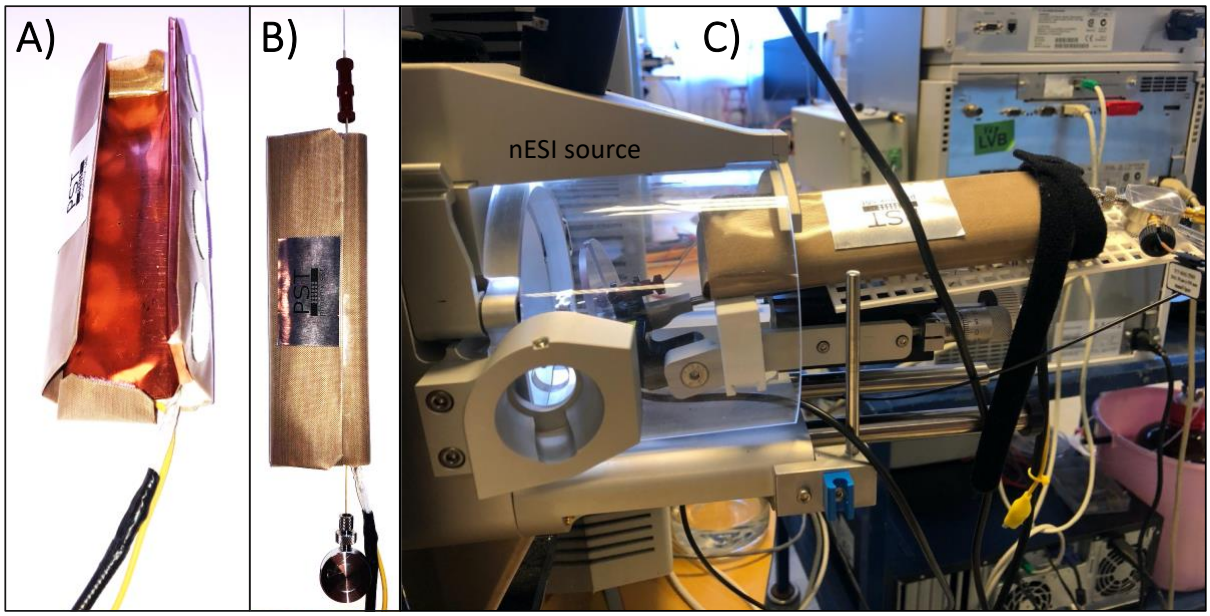

Figure 33. Pictures of the Butterfly Portfolio Heater A) in its open condition, B) in its closed condition with the nLC column inside, and C) operative lying inside the nESI source.

The Butterfly Portfolio Heater was introduced on Platform I to investigate its effect on the separation efficiency. The temperature of 55 °C was tested, resembling the conventional UHPLC-MS method. The linear velocity of 890 nL/min was now possible. The separation was optimized without the filter, trap column, and tubings, and the MP composition was systematically decreased from 45%, with the best separation reached at 39% B (**Figure 32B).** As expected, the % MP B was lower as the elution strength of the MP increases with

temperature. It should be mentioned that a new analytical column was used, which may have contributed to the improved efficiency.

All oxysterols were well-separated and eluted within 38 min. The filter, trap column, and tubings were attached using the optimized conditions producing the chromatogram shown in **Figure 32C**. The oxysterols were now barely separated and not even completely eluted within 60 min. These experiments made it clear that the majority of the band broadening was caused by extra-column volumes. Although contrary to previous results, this massive increase in band broadening was suspected to arise from trap column incompatibility. It was suspected that the optimized MP composition was insufficient to elute the oxysterols quickly off the trap column, thus, adding significant band broadening.

To sum up, the 5 μm PH particles showed to be inappropriate in the trap column after all (contrary to what earlier results showed), as the MP composition 61/39 A/B sufficient for oxysterol separation on a column packed with the 2.5 μm SPH particles alone was not sufficient to elute the oxysterols off the trap column. This contributed to the majority of the band broadening, and the 5 μm PH particles were hence not further used.

4.4.4 Redesign of the trap column and AFFL-set-up for extra-column volume reduction

As the extra-column volume showed major contributions to the band broadening, a redesign of the previous trap column and AFFL-set-up was performed, resulting in Platform III. The platform is described in **chapter 3.7.6**. Redesigning included moving the trap column closer to the analytical column as this allows the analytes to be eluted directly onto the analytical column hence, reducing band broadening. In practice, this meant moving the trap column from between ports 3 and 6 directly into the SST tee before the analytical column. The ID of the PEEK-tubings on the in- and outlets of the filter was also reduced from 100 μm to 64 μm. These changes reduced the extra-column volume by one nanoViper (150 mm x 20 μm ID), two rotor tracks (3 mm x 150 μm ID), and four stator holes (2 mm x 150 μm ID) and halved the total extra-column volume from 1881 nL to 938 nL. Changes are shown in **Figure 23** compared to **Figure 21**.

4.4.5 Investigating other trap column stationary phases

As the 5 µm PH particles were shown as inappropriate as trap column SP, other SPs had to be explored. The other SPs for the trap column tested are summarized in **Figure 34**.

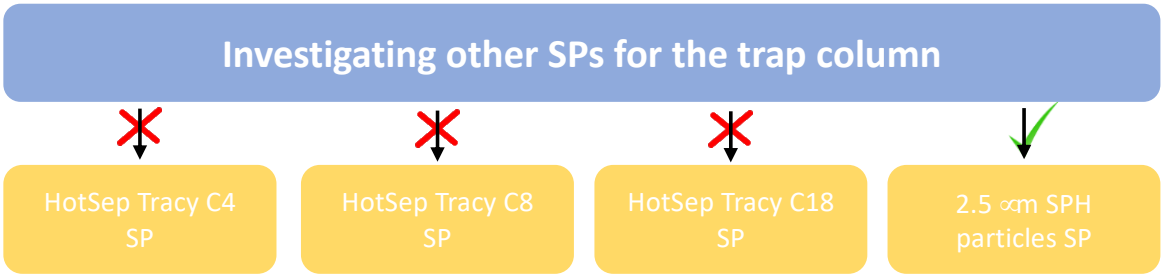

Figure 34. The different SPs tested as the trap column.

Testing HotSep Tracy C4, C8, and C18 (5 mm x 300 µm ID) as the trap column

Commercial HotSep Tracy (5 mm x 0.3 mm ID, 5 µm particles) columns were tested with C4, C8, and C18 as the SP. The SP with C4 and C8 were expected to be more suitable as their chemical structure suggests less retention of the oxysterols than on a PH SP. The SP with C18, however, was expected to have more retention. Experiments with the C18 and C8 SPs gave high-intensity noise, indicating that the oxysterols were present, however, lacking refocusing in the analytical column. These results were unexpected as these trap columns functioned in the conventional UHPLC-MS platform. For the C4 SP, no signal was obtained, suggesting that the SP was insufficient for oxysterol retention. It was also suspected that the loading pressure of 700 bar might have caused the oxysterols to "blow-off" the trap column during loading. Loading pressures of 400, 200, and 100 bar were therefore tested but without signal intensity improvements. The loading pressure did hence not seem to be the problem. Thus, the HotSep Tracy columns were not further investigated as trap columns for the 2.5 µm SPH particles.

Testing the 2.5 μm SPH particles as trap column

A trap column with identical SP as the analytical column is not ideal regarding refocusing. Additionally, an increased temperature on the analytical column could be problematic as it would decrease the retention factor compared to that on the trap column. However, a trap column with the 2.5 μm SPH particles was tested as the last option. In addition, 5% MeOH was added to the MP A to ensure that SP collapsing would not become an issue.

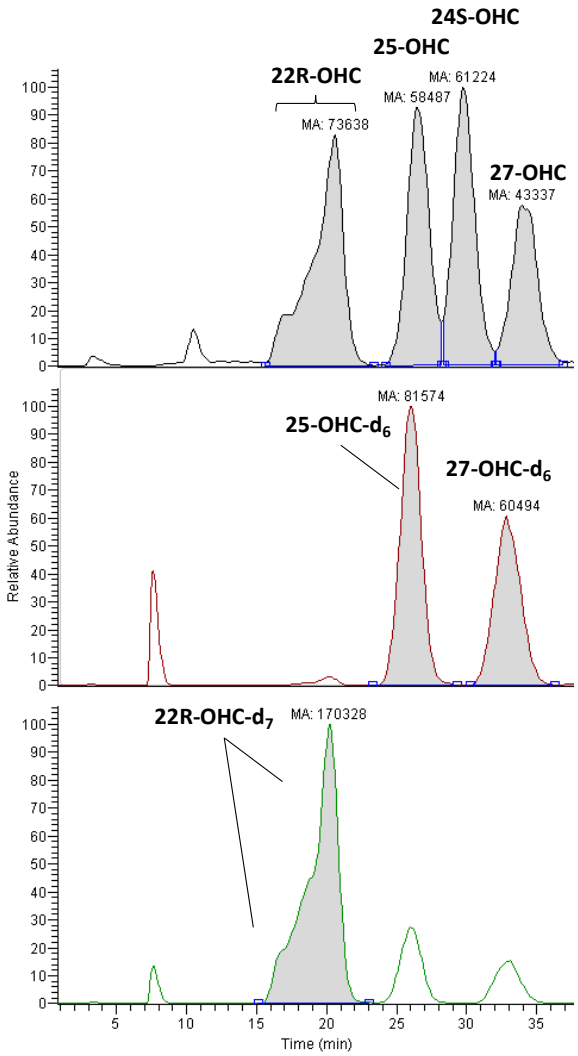

Figure 35. EIC of 0.54 fmol of the oxysterols on Platform III with a 2.5 μm SPH analytical column (185 mm x 75 μm ID) and a 2.5 μm SPH trap column (30 mm x 75 μm ID). Isocratic elution was at an 890 nL/min flow rate with 61/39 MP A/MP B at 55 °C.

A 2.5 μm SPH trap column (~3 cm x 75 μm ID) was packed, and a 108 pM evaluation solution was tested with 38-44% B (MF B increased by 1% for each run). All oxysterols and ISs were close to baseline separated and eluted within 37 min at 39% MP B (**Figure 35**). It should also be mentioned that a newly packed analytical column was used and had a length of 18.5 cm. The new column may have added to the improvement of the separation due to more plates. The oxysterols were now well-separated, although the peaks were still suffering from band broadening.

However, the chromatogram was not repeatable after the platform was detached and reattached to the MS, leaving a suspicion of short column lifetime, possibly due to large pressure drops (550-730 bar) between injections. As the columns only had frits at the outlet and not at the inlet, the particles could experience pull-back between injections, resulting in a more loosely packed bed and a poor lifetime. Newly packed columns were also tested but without improvement.

Hence, the efficient separation was not easily repeated. The challenges regarding repeatability of the efficiency resemble what was seen during column packing of 75 μm ID columns packed with 100% acetone as the variation in plate number between the columns was almost 21%, as described in **chapter 4.2.2**.

As the column efficiency had been an issue throughout this study, optimization of the slurry concentration should have been performed as proposed by Jorgenson and colleagues to be necessary with core-shell particles regarding particle size, particle roughness, column dimensions, and slurry solvents [131]. Perhaps the adapted slurry concentration of 30 mg particles/mL solvent held constant in this study was too high and created particle aggregation, or too low, not creating a dense enough packed bed.

To sum up, the combination of the 2.5 μm SPH particles in both the trap- and analytical column provided close to baseline separation of the oxysterols for two injections. However, the separation was difficult to repeat, both with the same columns and newly-packed ones. The repeatability challenges also resemble the variation in plate numbers between columns seen during column performance testing. The robustness of the columns was hence poor due to short lifetimes.

4.4.6 Investigating particle- and platform robustness

As the in-house packed nLC columns with the 2.5 μm SPH particles had issues regarding robustness, SEM images were taken of both the packed and unpacked 2.5 μm SPH particles to investigate if the particles could be damaged. Additionally, the nLC-MS platform robustness was tested with a commercial nLC analytical column.

Scanning electron microscope investigating 2.5 μm SPH particle robustness

The SEM images are presented in **Figure 36**. The particles looked similar in the unpacked (left) and packed (right, used for UHPLC-MS experiments) state. This indicated that no damage had happened during packing and that the particles were not the problem. Additionally, according to the producer, the commercial 2.5 μm SPH (150 x 2.1 mm ID) column can withstand backpressures up to 1000 bar, which supports the conclusion.

An attempt to get images of the 95 Å pores in the particles was also performed to investigate damage in the pores, but the resolution at such a small scale (~10 nm) was not successful, and

images of the pores were hence not retrieved. However, as the particles looked ordinary, it was not expected that the pores were damaged.

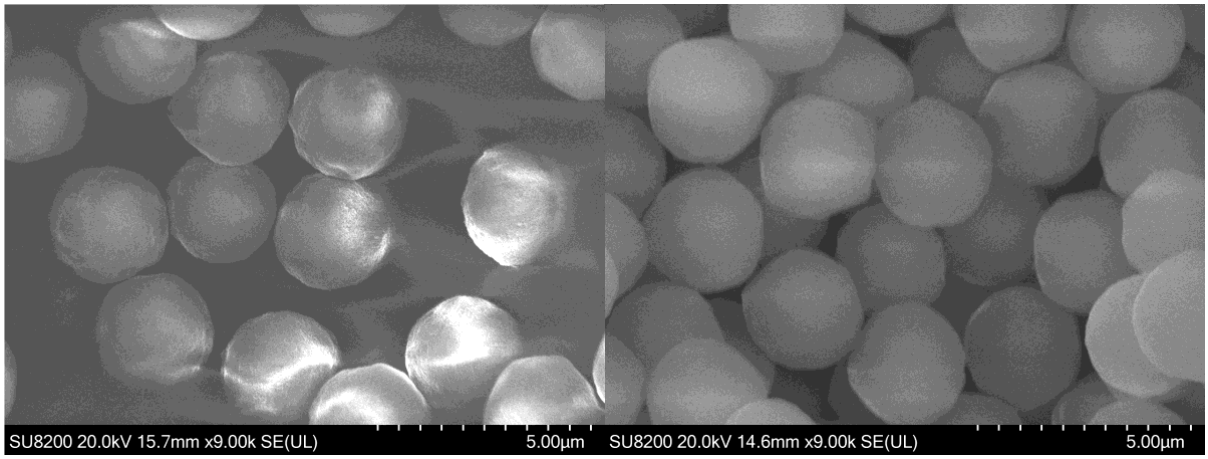

Figure 36. SEM images of the unpacked (left) and packed (right) 2.5 µm SPH-particles in a fused silica capillary used for UHPLC-MS experiments. The SEM images were taken by Inge Mikalsen.

To conclude, the 2.5 µm SPH particles in the in-house packed fused silica capillaries did not look damaged compared to the unpacked particles in the SEM images. This indicated that the particles were not the problem related to the poor robustness of the nLC columns.

Investigating platform robustness with a commercial nLC column

As the particles did not appear to be the problem, it was desired to explore the robustness of the platform. A commercial ACE 3 C8 nLC column (150 x 0.1 mm) was used as the analytical column combined with a commercial HotSep Tracy C8 (5 x 0.3 mm) as a trap column. Although the column had another SP, expected to provide a different selectivity, robustness regarding repeatable injections could still be explored. Platform IV was used, as described in **chapter 3.7.7**.

An 890 nL/min flow rate was used, and the optimized MP composition was found to be 57/43 MP A/MP B at ambient temperature. The oxysterols were baseline separated and eluted within 17 min, except the 25- and 24S-OHC. The 25- and 24S-OHC were assumed to totally coelute as 24S-OHC could not be seen at all, and the 25-OHC peak had over twice as a big peak area as the 22R-OHC and 27-OHC (**Figure 37**). An isocratic 45% B was tested to separate the coeluting peaks, but the C8 SP did not provide good enough selectivity, and the separation was unsuccessful.

The combination of the commercial columns proved to be more robust, as three injections of each evaluation solution (13, 27, 54, 81, and 108 pM) all provided similar separation, retention times, and peak shapes. The MP composition was also more robust as a 2%-increase in MP B only decreased the overall retention time by 3 min (vs. 7 min on 1%-increase on the 2.5 µm SPH columns). The enhanced repeatability indicated that it was not the extra-column volume of the platform that lacked robustness but rather the in-house packed analytical- and trap columns with the 2.5 µm SPH particles suffering from pressure drops during nLC-MS experiments, possibly creating a more loosely packed bed.

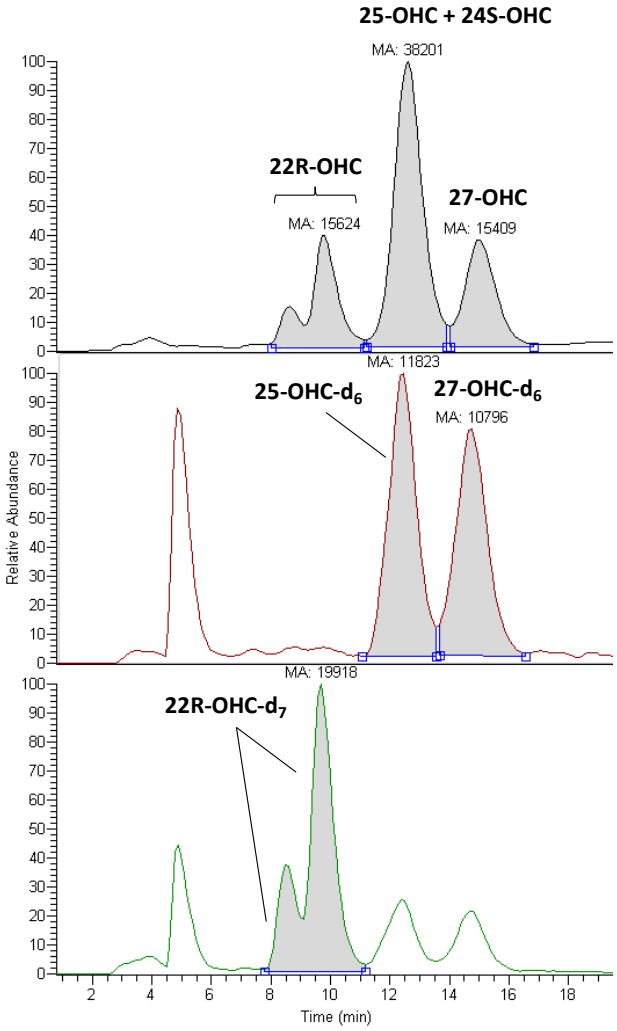

Figure 37. EIC of 0.54 fmol oxysterols on an ACE 3 C8 (150 x 0.1 mm ID) analytical column combined with a HotSep Tracy C8 (5 x 0.3 mm ID) trap column in Platform IV. A flow rate of 890 nL/min with 57/43 MF A/MF B was used at ambient temperature.

To sum up, the commercial ACE 3 C8 and HotSep Tracy C8 columns proved to be more robust than the in-house packed 2.5 µm SPH columns, indicating that the in-house packed columns with the 2.5 µm SPH particles were not robust enough to produce repeatable measurements of oxysterols in liver organoids.

4.5 Liver organoids

As stated, the plan was to analyze liver organoids. Still, due to unexpectedly many challenges regarding the development of the nLC-MS method, the time was not sufficient for further method development, and hence, organoid analysis was not conducted.

5 Conclusion and further work

In this study, an automated on-line sample preparation was successfully built in the nUHPLC-MS platform that contained an SST filter and a trap column. An SP for the trap column was successfully discovered (2.5 µm SPH particles), even though further advances can be made here. The 5 µm fully porous PH particles were found to be inappropriate as the SP in the trap column combined with the 2.5 µm SPH particles in the analytical column.

Efficient and highly sensitive 75 µm ID nLC columns with 2.5 µm SPH particles were successfully packed. However, the columns had poor lifetimes, and hence, were not particularly robust. The efficient nLC columns were also difficult to reproduce, confirming that core-shell particles are challenging to pack in narrow bore columns and possibly need more custom packing development. Specialized nLC-equipment in the form of the UHPLC-connections and the Butterfly column heater were successfully implemented in the nLC-MS platform, easing the handling of connections in nLC, and enhancing column efficiency, respectively. SEM images revealed that the 2.5 µm SPH particles did not seem to have suffered from column packing or high UHPLC-pressures during nLC-MS experiments. nLC-MS appears to be a promising tool for oxysterol quantification in liver organoids, although advances regarding nLC column robustness should be made. Due to the lack of robustness of the nLC columns, determination of 22R-, 24S-, 25-, and 27-OHC could not be done in liver organoids, either healthy or NAFLD-induced ones. The conclusions of the study are summarized in **Figure 38**.

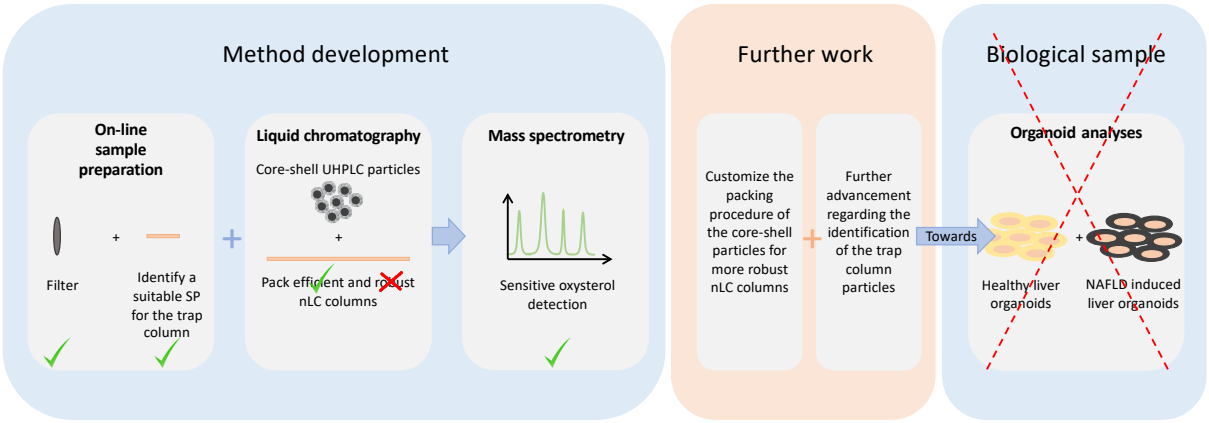

Figure 38. Summary of the conclusion and further work of the study. Further work towards the quantification of oxysterols in liver organoids should include customizing the packing procedure of the 2.5 µm SPH particles and advancements in optimizing the trap column, either by investigating other particles or using a column heater.

Further work should include investigating other suitable SP particles for the trap column or introducing temperature on the trap column as well to achieve the same or smaller retention factor on the trap column for improved refocusing. In addition, customizing the in-house packing procedure for the 2.5 μm SPH particles should be explored to obtain more robust nLC columns, perhaps by making frits on both ends of the column and optimizing the slurry concentration. Finally, if successful quantification of the oxysterols can be achieved, the nLC-MS method should be validated and used for quantification of 22R-, 24S-, 25-, and 27-OHC in liver organoids.

6 References

[1] S.V. Sokolov, K. Tschulik, C. Batchelor-McAuley, K. Jurkschat, R.G. Compton, *Reversible or Not? Distinguishing Agglomeration and Aggregation at the Nanoscale*, Analytical Chemistry, 87 (**2015**) 10033-10039.
[2] *excretion - Merriam Webster Dictionary*, [cited June 17th 2021], https://www.merriam-webster.com/dictionary/excretion
[3] L.S. Ettre, *Nomenclature for chromatography (IUPAC Recommendations 1993)*, Pure and Applied Chemistry, 65 (**1993**) 819-872.
[4] *ex vivo - Biology Online Dictionary*, [cited July 1st 2021], https://www.biologyonline.com/dictionary/ex-vivo
[5] *in vitro - Oxford Dictionary*, [cited June 17th 2021], https://www.oxfordlearnersdictionaries.com/definition/american_english/in-vitro
[6] *in vivo - Oxford Dictionary*, [cited June 17th 2021], https://www.oxfordlearnersdictionaries.com/definition/american_english/in-vivo
[7] T.M. Annesley, *Ion Suppression in Mass Spectrometry*, Clinical Chemistry, 49 (**2003**) 1041-1044.
[8] H. Hedlund, *Calculating Linear Flow Velocity from Volumetric Flow Rate*, Cold Spring Harbor Protocols, 2010 (**2010**) pdb.ip78.
[9] *parenchyma - Lexico by Oxford* [cited June 18th 2021], https://www.lexico.com/definition/parenchyma
[10] *phenotype - Merriam Webster Dictionary*, [cited June 17th 2021], https://www.merriam-webster.com/dictionary/phenotype
[11] L.A. Currie, G. Svehla, *Nomenclature for the presentation of results of chemical analysis (IUPAC Recommendations 1994)*, Pure and Applied Chemistry, 66 (**1994**) 595-608.
[12] J.G. Calvert, *Glossary of atmospheric chemistry terms (Recommendations 1990)*, Pure and Applied Chemistry, 62 (**1990**) 2167-2219.
[13] *sedimentation - Cambridge Dictionary*, [cited June 24th 2021], https://dictionary.cambridge.org/dictionary/english/sedimentation
[14] *surface tension - United States Geological Survey*, [cited June 17th 2021], https://www.usgs.gov/special-topic/water-science-school/science/surface-tension-and-water?qt-science_center_objects=0#qt-science_center_objects
[15] *suspension - Cambridge Dictionary*, [cited June 24th 2021], https://dictionary.cambridge.org/dictionary/english/suspension
[16] A.H. Mokdad, E.S. Ford, B.A. Bowman, W.H. Dietz, F. Vinicor, V.S. Bales, J.S. Marks, *Prevalence of Obesity, Diabetes, and Obesity-Related Health Risk Factors, 2001*, Journal of the American Medical Association, 289 (**2003**) 76-79.
[17] K.G.M.M. Alberti, P. Zimmet, J. Shaw, *The metabolic syndrome—a new worldwide definition*, The Lancet, 366 (**2005**) 1059-1062.
[18] R.H. Eckel, S.M. Grundy, P.Z. Zimmet, *The metabolic syndrome*, The Lancet, 365 (**2005**) 1415-1428.
[19] M.-A. Cornier, D. Dabelea, T.L. Hernandez, R.C. Lindstrom, A.J. Steig, N.R. Stob, R.E. Van Pelt, H. Wang, R.H. Eckel, *The Metabolic Syndrome*, Endocrine Reviews, 29 (**2008**) 777-822.
[20] N. Stefan, H.-U. Häring, K. Cusi, *Non-alcoholic fatty liver disease: causes, diagnosis, cardiometabolic consequences, and treatment strategies*, The Lancet Diabetes & Endocrinology, 7 (**2019**) 313-324.

[21] Z. Younossi, F. Tacke, M. Arrese, B. Chander Sharma, I. Mostafa, E. Bugianesi, V. Wai-Sun Wong, Y. Yilmaz, J. George, J. Fan, M.B. Vos, *Global Perspectives on Nonalcoholic Fatty Liver Disease and Nonalcoholic Steatohepatitis*, Hepatology, 69 (**2019**) 2672-2682.
[22] B. Li, C. Zhang, Y.-T. Zhan, *Nonalcoholic Fatty Liver Disease Cirrhosis: A Review of Its Epidemiology, Risk Factors, Clinical Presentation, Diagnosis, Management, and Prognosis*, Canadian Journal of Gastroenterology & Hepatology, 2018 (**2018**) 2784537-2784537.
[23] Q.M. Anstee, G. Targher, C.P. Day, *Progression of NAFLD to diabetes mellitus, cardiovascular disease or cirrhosis*, Nature Reviews Gastroenterology & Hepatology, 10 (**2013**) 330-344.
[24] A. Wree, L. Broderick, A. Canbay, H.M. Hoffman, A.E. Feldstein, *From NAFLD to NASH to cirrhosis—new insights into disease mechanisms*, Nature Reviews Gastroenterology & Hepatology, 10 (**2013**) 627-636.
[25] N. Chalasani, Z. Younossi, J.E. Lavine, M. Charlton, K. Cusi, M. Rinella, S.A. Harrison, E.M. Brunt, A.J. Sanyal, *The diagnosis and management of nonalcoholic fatty liver disease: Practice guidance from the American Association for the Study of Liver Diseases*, Hepatology, 67 (**2018**) 328-357.
[26] N. Pydyn, K. Miękus, J. Jura, J. Kotlinowski, *New therapeutic strategies in nonalcoholic fatty liver disease: a focus on promising drugs for nonalcoholic steatohepatitis*, Pharmacological Reports, 72 (**2020**) 1-12.
[27] BioRender, *https://biorender.com/*
[28] I. Wanless, K. Shiota, *The Pathogenesis of Nonalcoholic Steatohepatitis and Other Fatty Liver Diseases: A Four-Step Model including the Role of Lipid Release and Hepatic Venular Obstruction in the Progression to Cirrhosis*, Seminars in Liver Disease, 24 (**2004**) 99-106.
[29] R. Pais, A.S.t. Barritt, Y. Calmus, O. Scatton, T. Runge, P. Lebray, T. Poynard, V. Ratziu, F. Conti, *NAFLD and liver transplantation: Current burden and expected challenges*, Journal of Hepatology, 65 (**2016**) 1245-1257.
[30] Z.M. Younossi, G. Marchesini, H. Pinto-Cortez, S. Petta, *Epidemiology of Nonalcoholic Fatty Liver Disease and Nonalcoholic Steatohepatitis: Implications for Liver Transplantation*, Transplantation, 103 (**2019**) 22-27.
[31] D.L. Gorden, D.S. Myers, P.T. Ivanova, E. Fahy, M.R. Maurya, S. Gupta, J. Min, N.J. Spann, J.G. McDonald, S.L. Kelly, J. Duan, M.C. Sullards, T.J. Leiker, R.M. Barkley, O. Quehenberger, A.M. Armando, S.B. Milne, T.P. Mathews, M.D. Armstrong, C. Li, W.V. Melvin, R.H. Clements, M.K. Washington, A.M. Mendonsa, J.L. Witztum, Z. Guan, C.K. Glass, R.C. Murphy, E.A. Dennis, A.H. Merrill, Jr., D.W. Russell, S. Subramaniam, H.A. Brown, *Biomarkers of NAFLD progression: a lipidomics approach to an epidemic*, Journal of Lipid Research, 56 (**2015**) 722-736.
[32] T. Raselli, T. Hearn, A. Wyss, K. Atrott, A. Peter, I. Frey-Wagner, M.R. Spalinger, E.M. Maggio, A.W. Sailer, J. Schmitt, P. Schreiner, A. Moncsek, J. Mertens, M. Scharl, W.J. Griffiths, M. Bueter, A. Geier, G. Rogler, Y. Wang, B. Misselwitz, *Elevated oxysterol levels in human and mouse livers reflect nonalcoholic steatohepatitis*, Journal of Lipid Research, 60 (**2019**) 1270-1283.
[33] W. Cui, S.L. Chen, K.Q. Hu, *Quantification and mechanisms of oleic acid-induced steatosis in HepG2 cells*, American Journal of Translational Research, 2 (**2010**) 95-104.
[34] J. Henao-Mejia, E. Elinav, C. Jin, L. Hao, W.Z. Mehal, T. Strowig, C.A. Thaiss, A.L. Kau, S.C. Eisenbarth, M.J. Jurczak, J.P. Camporez, G.I. Shulman, J.I. Gordon, H.M. Hoffman, R.A. Flavell, *Inflammasome-mediated dysbiosis regulates progression of NAFLD and obesity*, Nature, 482 (**2012**) 179-185.
[35] W.K. Saeed, D.W. Jun, K. Jang, S.B. Ahn, J.H. Oh, Y.J. Chae, J.S. Lee, H.T. Kang, *Mismatched effects of receptor interacting protein kinase-3 on hepatic steatosis and*

inflammation in non-alcoholic fatty liver disease, World Journal of Gastroenterology, 24 (**2018**) 5477-5490.
[36] D. Jahn, S. Kircher, H.M. Hermanns, A. Geier, *Animal models of NAFLD from a hepatologist's point of view*, Biochim Biophys Acta Mol Basis Dis, 1865 (**2019**) 943-953.
[37] J. Kim, B.-K. Koo, J.A. Knoblich, *Human organoids: model systems for human biology and medicine*, Nature Reviews Molecular Cell Biology, 21 (**2020**) 571-584.
[38] P.K. Santhekadur, D.P. Kumar, A.J. Sanyal, *Preclinical models of non-alcoholic fatty liver disease*, Journal of Hepatology, 68 (**2018**) 230-237.
[39] J.R. Clapper, M.D. Hendricks, G. Gu, C. Wittmer, C.S. Dolman, J. Herich, J. Athanacio, C. Villescaz, S.S. Ghosh, J.S. Heilig, C. Lowe, J.D. Roth, *Diet-induced mouse model of fatty liver disease and nonalcoholic steatohepatitis reflecting clinical disease progression and methods of assessment*, American Journal of Physiology Gastrointestinal and Liver Physiology, 305 (**2013**) 483-495.
[40] P. Pingitore, K. Sasidharan, M. Ekstrand, S. Prill, D. Lindén, S. Romeo, *Human Multilineage 3D Spheroids as a Model of Liver Steatosis and Fibrosis*, International Journal of Molecular Sciences, 20 (**2019**) 1629.
[41] P.-A. Soret, J. Magusto, C. Housset, J. Gautheron, *In Vitro and In Vivo Models of Non-Alcoholic Fatty Liver Disease: A Critical Appraisal*, Journal of Clinical Medicine, 10 (**2021**) 36.
[42] S. Hassan, S. Sebastian, S. Maharjan, A. Lesha, A.-M. Carpenter, X. Liu, X. Xie, C. Livermore, Y.S. Zhang, A. Zarrinpar, *Liver-on-a-Chip Models of Fatty Liver Disease*, Hepatology, 71 (**2020**) 733-740.
[43] S.P. Harrison, S.F. Baumgarten, R. Verma, O. Lunov, A. Dejneka, G.J. Sullivan, *Liver Organoids: Recent Developments, Limitations and Potential*, Frontiers in Medicine, 8 (**2021**).
[44] T. Takebe, J.M. Wells, *Organoids by Design*, Science, 364 (**2019**) 956.
[45] X. Yin, Benjamin E. Mead, H. Safaee, R. Langer, Jeffrey M. Karp, O. Levy, *Engineering Stem Cell Organoids*, Cell Stem Cell, 18 (**2016**) 25-38.
[46] A. Lin, F. Sved Skottvoll, S. Rayner, S. Pedersen-Bjergaard, G. Sullivan, S. Krauss, S. Ray Wilson, S. Harrison, *3D cell culture models and organ-on-a-chip: Meet separation science and mass spectrometry*, Electrophoresis, 41 (**2020**) 56-64.
[47] J.P. Cotovio, T.G. Fernandes, *Production of Human Pluripotent Stem Cell-Derived Hepatic Cell Lineages and Liver Organoids: Current Status and Potential Applications*, Bioengineering, 7 (**2020**) 36.
[48] M.A. Lancaster, M. Huch, *Disease modelling in human organoids*, Disease Models & Mechanisms, 12 (**2019**) 39347.
[49] *Method of the Year 2017: Organoids*, Nature methods, 15 (**2018**) 1-1.
[50] L.A. Low, C. Mummery, B.R. Berridge, C.P. Austin, D.A. Tagle, *Organs-on-chips: into the next decade*, Nature Reviews Drug Discovery, 20 (**2021**) 345-361.
[51] Y. Wang, H. Wang, P. Deng, T. Tao, H. Liu, S. Wu, W. Chen, J. Qin, *Modeling Human Nonalcoholic Fatty Liver Disease (NAFLD) with an Organoids-on-a-Chip System*, ACS Biomaterials Science & Engineering, 6 (**2020**) 5734-5743.
[52] M. Kozyra, I. Johansson, Å. Nordling, S. Ullah, V.M. Lauschke, M. Ingelman-Sundberg, *Human hepatic 3D spheroids as a model for steatosis and insulin resistance*, Scientific Reports, 8 (**2018**) 14297.
[53] R. Ouchi, S. Togo, M. Kimura, T. Shinozawa, M. Koido, H. Koike, W. Thompson, R.A. Karns, C.N. Mayhew, P.S. McGrath, H.A. McCauley, R.-R. Zhang, K. Lewis, S. Hakozaki, A. Ferguson, N. Saiki, Y. Yoneyama, I. Takeuchi, Y. Mabuchi, C. Akazawa, H.Y. Yoshikawa, J.M. Wells, T. Takebe, *Modeling Steatohepatitis in Humans with Pluripotent Stem Cell-Derived Organoids*, Cell Metabolism, 30 (**2019**) 374-384.
[54] T.A. Miettinen, *Cholesterol Production in Obesity*, Circulation, 44 (**1971**) 842-850.

[55] K. Pinkwart, F. Schneider, M. Lukoseviciute, T. Sauka-Spengler, E. Lyman, C. Eggeling, E. Sezgin, *Nanoscale dynamics of cholesterol in the cell membrane*, Journal of Biological Chemistry, 294 (**2019**) 12599-12609.
[56] L. Iuliano, G. Lizard, *Oxysterols and related sterols in chemistry, biology and medicine: A dynamic European field of investigation*, Biochimie, 95 (**2013**) 445-447.
[57] J. Yang, L. Wang, R. Jia, *Role of de novo cholesterol synthesis enzymes in cancer*, Journal of Cancer, 11 (**2020**) 1761-1767.
[58] R.H. Nelson, *Hyperlipidemia as a Risk Factor for Cardiovascular Disease*, Primary Care: Clinics in Office Practice, 40 (**2013**) 195-211.
[59] R. Burkhardt, *Hyperlipidemia and cardiovascular disease: reinforcement for 'lower is better'*, Current Opinion in Lipidology, 26 (**2015**) 468-469.
[60] W.M. Pandak, G. Kakiyama, *The acidic pathway of bile acid synthesis: Not just an alternative pathway*, Liver Research, 3 (**2019**) 88-98.
[61] S. Lordan, J.J. Mackrill, N.M. O'Brien, *Oxysterols and mechanisms of apoptotic signaling: implications in the pathology of degenerative diseases*, The Journal of Nutritional Biochemistry, 20 (**2009**) 321-336.
[62] W. Griffiths, H. Jörnvall, *Oxysterols*, Biochemical and Biophysical Research Communications, 446 (**2014**) 645-646.
[63] K. Borah, O.J. Rickman, N. Voutsina, I. Ampong, D. Gao, E.L. Baple, I.H.K. Dias, A.H. Crosby, H.R. Griffiths, *A quantitative LC-MS/MS method for analysis of mitochondrial - specific oxysterol metabolism*, Redox biology, 36 (**2020**) 101595.
[64] A.J. Brown, W. Jessup, *Oxysterols: Sources, cellular storage and metabolism, and new insights into their roles in cholesterol homeostasis*, Molecular Aspects of Medicine, 30 (**2009**) 111-122.
[65] R.J. Fakheri, N.B. Javitt, *27-Hydroxycholesterol, does it exist? On the nomenclature and stereochemistry of 26-hydroxylated sterols*, Steroids, 77 (**2012**) 575-577.
[66] W.J. Griffiths, Y. Wang, *Oxysterols as lipid mediators: Their biosynthetic genes, enzymes and metabolites*, Prostaglandins & Other Lipid Mediators, 147 (**2020**) 106381.
[67] W.J. Griffiths, J. Abdel-Khalik, P.J. Crick, E. Yutuc, Y. Wang, *New methods for analysis of oxysterols and related compounds by LC–MS*, The Journal of Steroid Biochemistry and Molecular Biology, 162 (**2016**) 4-26.
[68] W.J. Griffiths, E. Yutuc, J. Abdel-Khalik, P.J. Crick, T. Hearn, A. Dickson, B.W. Bigger, T. Hoi-Yee Wu, A. Goenka, A. Ghosh, S.A. Jones, D.F. Covey, D.S. Ory, Y. Wang, *Metabolism of Non-Enzymatically Derived Oxysterols: Clues from sterol metabolic disorders*, Free Radical Biology and Medicine, 144 (**2019**) 124-133.
[69] R.B. Corcoran, M.P. Scott, *Oxysterols stimulate Sonic hedgehog signal transduction and proliferation of medulloblastoma cells*, Proceedings of the National Academy of Sciences, 103 (**2006**) 8408.
[70] S. He, E.R. Nelson, *27-Hydroxycholesterol, an endogenous selective estrogen receptor modulator*, Maturitas, 104 (**2017**) 29-35.
[71] A. Vejux, G. Lizard, *Cytotoxic effects of oxysterols associated with human diseases: Induction of cell death (apoptosis and/or oncosis), oxidative and inflammatory activities, and phospholipidosis*, Molecular Aspects of Medicine, 30 (**2009**) 153-170.
[72] T. Ikegami, H. Hyogo, A. Honda, T. Miyazaki, K. Tokushige, E. Hashimoto, K. Inui, Y. Matsuzaki, S. Tazuma, *Increased serum liver X receptor ligand oxysterols in patients with non-alcoholic fatty liver disease*, Journal of Gastroenterology, 47 (**2012**) 1257-1266.
[73] S. Ducheix, A. Montagner, A. Polizzi, F. Lasserre, M. Régnier, A. Marmugi, F. Benhamed, J. Bertrand-Michel, L. Mselli-Lakhal, N. Loiseau, P.G. Martin, J.M. Lobaccaro, L. Ferrier, C. Postic, H. Guillou, *Dietary oleic acid regulates hepatic lipogenesis through a liver X receptor-dependent signaling*, PLoS One, 12 (**2017**) 181393.

[74] I.H.K. Dias, S.R. Wilson, H. Roberg-Larsen, *Chromatography of oxysterols*, Biochimie, 153 (**2018**) 3-12.
[75] S. Dzeletovic, O. Breuer, E. Lund, U. Diczfalusy, *Determination of cholesterol oxidation products in human plasma by isotope dilution-mass spectrometry*, Analytical Biochemistry, 225 (**1995**) 73-80.
[76] V. Cardenia, M.T. Rodriguez-Estrada, E. Baldacci, S. Savioli, G. Lercker, *Analysis of cholesterol oxidation products by Fast gas chromatography/mass spectrometry*, Journal of Separation Science, 35 (**2012**) 424-430.
[77] S. Matysik, H.H. Klünemann, G. Schmitz, *Gas chromatography-tandem mass spectrometry method for the simultaneous determination of oxysterols, plant sterols, and cholesterol precursors*, Clinical Chemistry, 58 (**2012**) 1557-1564.
[78] H. Roberg-Larsen, K. Lund, T. Vehus, N. Solberg, C. Vesterdal, D. Misaghian, P.A. Olsen, S. Krauss, S.R. Wilson, E. Lundanes, *Highly automated nano-LC/MS-based approach for thousand cell-scale quantification of side chain-hydroxylated oxysterols*, Journal of Lipid Research, 55 (**2014**) 1531-1536.
[79] J.G. McDonald, D.D. Smith, A.R. Stiles, D.W. Russell, *A comprehensive method for extraction and quantitative analysis of sterols and secosteroids from human plasma*, Journal of Lipid Research, 53 (**2012**) 1399-1409.
[80] W.J. Griffiths, Y. Wang, *Analysis of oxysterol metabolomes*, Biochimica et Biophysica Acta (BBA) - Molecular and Cell Biology of Lipids, 1811 (**2011**) 784-799.
[81] W.J. Griffiths, Y. Wang, *Oxysterol research: a brief review*, Biochemical Society Transactions, 47 (**2019**) 517-526.
[82] P.J. Crick, T. William Bentley, J. Abdel-Khalik, I. Matthews, P.T. Clayton, A.A. Morris, B.W. Bigger, C. Zerbinati, L. Tritapepe, L. Iuliano, Y. Wang, W.J. Griffiths, *Quantitative Charge-Tags for Sterol and Oxysterol Analysis*, Clinical Chemistry, 61 (**2015**) 400-411.
[83] Z. Pataj, G. Liebisch, G. Schmitz, S. Matysik, *Quantification of oxysterols in human plasma and red blood cells by liquid chromatography high-resolution tandem mass spectrometry*, Journal of Chromatography A, 1439 (**2016**) 82-88.
[84] X. Jiang, D.S. Ory, X. Han, *Characterization of oxysterols by electrospray ionization tandem mass spectrometry after one-step derivatization with dimethylglycine*, Rapid Communications in Mass Spectrometry, 21 (**2007**) 141-152.
[85] A. Honda, K. Yamashita, T. Hara, T. Ikegami, T. Miyazaki, M. Shirai, G. Xu, M. Numazawa, Y. Matsuzaki, *Highly sensitive quantification of key regulatory oxysterols in biological samples by LC-ESI-MS/MS*, Journal of Lipid Research, 50 (**2009**) 350-357.
[86] A. Meljon, S. Theofilopoulos, C.H.L. Shackleton, G.L. Watson, N.B. Javitt, H.-J. Knölker, R. Saini, E. Arenas, Y. Wang, W.J. Griffiths, *Analysis of bioactive oxysterols in newborn mouse brain by LC/MS*, Journal of Lipid Research, 53 (**2012**) 2469-2483.
[87] O. Lavrynenko, R. Nedielkov, H.M. Möller, A. Shevchenko, *Girard derivatization for LC-MS/MS profiling of endogenous ecdysteroids in Drosophila*, Journal of Lipid Research, 54 (**2013**) 2265-2272.
[88] K. Karu, M. Hornshaw, G. Woffendin, K. Bodin, M. Hamberg, G. Alvelius, J. Sjövall, J. Turton, Y. Wang, W.J. Griffiths, *Liquid chromatography-mass spectrometry utilizing multi-stage fragmentation for the identification of oxysterols*, Journal of Lipid Research, 48 (**2007**) 976-987.
[89] H. Roberg-Larsen, C. Vesterdal, S.R. Wilson, E. Lundanes, *Underivatized oxysterols and nanoLC–ESI-MS: A mismatch*, Steroids, 99 (**2015**) 125-130.
[90] W.J. Griffiths, P.J. Crick, Y. Wang, M. Ogundare, K. Tuschl, A.A. Morris, B.W. Bigger, P.T. Clayton, Y. Wang, *Analytical strategies for characterization of oxysterol lipidomes: Liver X receptor ligands in plasma*, Free Radical Biology and Medicine, 59 (**2013**) 69-84.

[91] Y. Wang, K.M. Sousa, K. Bodin, S. Theofilopoulos, P. Sacchetti, M. Hornshaw, G. Woffendin, K. Karu, J. Sjövall, E. Arenas, W.J. Griffiths, *Targeted lipidomic analysis of oxysterols in the embryonic central nervous system*, Molecular bioSystems, 5 (**2009**) 529-541.
[92] S. Solheim, S.A. Hutchinson, E. Lundanes, S.R. Wilson, J.L. Thorne, H. Roberg-Larsen, *Fast liquid chromatography-mass spectrometry reveals side chain oxysterol heterogeneity in breast cancer tumour samples*, The Journal of Steroid Biochemistry and Molecular Biology, 192 (**2019**) 105309.
[93] H.K. Walker, W.D. Hall, J.W. Hurst, *Chapter 31 - Cholesterol, triglycerides, and related Lipoproteins*, in: Clinical Methods: The History, Physical, and Laboratory Examinations, Butterworth Publishers, Boston, (**1990)**.
[94] M. Rogeberg, H. Malerod, H. Roberg-Larsen, C. Aass, S.R. Wilson, *On-line solid phase extraction–liquid chromatography, with emphasis on modern bioanalysis and miniaturized systems*, Journal of Pharmaceutical and Biomedical Analysis, 87 (**2014**) 120-129.
[95] K.O. Svendsen, H.R. Larsen, S.A. Pedersen, I. Brenna, E. Lundanes, S.R. Wilson, *Automatic filtration and filter flush for robust online solid-phase extraction liquid chromatography*, Journal of Separation Science, 34 (**2011**) 3020-3022.
[96] S.R. Wilson, T. Vehus, H.S. Berg, E. Lundanes, *Nano-LC in proteomics: recent advances and approaches*, Bioanalysis, 7 (**2015**) 1799-1815.
[97] C.S. Ho, C.W.K. Lam, M.H.M. Chan, R.C.K. Cheung, L.K. Law, L.C.W. Lit, K.F. Ng, M.W.M. Suen, H.L. Tai, *Electrospray ionisation mass spectrometry: principles and clinical applications*, The Clinical Biochemist Reviews, 24 (**2003**) 3-12.
[98] R. Bąchor, P. Mielczarek, M. Rudowska, J. Silberring, Z. Szewczuk, *Sensitive detection of charge derivatized peptides at the attomole level using nano-LC-ESI–MRM analysis*, International Journal of Mass Spectrometry, 362 (**2014**) 32-38.
[99] E. Ciccimaro, I.A. Blair, *Stable-isotope dilution LC–MS for quantitative biomarker analysis*, Bioanalysis, 2 (**2010**) 311-341.
[100] G.I. Taylor, *Disintegration of water drops in an electric field*, Proceedings of the Royal Society of London. Series A. Mathematical and Physical Sciences, 280 (**1964**) 383-397.
[101] M. Yamashita, J.B. Fenn, *Electrospray ion source. Another variation on the free-jet theme*, The Journal of Physical Chemistry, 88 (**1984**) 4451-4459.
[102] C.M. Whitehouse, R.N. Dreyer, M. Yamashita, J.B. Fenn, *Electrospray interface for liquid chromatographs and mass spectrometers*, Analytical Chemistry, 57 (**1985**) 675-679.
[103] M. Wilm, *Principles of electrospray ionization*, Molecular & Cellular Proteomics, 10 (**2011**) 9407.
[104] M.S. Wilm, M. Mann, *Electrospray and Taylor-Cone theory, Dole's beam of macromolecules at last?*, International Journal of Mass Spectrometry and Ion Processes, 136 (**1994**) 167-180.
[105] E. Hoffmann, V. Stroobant, *Mass Spectrometry: Principles and Applications*, Third ed., John Wiley & Sons, West Sussex, England, (**2007)**.
[106] K.K. Murray, *The term 'multiple reaction monitoring' is recommended*, Rapid Communications in Mass Spectrometry, 29 (**2015**) 1926-1928.
[107] E. Lundanes, L. Reubsaet, T. Greibrokk, *Chromatography; basic principles, sample preparations and related methods*, Wiley-VHC Verlag, (**2014)**.
[108] A.J. Martin, R.L. Synge, *A new form of chromatogram employing two liquid phases: A theory of chromatography. 2. Application to the micro-determination of the higher monoamino-acids in proteins*, The Biochemical Journal, 35 (**1941**) 1358-1368.
[109] U.S. FDA, *Reviewer Guidance; Validation of Chromatographic Methods*, (**1994**)
[110] J.E. MacNair, K.C. Lewis, J.W. Jorgenson, *Ultrahigh-Pressure Reversed-Phase Liquid Chromatography in Packed Capillary Columns*, Analytical Chemistry, 69 (**1997**) 983-989.

[111] S. Fekete, I. Kohler, S. Rudaz, D. Guillarme, *Importance of instrumentation for fast liquid chromatography in pharmaceutical analysis*, Journal of Pharmaceutical and Biomedical Analysis, 87 (**2014**) 105-119.
[112] N. Wu, J.A. Lippert, M.L. Lee, *Practical aspects of ultrahigh pressure capillary liquid chromatography*, Journal of Chromatography A, 911 (**2001**) 1-12.
[113] S. Fekete, J. Schappler, J.-L. Veuthey, D. Guillarme, *Current and future trends in UHPLC*, TrAC Trends in Analytical Chemistry, 63 (**2014**) 2-13.
[114] Y. Wu, X. Sun, J. Zhu, J. Shen, H. Wang, L. Zhu, Y. Zhou, Y. Ke, *Monodisperse core–shell silica particles as a high-performance liquid chromatography packing material: Facile in situ silica sol-gel synthesis*, Journal of Chromatography A, 1625 (**2020**) 461282.
[115] R. Hayes, A. Ahmed, T. Edge, H. Zhang, *Core–shell particles: Preparation, fundamentals and applications in high performance liquid chromatography*, Journal of Chromatography A, 1357 (**2014**) 36-52.
[116] L.E. Blue, J.W. Jorgenson, *1.1 μm superficially porous particles for liquid chromatography: part II: column packing and chromatographic performance*, Journal of Chromatography A, 1380 (**2015**) 71-80.
[117] F. Gritti, A. Cavazzini, N. Marchetti, G. Guiochon, *Comparison between the efficiencies of columns packed with fully and partially porous C18-bonded silica materials*, Journal of Chromatography A, 1157 (**2007**) 289-303.
[118] F. Capriotti, I. Leonardis, A. Cappiello, G. Famiglini, P. Palma, *A Fast and Effective Method for Packing Nano-LC Columns with Solid-Core Nano Particles Based on the Synergic Effect of Temperature, Slurry Composition, Sonication and Pressure*, Chromatographia, 76 (**2013**) 1079-1086.
[119] F. Gritti, G. Guiochon, *Theoretical and experimental impact of the bed aspect ratio on the axial dispersion coefficient of columns packed with 2.5μm particles*, Journal of Chromatography A, 1262 (**2012**) 107-121.
[120] F. Gritti, G. Guiochon, *Perspectives on the Evolution of the Column Efficiency in Liquid Chromatography*, Analytical Chemistry, 85 (**2013**) 3017-3035.
[121] G. Guiochon, F. Gritti, *Shell particles, trials, tribulations and triumphs*, Journal of Chromatography A, 1218 (**2011**) 1915-1938.
[122] M.R. Gama, C.H. Collins, C.B.G. Bottoli, *Nano-Liquid Chromatography in Pharmaceutical and Biomedical Research*, Journal of Chromatographic Science, 51 (**2013**) 694-703.
[123] K. Vanhoutte, W. Van Dongen, I. Hoes, F. Lemière, E.L. Esmans, H. Van Onckelen, E. Van den Eeckhout, R.E.J. van Soest, A.J. Hudson, *Development of a Nanoscale Liquid Chromatography/Electrospray Mass Spectrometry Methodology for the Detection and Identification of DNA Adducts*, Analytical Chemistry, 69 (**1997**) 3161-3168.
[124] J.P. Chervet, M. Ursem, J.P. Salzmann, *Instrumental Requirements for Nanoscale Liquid Chromatography*, Analytical Chemistry, 68 (**1996**) 1507-1512.
[125] T. Vehus, H. Roberg-Larsen, J. Waaler, S. Aslaksen, S. Krauss, S.R. Wilson, E. Lundanes, *Versatile, sensitive liquid chromatography mass spectrometry – Implementation of 10 μm OT columns suitable for small molecules, peptides and proteins*, Scientific Reports, 6 (**2016**) 37507.
[126] D.V. McCalley, *Instrumental considerations for the effective operation of short, highly efficient fused-core columns. Investigation of performance at high flow rates and elevated temperatures*, Journal of Chromatography A, 1217 (**2010**) 4561-4567.
[127] X. Zhao, X. Xie, S. Sharma, L.T. Tolley, A. Plistil, H.E. Barnett, M.P. Brisbin, A.C. Swensen, J.C. Price, P.B. Farnsworth, H.D. Tolley, S.D. Stearns, M.L. Lee, *Compact Ultrahigh-Pressure Nanoflow Capillary Liquid Chromatograph*, Analytical Chemistry, 89 (**2017**) 807-812.

[128] J.W. Jorgenson, K.D. Lukacs, *Zone electrophoresis in open-tubular glass capillaries*, Analytical Chemistry, 53 (**1981**) 1298-1302.
[129] F. Gritti, M. Martin, G. Guiochon, *Influence of Viscous Friction Heating on the Efficiency of Columns Operated under Very High Pressures*, Analytical Chemistry, 81 (**2009**) 3365-3384.
[130] F. Gritti, G. Guiochon, *Measurement of the axial and radial temperature profiles of a chromatographic column: Influence of thermal insulation on column efficiency*, Journal of Chromatography A, 1138 (**2007**) 141-157.
[131] A.E. Reising, J.M. Godinho, K. Hormann, J.W. Jorgenson, U. Tallarek, *Larger voids in mechanically stable, loose packings of 1.3μm frictional, cohesive particles: Their reconstruction, statistical analysis, and impact on separation efficiency*, Journal of Chromatography A, 1436 (**2016**) 118-132.
[132] G. Instruments, *PHMT Thermoshaker for Microtubes and Microplates*, [assessed June 15th 2021], https://grantinstruments.com/scientific/life-science/thermoshakers/phmt-thermoshaker-for-microtubes-and-microplates
[133] H.S. Berg, K.E. Seterdal, T. Smetop, R. Rozenvalds, O.K. Brandtzaeg, T. Vehus, E. Lundanes, S.R. Wilson, *Self-packed core shell nano liquid chromatography columns and silica-based monolithic trap columns for targeted proteomics*, Journal of Chromatography A, 1498 (**2017**) 111-119.
[134] V. Valco Instruments Co. Inc., *Direct-Connect 360 µm FS Tubing to 1/16" Fitting Detail*, [assessed April 19th 2021], https://www.vici.com/uhplc/360um-to-1-16th.php
[135] V. Valco Instruments Co. Inc., *Technical Note 512: Installation Instructions for 360µm to 1/16" Fitting Adapter* [assessed April 19th 2021], https://www.vici.com/support/tn/tn512.pdf
[136] T. Scientific, *EASY-nLC™ 1200 System*, [assessed April 19th 2021], https://www.thermofisher.com/order/catalog/product/LC140#/LC140
[137] T. Scientific, *Nanospray Flex™ Ion Sources*, [assessed April 19th 2021], https://www.thermofisher.com/order/catalog/product/ES071#/ES071
[138] T. Scientific, *Thermo Scientific TSQ Quantiva Triple-Stage Quadrupole Mass Spectrometer*, [assessed April 19th 2021], https://tools.thermofisher.com/content/sfs/brochures/PS-64079-MS-TSQ-Quantiva-PS64079-EN.pdf
[139] Eurachem, *The Fitness for Purpose of Analytical Methods: A Laboratory Guide to Method Validation and Related Topics* (**2014**)
[140] A.E. Reising, J.M. Godinho, J. Bernzen, J.W. Jorgenson, U. Tallarek, *Axial heterogeneities in capillary ultrahigh pressure liquid chromatography columns: Chromatographic and bed morphological characterization*, Journal of Chromatography A, 1569 (**2018**) 44-52.
[141] S. Fanali, S. Rocchi, B. Chankvetadze, *Use of novel phenyl-hexyl core-shell particles in nano-LC*, Electrophoresis, 34 (**2013**) 1737-1742.
[142] J.W. Treadway, K.D. Wyndham, J.W. Jorgenson, *Highly efficient capillary columns packed with superficially porous particles via sequential column packing*, Journal of Chromatography A, 1422 (**2015**) 345-349.
[143] A.E. Reising, J.M. Godinho, J.W. Jorgenson, U. Tallarek, *Bed morphological features associated with an optimal slurry concentration for reproducible preparation of efficient capillary ultrahigh pressure liquid chromatography columns*, Journal of Chromatography A, 1504 (**2017**) 71-82.

[144] S. Bruns, E.G. Franklin, J.P. Grinias, J.M. Godinho, J.W. Jorgenson, U. Tallarek, *Slurry concentration effects on the bed morphology and separation efficiency of capillaries packed with sub-2μm particles*, Journal of Chromatography A, 1318 (**2013**) 189-197.
[145] F. Gritti, M. Farooq Wahab, *Understanding the science behind packing high-efficiency columns and capillaries: Facts, fundamentals, challenges, and future directions*, LC GC North America, 36 (**2018**) 82-98.
[146] P.A. Bristow, J.H. Knox, *Standardization of test conditions for high performance liquid chromatography columns*, Chromatographia, 10 (**1977**) 279-289.
[147] F. Gritti, M. Dion, A. Felinger, M. Savaria, *Characterization of radial and axial heterogeneities of chromatographic columns by flow reversal*, Journal of Chromatography A, 1567 (**2018**) 164-176.
[148] F. Gritti, T. McDonald, M. Gilar, *Impact of the column hardware volume on resolution in very high pressure liquid chromatography non-invasive investigations*, Journal of Chromatography A, 1420 (**2015**) 54-65.
[149] F. Gritti, M. Gilar, *Impact of frit dispersion on gradient performance in high-throughput liquid chromatography*, Journal of Chromatography A, 1591 (**2019**) 110-119.
[150] N. Lambert, S. Miyazaki, M. Ohira, N. Tanaka, A. Felinger, *Comparison of the kinetic performance of different columns for fast liquid chromatography, emphasizing the contributions of column end structure*, Journal of Chromatography A, 1473 (**2016**) 99-108.
[151] O.K. Brandtzaeg, E. Johnsen, H. Roberg-Larsen, K.F. Seip, E.L. MacLean, L.R. Gesquiere, S. Leknes, E. Lundanes, S.R. Wilson, *Proteomics tools reveal startlingly high amounts of oxytocin in plasma and serum*, Scientific Reports, 6 (**2016**) 31693.
[152] H. Roberg-Larsen, K. Lund, K.E. Seterdal, S. Solheim, T. Vehus, N. Solberg, S. Krauss, E. Lundanes, S.R. Wilson, *Mass spectrometric detection of 27-hydroxycholesterol in breast cancer exosomes*, The Journal of Steroid Biochemistry and Molecular Biology, 169 (**2017**) 22-28.
[153] R. Parker, *The role of adipose tissue in fatty liver diseases*, Liver Research, 2 (**2018**) 35-42.
[154] J.M. Lee, B.I. Choi, *Hepatocellular nodules in liver cirrhosis: MR evaluation*, Abdominal Imaging, 36 (**2011**) 282-289.
[155] Z.D. Goodman, *Neoplasms of the liver*, Modern Pathology, 20 (**2007**) S49-S60.
[156] *Fundamentals of Statistics - Grubb's Test*, http://www.statistics4u.com/fundstat_eng/ee_grubbs_outliertest.html

7 Appendix

7.1 Supplementary theory

7.1.1 Evolution of non-alcoholic fatty liver disease

In NAFLD, obesity induces NAFL and further on NASH through two main pathways, as illustrated in **Figure 39.** Obesity alters the function of the adipose tissue [153]. The adipose tissue, normally performing uptake and storing of FFA itself, delivers the FFAs to the liver, resulting in FFA-accumulation in the liver [153]. The hepatocytes synthesize triglycerides from the FFAs, inducing lipotoxicity in the liver. This generates ER stress, mitochondrial dysfunction, reactive oxygen species (ROS), and secretion of cytokines. Secretion of cytokines from the triglycerides announces a threat and activates macrophages (white blood cells) called Kupffer cells which are liver-resident cells only. This infiltration of macrophages induces inflammation in the hepatocyte tissue [36].

Further on, the inflammatory response activates HSCs through macrophage secretion of the inflammatory cytokines tumor necrosis factor α (TNFα) or interleukin-6 (IL-6) and growth factors like transforming growth factor-β (TGFβ) [38]. TNFα induces hepatocyte apoptosis and modulates a hepatic immune response. In chronic damage, IL-6 can provoke hepatic insulin resistance [153]. HSCs are the cells involved in fibrotic activation. There is a direct relationship between FFA flux and the degree of hepatic steatosis [153].

Additionally, adipose tissue can signal directly to the hepatic tissue through adipokines called leptin, and the cytokines TNFα, inducing macrophage activity in the liver and inflammation and NASH this way.

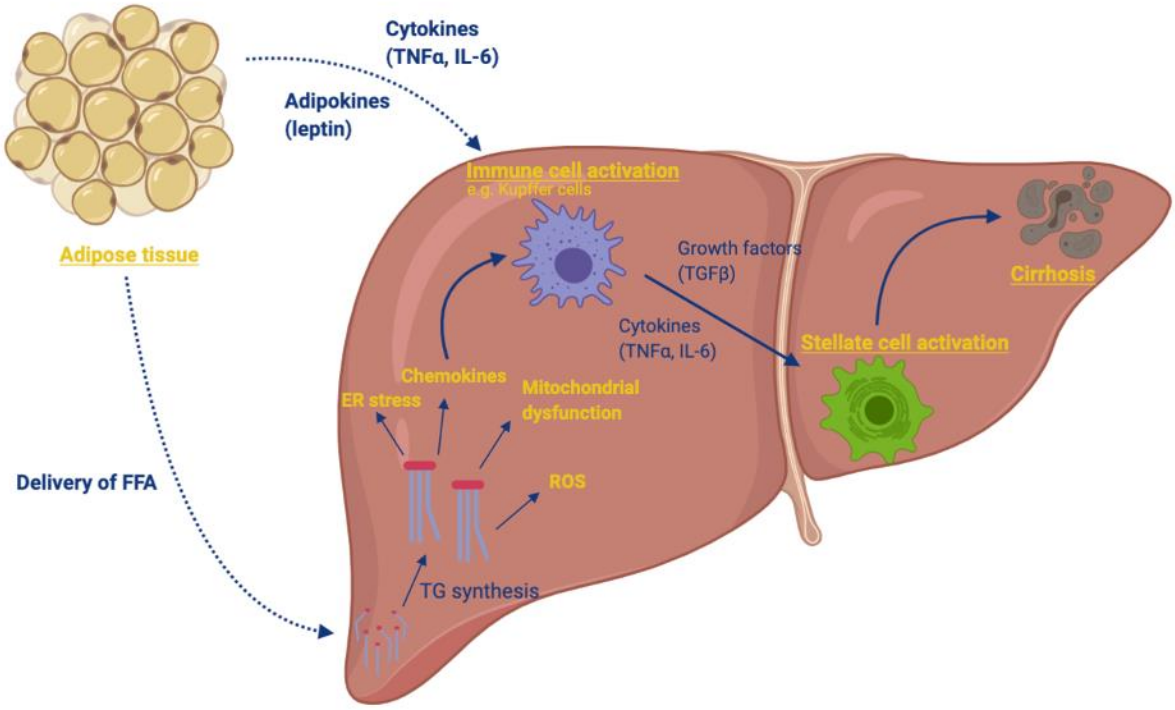

Figure 39. The two pathways that can induce NAFLD development on a cellular and molecular level. The illustration was adapted from [36] and was made in BioRender [27].

When the evolution of fibrosis gets far enough, the connective tissue created starts generating hepatocellular nodules like regenerative nodules, dysplastic nodules (DNs), and neoplastic nodules. DNs are large and benign lesions, and the latter causes tumor growth, either benign or malignant [154]. Eventually, the fibrosis will encapsulate the nodules completely, giving rise to cirrhosis, potentially followed by hepatocellular carcinoma (HCC) development. A stepwise progression from regenerative nodules to low-grade dysplastic nodules (have minimal abnormal cells) to high-grade dysplastic nodules (have small cell changes suggesting cellular proliferation) to HCC occurs [154, 155]. High-grade dysplastic nodules have features creating a node-in-node look, giving the cirrhotic liver its characteristic appearance [155].

7.1.2 Column contributions to band broadening

Eddy dispersion is considered the major contributor to band broadening in HPLC and occurs due to differences in the widths and lengths of the intra- and interparticle pores. Therefore, the analyte molecules move through different paths throughout the column, promoting band broadening [116]. Both particle size and inhomogeneous particle size distribution are proportional to the size of the eddy dispersion in a packed column [107]. Eddy dispersion is expressed by **equation 8**.

$$H = C_e * d_p \qquad (eq. 8)$$

Here H is the plate height, C_e is a constant, and d_p is the diameter of the particles.

Longitudinal diffusion occurs due to the natural phenomenon of molecules diffusing from concentrated zones to less concentrated zones. In HPLC, this type of diffusion is reliant on the diffusion coefficient of the analyte in the MP and the linear velocity of the MP – a higher flow rate gives a lower plate height, hence less contribution to band broadening, as seen from the equation for longitudinal diffusion (**equation 9**).

$$H = \frac{c_1 * D_m}{u} \qquad (eq. 9)$$

Here H is the plate height, c_1 is a constant, D_m is the diffusion coefficient of the analyte in the MP, and u is the linear velocity of the MP [107].

Resistance to mass transfer is inversely proportional to the diffusion constants of the analyte in both the SP and MP [107]. Resistance to mass transfer in the MP and the stagnant MP in a packed column is expressed by **equations 10** and **11**, respectively.

$$H_m = \frac{c_m * d^2_p * u}{D_m} \qquad (eq. 10)$$

$$H_{stm} = \frac{c_{stm} * d^2_p * u}{D_m} \qquad (eq. 11)$$

Here c_m and c_{stm} are constants, and the other parameters are as before.

Higher diffusion constants result in faster-restored equilibria of the analyte between the two phases, reducing the resistance to mass transfer contributions, increasing the column efficiency.

7.2 Experimental: The conventional UHPLC-MS platform

The conventional UHPLC-MS platform used for preliminary experiments is shown in **Figure 40**.

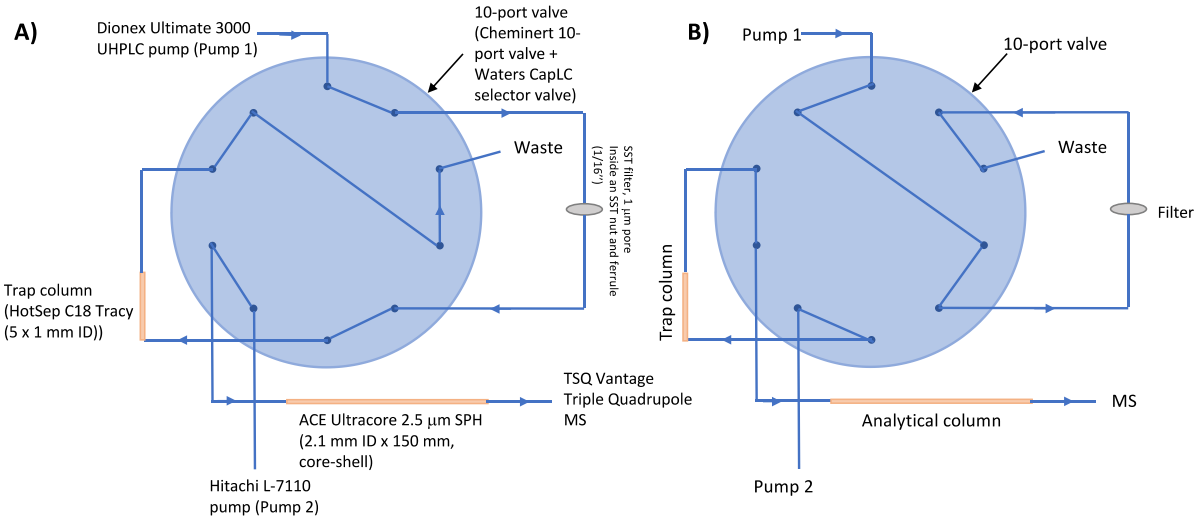

Figure 40. A Dionex Ultimate 3000 UHPLC from Thermo Scientific was coupled to a TSQ Vantage TQMS from Thermo Scientific and operated in MRM mode. The injection volume was 60 µL. All connections were Thermo Scientific Viper SST finger tight fittings (180 µm ID). Isocratic elution was performed with 0.1% FA in 57/33/10 water/ACN/MeOH at a 700 µL/min flow rate.

7.3 Supplementary results

7.3.1 Preliminary experiments

In the preliminary experiments, the current conventional UHPLC-MS method needed to be tested for training purposes and to see if the method was operational. Therefore, evaluation solutions containing 22R-, 24S-, 25-, and 27-OHC in the 50-500 pM range also containing 200 pM IS (22R-OHC-d_7, 25-OHC-d_6, and 27-OHC-d_6) and 6 μM heavy cholesterol was prepared before quantification by LC-MS.

Cholesterol oxidase enzyme assessment

The initial focus was to determine if the enzyme cholesterol oxidase containing phosphate buffer functioned properly to oxidize the oxysterols.

To investigate the cholesterol oxidase enzyme performance, 3x2 calibration solution series (50-500 pM concentration range) were compared containing cholesterol oxidase phosphate buffer made by me (cholesterol oxidase 1) and former M.Sc. student Stian Solheim (cholesterol oxidase 2). LC-MS determination of the calibration solutions showed that the TSQ Vantage mass spectrometer produced signals, indicating that both enzymes worked. However, the peak areas were ~10-fold lower than normally experienced by the research group (e.g., 50 pM of 25-OHC had peak areas of ~500 vs. ~5 000). See **Table 14** for linearity and RSD results. The analytical method for the determination of 22R-, 24S-, 25-, and 27-OHC were hence operational. However, issues regarding the sensitivity of the MS were discovered and had to be further explored. Poor sensitivity of the MS can, in this case, be due to the instrument being old and hence having suffered continuous application over the years.

Method evaluation of the conventional chromatographic platform

Neither washing and calibrating the MS in-house or periodic maintenance by a service technician improved the sensitivity. Therefore, a method evaluation was necessary to test if the method performance was fit for the purpose of this study regarding analytical sensitivity, working range, and precision. Eurachem's guidelines were used to perform the method evaluation [139].

Analytical sensitivity

The S/N for the 50 pM calibration solutions were varying and not always detected. 50 pM of the oxysterols were hence sometimes detectable but below the LOQ (S/N = 10) and did not ensure the certainty needed regarding accuracy for quantification. All evaluation solutions gave significantly lower S/N compared to earlier signals provided by the MS (Solheim *et al.* determined the LOQ of this instrument to be 15-31 pM for the oxysterols in 2018 [92]).

Working range and precision

It was important to confirm that the method could be used over the desired interval. Linearity refers to what extent the detector delivers results within the desired concentration range. The lowest concentration of the 25-OHC standard (50 pM) was below the LOQ of the method, eliminating the possibility of quantifying concentrations of the oxysterols at this level with acceptable certainty.

Intra- and inter-vial oxysterol quantification revealed the working range and the precision of the analytical method, none of which fulfilled the acceptable analytical criteria. Intra-vial cholesterol oxidase 2 provided the best linearity and precision within this experiment. However, it was insufficient to meet analytical demands (RSD < 20% and linearity where r^2 > 0.99). Linearity and precision are summarized in **Table 14**. The precision at low oxysterol concentrations (50-200 pM) was throughout poor, independent of the enzyme used, but was better at higher concentrations. Due to the overall small peak areas and S/N, it was suspected that either the sensitivity of the MS had become poorer or that the working solutions were diluted incorrectly.

Table 14. The linearity and precision obtained from initial testing of the conventional UHPLC-MS method for oxysterol quantification.

		Linearity	**RSD**
Cholesterol oxidase 1	Intra-vial	0.4-0.8	3-35%
	Inter-vial	0.92-0.99	2-49%
Cholesterol oxidase 2	Intra-vial	0.96-0.99	2-33%
	Inter-vial	0.81-0.98	11-41%

New working solutions were made, and the experiment was repeated. Peak areas and S/N remained low, supporting the conclusion that the sensitivity of the MS had become insufficient.

7.3.2 Testing the 5 μm phenyl-hexyl particles in the analytical column

To enhance the oxysterol separation in the nLC-MS platform, 5 μm PH particles were tested in the analytical column. Until now, a 5 μm PH in-house packed trap column (90 mm x 180 μm ID) had been used. The length was necessary due to the coupling of the UHPLC-connections requiring space on the column. However, when the trap column was substituted with a 3 cm long trap column (coupled with vespel/graphite ferrule and SST nut and union) to lower the backpressure of the platform, a lot of selectivity was lost, resulting in faster analysis time, but a worse separation of the oxysterols. The loss of selectivity indicated that some separation of the oxysterols may have occurred in the trap column, proposing that the 5 μm PH particles might separate the oxysterols well.

The 5 μm PH particles were packed in a 75 μm ID column (17 cm long), and the 5 μm PH particles (90 mm x 180 μm ID) were still used as the trap column. A 5-95% B gradient was run over 25 min with a 1000 nL/min flow rate (larger particles generate less backpressure, allowing a faster flow rate), which made the oxysterols coelute at ~15-16 min. Calculations revealed that coelution happened at ~60% B in the gradient. Isocratic elution was systematically decreased 5% from 50% B to 35% B, reaching the best separation at 38% B (**Figure 41A**), even though the separation was still poor. Different gradients were tested without separation success.

For easier comparison with the 2.5 μm SPH particles (**Figure 30C**), the same flow rate and MP composition as "optimized" on the 2.5 μm SPH column was tested. Isocratic 45% B with a flow rate of 500 nL/min was tested, achieving better separation between 25- and 24S-OHC than ever experienced in the study, but worse separation between the other analytes, as shown in **Figure 41B**. All oxysterols eluted within ~30 min which again indicated that the oxysterols have less retention on the 5 μm PH particles than on the 2.5 μm SPH particles (50 min analysis time).

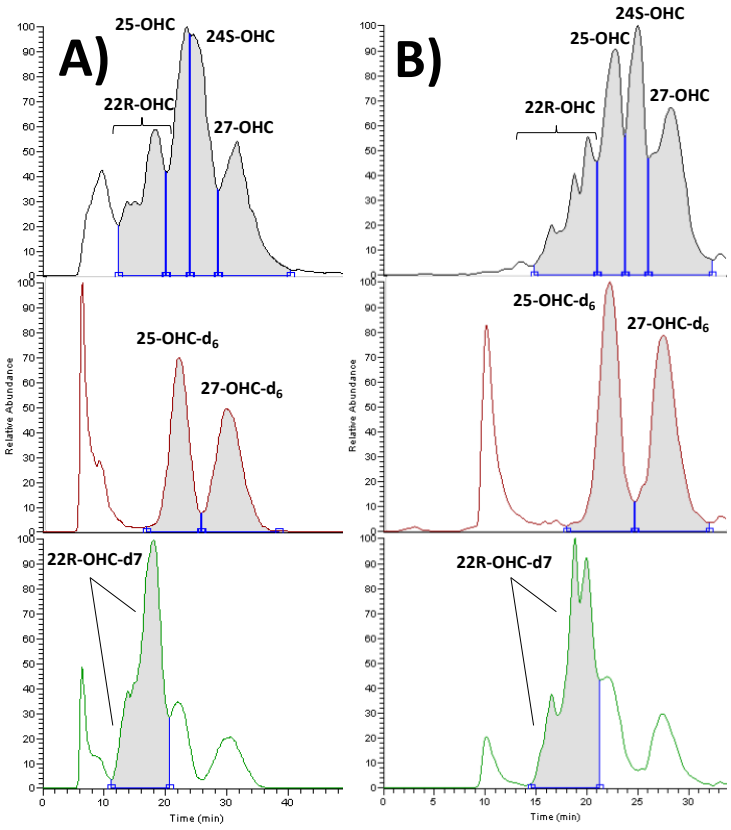

Figure 41. The separation of 22R-, 24S-, 25-, and 27-OHC and the ISs 25-OHC-d_6, 27-OHC-d_6, and 22R-OHC-d_7 on the 5 µm PH analytical- (170 mm x 75 µm ID) and trap (90 mm x 180 µm ID) column with A) 38% B at a 1000 nL/min flow rate at ambient temperature and, B) 45% B at a 500 nL/min flow rate at ambient temperature.

To conclude, the 5 µm PH particles in the analytical column did not provide sufficient separation and were not investigated further. Band broadening was still a problem.

7.4 Calculations

7.4.1 Comparison of two means: T-test calculation

Several significance tests were performed in the plate number, asymmetry, and retention factor testing comparing slurry concentrations and column IDs. Only one example is shown here (if the plate number of 100 µm ID columns packed with 80% ACN vs. 90% ACN was significantly different). As the difference between the means of the two groups was tested, all significance tests performed were a two-tailed t-test at a 95% confidence interval ($\alpha = 0.05$). The tests were performed in Excel.

Firstly, an F-test was executed to test the equality of variance between the two groups. The data analysis tool in excel was used and gave the table in **Table 15**.

Table 15. The F-test was performed using the data analysis tool in Excel. If the one-tail P-value is less than the associated confidence interval (0.05), the variances are not equal, as in this example (5E-07 < 0.05). Therefore, the test should be continued using the t-test assuming non-equal variances.

F-Test Two-sample for variances

	Variable 1	*Variable 2*
Mean	2802,79673	1944,539494
Variance	5060122,9	7959,470629
Observations	6	6
df	5	5
F	635,73611	
P(F<=f) one-tail	5,3011E-07	
F Critical, one-tail	5,05032906	

To determine whether the null hypothesis (the means of the two groups are equal) should be rejected or not, a P-value was calculated in Excel using the "T.TEST" function shown in **Figure 42**. The calculated P-value was compared to the α-value of a t-test at a 95% confidence interval ($\alpha = 0.05$). The null hypothesis was rejected if the calculated P-value was smaller than α, meaning that the two groups were significantly different.

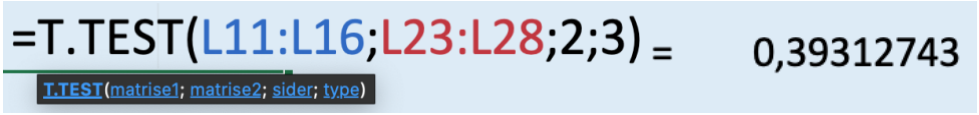

Figure 42. «matrise1» are the values from group 1, "matrise2" are the values from group 2, "sider" is whether the t-test is one-tailed (1) or two-tailed (2), and "type" is whether the t-test is paired (1), two samples with equal variance (2) or two samples with unequal variance (3). In this case, a two-tailed t-test assuming unequal variances was used. The calculated P-value is shown to the right.

In this case, the calculated P-value was larger than α (0.39 > 0.05), and the null hypothesis was not rejected, meaning that the plate number of 100 µm ID columns packed with 80% ACN vs. 90% ACN was not significantly different.

7.4.2 Outlier determination: Grubb's test

To discover an outlier (a data point that significantly differs from the other data points at a certain level of confidence) when testing columns for plate numbers, asymmetry, and retention factors, Grubb's test was used. In all cases, it was desired to test whether the data point was an upper or lower outlier. Hence, a one-sided Grubb's test was used at a 95% confidence interval. Grubb's test is expressed by **equation 12**.

$$G = \frac{|x - \tilde{x}|}{s} \qquad (eq.\ 12)$$

The calculated G value was compared against a G_{crit}-value for a one-sided test found in [156] at $\alpha = 0.05$. If $G_{calc} > G_{crit}$, the data point was considered an outlier.

7.5 Raw data

7.5.1 Sensitivity evaluation of the conventional chromatographic method

The raw data of S/N and signal intensities used for method evaluation on sensitivity is summarized in **Table 16**. In addition, the signal intensities and S/N obtained in 2018 are also included for comparison.

Table 16. S/N of evaluation solutions of 50, 300, and 500 pM 25-OHC made by Alex Websdale and me. The S/N are also compared against former calibration solution experiments performed in 2018 by Associate Professor Hanne Røberg-Larsen. Average signal intensities are highlighted in blue, and average S/N are highlighted in green. ND = not detected.

WS	Henriette				Alex	Hanne				
C 25-OHC (pM)	Rep 1	Rep 2	Rep 3	Average	Rep 1	Rep 1	Rep 2	Rep 3	Rep 4	Average
	Signal intensity				Signal intensity	Signal intensity				
50	ND	ND	ND	ND	ND	1,00E+03	5,00E+02	4,00E+02		6,33E+02
300	1,90E+02	2,50E+02	1,70E+02	2,03E+02	6,30E+02	7,00E+03	2,00E+03	3,00E+03		4,00E+03
500	4,90E+02	4,30E+02	3,00E+02	4,07E+02	1,13E+03	1,00E+04	4,00E+03	4,00E+03		6,00E+03
	S/N				S/N	S/N				
50	ND	ND	ND	ND	ND	2	4	3	2	3
300	1	1	1	1	1	12	34	29	14	22
500	2	2	1	2	1	43	46	122	79	73

7.5.2 Column flushing and testing

After each of the 18 nLC columns were packed, they were flushed for particle settlement – 75 and 100 µm ID with a 300 and 400 nL/min flow rate, respectively. The backpressures generated by each column are summarized in **Table 17**, together with the backpressures generated in an evaluation solution run.

Table 17. The backpressures generated by each of the 18 columns during both flushing and evaluation solution run. Pressure A and B refer to pump A and B. The blank spaces in column 17 are due to forgetting to collect the data. The lengths in red only highlight the shorter columns.

Column	ID (µm)	Solvent	Part. Batch	Length (cm)	Flush 400 nL/min		Run 600 nL/min	
			Serienummer		Pressure A (bar)	Pressure B (bar)	Pressure A (bar)	Pressure B (bar)
1	100	80% ACN	A174508	14,2	96	107	235	240
2	100	80% ACN	A174508	15,2	104	114	247	253
3	100	80% ACN	A174508	15,5	115	122	236	240
4	100	90% ACN	A174508	14,3	136	147	286	291
5	100	90% ACN	A174508	15,2	113	122	226	232
6	100	90% ACN	A174508	14,3	106	116	212	217
7	100	100% acetone	A226044	11,8			286	291
8	100	100% acetone	A226044	15,4	123	132	182	187
9	100	100% acetone	A226044	15,5	123	133	210	215
					Flush 300 nL/min		Run 450 nL/min	
10	75	80% ACN	A174508	15,5	98	106	240	245
11	75	80% ACN	A174508	13,1	125	133	297	301
12	75	80% ACN	A174508	15,0	126	132	255	250
13	75	90% ACN	A226044	11,6	219	240	297 (490)	294 (493)
14	75	90% ACN	A226044	15,4	144	151	230	232
15	75	90% ACN	A226044	15,2	124	132	230	233
16	75	100% acetone	A226044	15,4	192	200	264	268
17	75	100% acetone	A226044	15,4	-	-	230	233
18	75	100% acetone	A226044	15,2	160	168	208	210

7.5.3 Column performance testing

Plate number

The raw data of the chromatograms of thiourea and toluene used for calculating the plate number during column performance factor testing is summarized in **Table 18**.

Table 18. The raw data used for plate number calculation during column performance testing. The raw data are in white boxes and calculations in green boxes. The box in orange is considered an outlier. The blank spaces in column 3 are due to injection fail due to switching issues during loading. Thus, data were not collected.

Column	Replicate	Length (cm)	Retention time (min)			FWHM toluene			Plate number N			All
			Thiourea	Toluene	Difference	Start	End	Difference	Value	Mean	RSD (%)	RSD (%)
1	2	14,2	2,30	3,27	3,27	3,21	3,32	0,11	4895,8			
	1		2,31	3,26	3,26	3,22	3,33	0,11	4865,9			
	3		2,31	3,24	3,24	3,17	3,28	0,11	4806,3	4856,0	0,9	
2	2	15,2	2,50	3,59	3,59	3,50	3,80	0,30	793,3			
	1		2,54	3,65	3,65	3,53	3,85	0,32	720,8			
	3		2,48	3,57	3,57	3,45	3,76	0,31	734,7	749,6	5,1	80,3
3	1	15,5	2,66	6,98	4,32	6,86	7,12	0,26				
	2		-	-	-	-	-	-	-			
	3		-	-	-	-	-	-	-	-	-	
4	3	14,3	3,50	4,46	4,46	4,40	4,56	0,16	4304,7			
	1		3,56	4,54	4,54	4,46	4,62	0,16	4460,5			
	2		3,51	4,46	4,46	4,39	4,55	0,16	4304,7	4356,6	2,1	
5	3	15,2	2,39	3,42	3,42	3,34	3,52	0,18	1999,9			
	1		2,35	3,37	3,37	3,30	3,47	0,17	2177,1			
	2		2,36	3,38	3,38	3,31	3,48	0,18	1953,4	2043,5	5,8	
6	3	14,3	3,20	4,26	4,26	4,16	4,38	0,22	2077,2			
	1		3,17	4,19	4,19	4,07	4,30	0,23	1838,6			
	2		3,18	4,21	4,21	4,11	4,34	0,23	1856,2	1924,0	6,9	49,4
7	2	11,8	3,44	4,22	4,22	4,15	4,38	0,23	1865,0			
	1		3,46	4,22	4,22	4,15	4,37	0,22	2038,4			
	3		3,46	4,24	4,24	4,16	4,38	0,22	2057,8	1987,1	5,3	
8	2	15,4	2,23	3,20	3,20	3,12	3,32	0,20	1418,2			
	1		2,23	3,20	3,20	3,11	3,30	0,19	1571,5			
	3		2,23	3,23	3,23	3,13	3,33	0,20	1445,0	1478,2	5,5	
9	2	15,5	2,18	3,14	3,14	3,07	3,24	0,17	1890,0			
	1		2,17	3,12	3,12	3,06	3,22	0,16	2106,6			
	3		2,17	3,12	3,12	3,08	3,25	0,17	1866,0	1954,2	6,8	15,8
10	1	15,5	2,60	3,49	3,49	3,40	3,62	0,22	1394,2			
	2		2,60	3,50	3,50	3,40	3,63	0,23	1282,9			
	3		2,60	3,50	3,50	3,41	3,64	0,23	1282,9	1320,0	4,9	
11	1	13,1	2,60	3,39	3,39	3,30	3,52	0,22	1315,4			
	2		2,54	3,33	3,33	3,25	3,47	0,22	1269,3			
	3		2,55	3,34	3,34	3,27	3,50	0,23	1168,3	1251,0	6,0	
12	1	15,0	3,76	4,82	4,82	4,72	5,05	0,33	1181,9			
	2		3,70	4,76	4,76	4,66	4,98	0,32	1225,8			
	3		3,68	4,73	4,73	4,62	4,95	0,33	1138,2	1182,0	3,7	5,5
13	1	11,6	3,65	4,30	4,30	4,18	4,51	0,33	940,6			
	2		3,73	4,38	4,38	4,27	4,58	0,31	1105,9			
	3		3,83	4,50	4,50	4,39	4,73	0,34	970,5	1005,7	8,8	
14	1	15,4	2,60	3,43	3,43	3,37	3,64	0,27	894,1			
	2		2,58	3,41	3,41	3,32	3,60	0,28	821,7			
	3		2,56	3,40	3,40	3,31	3,59	0,28	816,9	844,2	5,1	
15	1	15,2	2,39	3,12	3,12	3,01	3,28	0,27	739,8			
	2		2,41	3,14	3,14	3,04	3,32	0,28	696,7			
	3		2,40	3,14	3,14	3,04	3,32	0,28	696,7	711,1	3,5	17,3
16	1	15,4	2,27	3,06	3,06	2,99	3,19	0,20	1296,9			
	2		2,27	3,06	3,06	3,01	3,20	0,19	1437,0			
	3		2,28	3,07	3,07	3,00	3,19	0,19	1446,4	1393,4	6,0	
17	1	15,4	3,11	3,87	3,87	3,79	4,00	0,21	1881,5			
	2		3,12	3,90	3,90	3,80	4,00	0,20	2106,6			
	3		3,10	3,86	3,86	3,78	3,98	0,20	2063,6	2017,2	5,9	
18	1	15,2	3,27	4,36	4,36	4,27	4,49	0,22	2175,9			
	2		3,17	4,23	4,23	4,14	4,36	0,22	2048,1			
	3		3,13	4,16	4,16	4,07	4,29	0,22	1980,8	2068,3	4,8	20,6

Asymmetry

The raw data of the chromatograms of toluene used for calculating the asymmetry during column performance factor testing is summarized in **Table 19.**

Table 19. The raw data used for asymmetry calculation during column performance testing. The raw data are in white boxes, and calculations are in green boxes. The blank spaces in column 3 are due to injection fail due to switching issues during loading. Thus, data were not collected.

Column	Replicate	Length (cm)	Height toluene		Width toluen 10% height				Asymmetry		All	
			Full height	Height 10%	Middle	a (start)	b (end)	b/a ratio	Mean	RSD %	Mean	RSD %
1	1	14,2	31,00	3,10	3,25	3,19	3,58	5,5				
	2		32,00	3,20	3,21	3,15	3,55	5,7				
	3		31,80	3,18	3,20	3,14	3,52	5,3	5,5	2,5		
2	2	15,2	18,00	1,80	3,57	3,44	4,04	3,6				
	1		19,30	1,93	3,62	3,50	4,08	3,8				
	3		17,70	1,77	3,54	3,42	4,01	3,9	3,8	3,4	4,6	26,1
3	1	15,5	23,00	2,30		6,86	7,12	0,3				
	2	-	-	-	-	-	-	-				
	3	-	-	-	-	-	-	-	-	-	-	-
4	1	14,3	19,00	1,90	4,54	4,43	4,87	3,0				
	2		19,70	1,97	4,47	4,37	4,77	3,0				
	3		19,80	1,98	4,45	4,35	4,76	3,1	3,0	1,6		
5	1	15,2	25,60	2,56	3,33	3,24	3,70	4,1				
	2		24,40	2,44	3,36	3,27	3,73	4,1				
	3		26,20	2,62	3,41	3,32	3,77	4,0	4,1	1,3		
6	1	14,3	8,50	0,85	4,18	4,03	4,53	2,3				
	2		12,20	1,22	4,21	4,07	4,53	2,3				
	3		10,40	1,04	4,25	4,14	4,50	2,3	2,3	1,1	3,1	28,5
7	1	11,8	23,90	2,39	4,23	4,11	4,64	3,4				
	2		22,70	2,27	4,23	4,11	4,62	3,2				
	3		23,90	2,39	4,24	4,12	4,62	3,2	3,3	3,2		
8	1	15,4	22,70	2,27	3,19	3,09	3,58	3,9				
	2		22,90	2,29	3,20	3,10	3,57	3,7				
	3		22,30	2,23	3,20	3,10	3,59	3,9	3,8	2,5		
9	1	15,5	21,30	2,13	3,12	3,02	3,53	4,1				
	2		22,30	2,23	3,14	3,04	3,53	3,9				
	3		21,30	2,13	3,14	3,04	3,55	4,1	4,0	2,3	3,7	10,5
10	1	15,5	28,70	2,87	3,46	3,36	3,95	4,9				
	2		29,00	2,90	3,47	3,37	3,97	5,0				
	3		28,70	2,87	3,48	3,38	3,97	4,9	4,9	1,0		
11	1	13,1	40,10	4,01	3,36	3,28	3,84	6,0				
	2		40,00	4,00	3,31	3,22	3,82	5,7				
	3		38,30	3,83	3,32	3,23	3,85	5,9	5,9	2,4		
12	1	15,0	30,70	3,07	4,81	4,70	5,31	4,5				
	2		31,50	3,15	4,75	4,62	5,30	4,2				
	3		31,90	3,19	4,71	4,58	5,26	4,2	4,3	3,4	5,0	15,2
13	1	11,6	22,90	2,29	4,26	4,13	5,02	5,8				
	2		22,20	2,22	4,35	4,23	5,00	5,4				
	3		23,30	2,33	4,48	4,35	5,23	5,8	5,7	3,3		
14	1	15,4	28,70	2,87	3,43	3,32	4,03	5,5				
	2		30,00	3,00	3,40	3,30	3,93	5,3				
	3		30,60	3,06	3,37	3,27	3,91	5,4	5,4	1,2		
15	1	15,2	30,70	3,07	3,08	2,97	3,61	4,8				
	2		29,50	2,95	3,11	3,00	3,65	4,9				
	3		30,30	3,03	3,12	3,00	3,66	4,5	4,7	3,7	5,3	9,1
16	1	15,4	14,30	1,43	3,07	2,97	3,52	4,5				
	2		13,40	1,34	3,07	2,97	3,52	4,5				
	3		14,80	1,48	3,07	2,97	3,55	4,8	4,6	3,1		
17	1	15,4	24,50	2,45	3,86	3,75	4,33	4,3				
	2		25,40	2,54	3,86	3,75	4,32	4,2				
	3		20,90	2,09	3,86	3,75	4,32	4,2	4,2	1,0		
18	1	15,2	24,70	2,47	4,33	4,22	4,81	4,4				
	2		24,00	2,40	4,20	4,10	4,62	4,2				
	3		23,50	2,35	4,15	4,04	4,63	4,4	4,3	1,8	4,4	4,6

Retention factor

The raw data of the chromatograms of thiourea and toluene used for calculating the retention factor during column performance factor testing is summarized in **Table 20**.

Table 20. The raw data used for retention factor calculation during column performance testing. The raw data are in white boxes, and calculations are in green boxes. The box in orange is considered an outlier. The blank spaces in column 3 are due to injection fail due to switching issues during loading. Thus, data were not collected.

Column	Replicate	Length	Retention time (min)			Height toluene		FWHM toluene			Retention factor k			All
			Thiourea	Toluene	Difference	Full height	Half height	Start	End	Difference	Value	Mean	RSD (%)	RSD (%)
1	2	14,2	2,30	3,27	0,97	32,00	16,00	3,21	3,32	0,11	0,42			
	1		2,31	3,26	0,95	31,00	15,50	3,22	3,33	0,11	0,41			
	3		2,31	3,24	0,93	31,80	15,90	3,17	3,28	0,11	0,40	0,41	2,33	
2	2	15,2	2,50	3,59	1,09	18,00	9,00	3,50	3,80	0,30	0,44			
	1		2,54	3,65	1,11	19,30	9,65	3,53	3,85	0,32	0,44			
	3		2,48	3,57	1,09	17,70	8,85	3,45	3,76	0,31	0,44	0,44	0,41	3,61
3	1	15,5	2,66	6,98	4,32	23,00	11,50	6,86	7,12	0,26	1,62			
	2	-	-	-	-	-	-	-	-	-	-			
	3	-	-	-	-	-	-	-	-	-	-	-	-	
4	3	14,3	3,50	4,46	0,96	19,00	9,50	4,40	4,56	0,16	0,27			
	1		3,56	4,54	0,98	19,70	9,85	4,45	4,62	0,17	0,28			
	2		3,51	4,46	0,95	19,80	9,90	4,39	4,55	0,16	0,27	0,27	0,89	
5	3	15,2	2,39	3,42	1,03	25,60	12,80	3,34	3,52	0,18	0,43			
	1		2,35	3,37	1,02	24,40	12,20	3,29	3,47	0,18	0,43			
	2		2,36	3,38	1,02	26,20	13,10	3,31	3,48	0,17	0,43	0,43	0,36	
6	3	14,3	3,20	4,26	1,06	8,50	4,25	4,16	4,38	0,22	0,33			
	1		3,17	4,19	1,02	12,20	6,10	4,07	4,30	0,23	0,32			
	2		3,18	4,21	1,03	10,40	5,20	4,11	4,34	0,23	0,32	0,33	1,53	20,43
7	2	11,8	3,44	4,22	0,78	23,90	11,95	4,15	4,38	0,23	0,23			
	1		3,46	4,22	0,76	22,70	11,35	4,15	4,37	0,22	0,22			
	3		3,46	4,24	0,78	23,90	11,95	4,16	4,38	0,22	0,23	0,22	1,68	
8	2	15,4	2,23	3,20	0,97	22,70	11,35	3,12	3,32	0,20	0,43			
	1		2,23	3,20	0,97	22,90	11,45	3,11	3,30	0,19	0,43			
	3		2,23	3,23	1,00	22,30	11,15	3,13	3,33	0,20	0,45	0,44	1,77	
9	2	15,5	2,18	3,14	0,96	21,30	10,65	3,07	3,24	0,17	0,44			
	1		2,17	3,12	0,95	22,30	11,15	3,06	3,22	0,16	0,44			
	3		2,17	3,12	0,95	21,30	10,65	3,08	3,25	0,17	0,44	0,44	0,34	1,14
10	1	15,5	2,60	3,49	0,89	28,70	14,35	3,40	3,62	0,22	0,34			
	2		2,60	3,50	0,90	29,00	14,50	3,40	3,63	0,23	0,35			
	3		2,60	3,50	0,90	28,70	14,35	3,41	3,64	0,23	0,35	0,34	0,64	
11	1	13,1	2,60	3,39	0,79	40,10	20,05	3,30	3,51	0,21	0,30			
	2		2,54	3,33	0,79	40,00	20,00	3,25	3,47	0,22	0,31			
	3		2,55	3,34	0,79	38,30	19,15	3,27	3,50	0,23	0,31	0,31	1,25	
12	1	15,0	3,76	4,82	1,06	30,70	15,35	4,72	5,05	0,33	0,28			
	2		3,70	4,76	1,06	31,50	15,75	4,66	4,98	0,32	0,29			
	3		3,68	4,73	1,05	31,90	15,95	4,62	4,95	0,33	0,29	0,28	0,84	8,46
13	1	11,6	3,65	4,30	0,65	22,90	11,45	4,18	4,51	0,33	0,18			
	2		3,73	4,38	0,65	22,20	11,10	4,27	4,58	0,31	0,17			
	3		3,83	4,50	0,67	23,30	11,65	4,39	4,73	0,34	0,17	0,18	1,16	
14	1	15,4	2,60	3,43	0,83	28,70	14,35	3,37	3,64	0,27	0,32			
	2		2,58	3,41	0,83	30,00	15,00	3,32	3,60	0,28	0,32			
	3		2,56	3,40	0,84	30,60	15,30	3,31	3,59	0,28	0,33	0,32	1,42	
15	1	15,2	2,39	3,12	0,73	30,70	15,35	3,01	3,28	0,27	0,31			
	2		2,41	3,14	0,73	29,50	14,75	3,04	3,32	0,28	0,30			
	3		2,40	3,14	0,74	30,30	15,15	3,04	3,32	0,28	0,31	0,31	0,89	3,23
16	1	15,4	2,27	3,06	0,79	14,30	7,15	2,99	3,19	0,20	0,35			
	2		2,27	3,06	0,79	13,40	6,70	3,01	3,20	0,19	0,35			
	3		2,28	3,07	0,79	14,80	7,40	3,00	3,19	0,19	0,35	0,35	0,25	
17	1	15,4	3,11	3,87	0,76	24,50	12,25	3,79	4,00	0,21	0,24			
	2		3,12	3,90	0,78	25,40	12,70	3,80	4,00	0,20	0,25			
	3		3,10	3,86	0,76	20,90	10,45	3,78	3,98	0,20	0,25	0,25	1,24	
18	1	15,2	3,27	4,36	1,09	24,70	12,35	4,27	4,48	0,21	0,33			
	2		3,17	4,23	1,06	24,00	12,00	4,14	4,36	0,22	0,33			
	3		3,13	4,16	1,03	23,50	11,75	4,07	4,29	0,22	0,33	0,33	0,85	15,29

7.5.4 Retention factor testing of the 5 μm PH particles

The raw data from chromatograms of toluene used during the calculation of the retention factor is summarized in **Table 21**.

Table 21. The raw data and the calculated average retention factor for toluene on a column packed 5 μm PH particles (n=1).

Particles		Length (cm)	t_M (min)	t_R 25-OHC (min)	Difference (min)	k	x̃	RSD (%)
5 μm PH	1	15.3	2.59	4.12	1.53	0.59		
	2		2.76	4.14	1.38	0.50		
	3		2.76	4.20	1.44	0.52	0.54	8.8

The raw data from chromatograms of 25-OHC used during the calculation of the retention factor is summarized in **Table 22**.

Table 22. The raw data and the calculated average retention factor for 25-OHC on columns packed with both 2.5 μm SPH particles and 5 μm PH particles.

Particles		Length (cm)	t_M (min)	t_R 25-OHC (min)	Difference (min)	k	x̃	RSD (%)
2.5 μm SPH	1	12.3	1.23	6.22	4.99	4.06		
	2		1.23	6.33	5.10	4.15		
	3		1.23	6.25	5.02	4.08		
	4		1.21	6.25	5.04	4.17	4.11	1.2
5 μm PH	1	12.3	1.22	2.47	1.25	1.02		
	2		1.15	2.63	1.48	1.29		
	3		1.25	2.73	1.48	1.18		
	4		1.20	2.46	1.26	1.05	1.14	10.8